THE UNDERLYING MOLECULAR MECHANISM OF BUFEI YISHEN PRESCRIPTION FOR COPD IN MICE MODEL BASED ON NRF2/PPAR γ PATHWAY

Xu Cong

DOCTOR OF PHILOSOPHY

(CHINESE MEDICINE)

M. KANDIAH FACULTY OF MEDICINE AND HEALTH SCIENCES

UNIVERSITI TUNKU ABDUL RAHMAN

Dec 2023

THE UNDERLYING MOLECULAR MECHANISM OF BUFEI YISHEN
PRESCRIPTION FOR COPD IN MICE MODEL BASED ON NRF2/PPAR
γ PATHWAY

By

Xu Cong

A thesis submitted to the Department of Chinese Medicine,

M. Kandiah Faculty of Medicine and Health Sciences,

Universiti Tunku Abdul Rahman, in partial fulfillment of the requirements

for the degree of

Doctor of Philosophy (Chinese Medicine)

Dec 2023

ABSTRACT

**THE UNDERLYING MOLECULAR MECHANISM OF BUFEI YISHEN
PRESCRIPTION FOR COPD IN MICE MODEL BASED ON
NRF2/PPAR γ PATHWAY**

Xu Cong

Chronic Obstructive Pulmonary Disease (COPD) is a debilitating respiratory disorder characterized by persistent airflow limitation and oxidative stress-induced inflammation. Bufei Yishen Prescription (BYP), a traditional Chinese medicine formula, has shown promising therapeutic effects on COPD. However, the precise molecular mechanisms underlying its efficacy remain unclear. This study investigates the potential therapeutic mechanisms of BYP in a COPD mice model, focusing on the NRF2/PPARγ signaling pathway.

Using a murine model of COPD induced by cigarette smoke exposure, we found that Bufei Yishen prescription can effectively improve the general condition, lung function and lung tissue injury of COPD mice model, reduce the expression level of pulmonary inflammatory factors, improve the efferocytosis function of alveolar macrophages in COPD mice model, reduce the apoptosis rate of lung tissue, and inhibit the number and polarization of macrophages.

In conclusion, our study elucidates the molecular mechanisms underlying the therapeutic effects of Bufei Yishen Prescription in a COPD mice model. BYP

exerts its beneficial effects by activating the NRF2/PPARγ pathway, leading to enhanced antioxidant defense and reduced inflammation. These findings provide valuable insights into the potential of BYP as a complementary therapeutic approach for COPD and underscore the importance of NRF2/PPARγ signaling in COPD pathogenesis. Further clinical studies are warranted to validate these findings and explore the translational potential of BYP in COPD management.

Key Words

ACKNOWLEDGEMENT

point of being unworthy of mention, but your words describe everything that ordinary people go through. The ordinary and authentic have a power of their own. I wish you all success in your careers, good health, and happy families.

Guo Kai, Yu Huihui, Jiang Bohan, and Yan Lipeng, I miss you all very much, and I will visit you with my wife. Thanks to Wang Lin, I appreciate the time you took in freshman year to chat with me, and I am even more grateful that you helped me meet my wife. I wish you, your child, and your husband good health.

I also want to thank my father-in-law and mother-in-law for providing my wife with a relaxed childhood and suitable job. Thus, the person I am most grateful to is my wife. In the blink of an eye, it has been two and a half years since we first met. Lee Teng does not know that every time I went to see her, it was actually my wife urging me behind the scenes. She is more sensitive and thoughtful than I am. Even though she is just a somewhat thin and dark-skinned ordinary girl in the eyes of most people, only I know how much she depends on me and how much she indulges me. The hopeful look in her eyes is my greatest motivation to complete this article.

If successful, benefit the world; if not, take care of oneself. In such a chaotic world, having a healthy and harmonious family is my greatest fortune. Therefore, no one can prevent me from going home, including myself, even my high blood

pressure and fatty liver are no exceptions.

Finally, I would like to express my gratitude to the firefighting and healthcare institutions of Zhengzhou City, as well as to all the people living in this mega-city with a population of 12 million. From July 17th to July 20th, 2021, Zhengzhou City experienced the most intense rainfall in China's recorded meteorological history and the strongest precipitation among major cities worldwide. The maximum rainfall in an hour is 201.9 mm, 10 times that of the Chinese mainland standard for short-term heavy precipitation, nearly 7 times the red warning standard for rainstorm, and nearly 3 times the "Black rainstorm warning" standard for the highest-level warning of the Hong Kong Observatory. Never before in meteorological records has any mega-city in the world encountered such terrifying torrential rainfall. In the face of this historic-level natural disaster, my home's public utilities, including electricity, water supply, internet, telephone, and natural gas, did not experience even a minute of paralysis. In contrast, I saw that the road outside the window had already become a river, the lights beside the road had long gone out, and the cars were paralyzed on the road. I am proud of my city, and I would like to extend my gratitude to every citizen and military personnel involved in the post-disaster reconstruction.

Thank you for your dedication and efforts.

SUBMISSION OF THESIS

It is hereby certified that **Xu Cong** (ID No:**1905128**) has completed this thesis entitled "**THE UNDERLYING MOLECULAR MECHANISM OF BUFEI YISHEN PRESCRIPTION FOR COPD IN MICE MODEL BASED ON NRF2/PPAR γ PATHWAY**" under the supervision of Dr. Te Kian Keong (Supervisor) from the Department of Chinese Medicine, M. Kandiah Faculty of Medicine and Health Sciences, and Dr. Choy Wai Chong (Co-Supervisor) from the Department of Chinese Medicine, M. Kandiah Faculty of Medicine and Health Sciences, and Prof. Chen Yu Long（External Co-Supervisor）of Academy of Chinese Medicine Sciences

I understand that University will upload softcopy of my thesis in pdf format into UTAR Institutional Repository, which may be made accessible to UTAR community and public.

Yours truly,

Xu Cong

APPROVAL SHEET

This thesis entitled **"THE UNDERLYING MOLECULAR MECHANISM OF BUFEI YISHEN PRESCRIPTION FOR COPD IN MICE MODEL BASED ON NRF2/PPAR γ PATHWAY"** was prepared by **Xu Cong** and submitted as partial fulfillment of the requirements for the degree of **Doctor of Philosophy (CHINESE MEDICINE)** at Universiti Tunku Abdul Rahman.

Approved by:

(Dr. Te Kian Keong)   Date: 5/Dec/2023

Associate Professor/Supervisor Department of Chinese Medicine

M. Kandiah Faculty of Medicine and Health Sciences

Universiti Tunku Abdul Rahman

(Dr. Choy Wai Chong)   Date: 5/Dec/2023

Associate Professor/Co-Supervisor Department of Chinese Medicine

M. Kandiah Faculty of Medicine and Health Sciences

Universiti Tunku Abdul Rahman

(Prof. Chen Yu Long)   Date: 5/Dec/2023

Professor/External Co-Supervisor Academy of Chinese Medicine Sciences

Henan University of Chinese Medicine

M. KANDIAH FACULTY OF MEDICINE AND HEALTH SCIENCES

UNIVERSITI TUNKU ABDUL RAHMAN

Date: 5/Dec/2023

DECLARATION

I Xu Cong hereby declare that the thesis is based on my original work except

for quotations and citations which have been duly acknowledged. I also

declare that it has not been previously or concurrently submitted for any

other degree at UTAR or other institutions.

(Xu Cong)

Date: 5/Dec/2023

TABLE OF CONTENTS

LIST OF TABLES

LIST OF FIGURES

LIST OF APPENDICES

LIST OF ABBREVIATIONS

AM	Alveolar macrophage
BALF	Bronchoalveolar lavage fluid
CD	Cluster of Differentiation
COPD	Chronic Obstructive Pulmonary Disease
DMSO	Dimethyl Sulfoxide
EF50	Expiratory flow at 50% expired volume
ELISA	Enzyme-linked immunosorbent assay
FCM	Flow cytometry
HE	Hematoxylin and Eosin
IHC	Immunohistochemistry
IL-4	Interleukin-4
INOS	Inducible nitric oxide synthase
IOD	Integral optical density
M1	Classically activated macrophage
M2	Alternatively activated macrophage
MV	Minute volume
Nrf2	Nuclear factor erythroid-2 related factor 2
OD	Optical Density
PBS	Phosphate Buffer Saline
PEF	Peak expiratory flow
PPAR γ	Peroxisome Proliferator-activated

	Receptor
TNF α	Tumor necrosis factor-α
TV	Tidal volume

CHAPTER 1.0: INTRODUCTION

Chronic obstructive pulmonary disease (COPD) represents a significant burden on global health resources. The primary etiological factors for COPD including of exposure to cigarette smoke (CS), and inhalation of toxic particles and gases, in which the toxicants will precipitate in the lung tissue and cause extensive injury to lung tissue and subsequent recession in lung function (Mirza et al., 2018).

The disease is typified by persistent dyspnea and a restriction in airflow. The symptom of COPD is diverse, and symptoms become increasingly pronounced as the disease progresses towards its later stages (Leung and Sin, 2017).

The pathogenesis of COPD is multifactorial, often co-existing with a range of other diseases (Rabe and Watz, 2017). In the absence of timely and appropriate intervention, patients may experience an exacerbation of symptoms, including chronic persistent cough, dyspnea, frequent respiratory infections. These conditions can lead to a progressive and irreversible decline in lung function, thereby posing a significant threat to patient survival.

The incidence of COPD is increasing, particularly among individuals aged 40

and above. In terms of age, COPD is the second leading factor in leading to high mortality in 1990 and in 2019, COPD is the third leading factor (Collaborators, 2020).

According to a report, the prevalence of COPD increased by 15.6% from 2007 to 2017, despite a 10.1% decrease in age-standardized prevalence among males (James SL, et al., 2018). This discrepancy underscores the complex epidemiology of COPD and highlights the urgent need for further study and the development of effective intervention strategies to mitigate the impact of this debilitating disease.

Study conducted by Yin and coworker (2022) suggests that as of 2019, one in four global COPD patients' lives in China. Currently, China has 300 million active adult smokers, the largest number in the world (Wang et al., 2019). Compared to survey results from a decade ago, the COPD prevalence in Middle-aged and elderly people, the middle-aged and elderly are defined as people aged 40 and above, increased by 67% between 2012 and 2015, reaching epidemic proportions (Wang et al., 2018a).

As China's population is aging rapidly and predictably, the cost of managing COPD patients is expected to increase substantially in the coming years (Yin et al., 2022). COPD is the primary reason of death and disability, which brings huge

economic burden to people.

The persistent chronic inflammatory response is a central component in the continuous progression of COPD (Barnes, 2019). Exogenous bacteria, harmful particles, and gases, among other inflammatory factors, induce the activation of eosinophils, neutrophils, basophils, macrophages, and other inflammatory cells in lungs, leading to the inflammatory factor's secretion and the onset of inflammatory response in the body in triggering lung disease (Barnes, 2019).

Inflammatory factors induced lung disease can generate endogenous reactive oxygen species (ROS) in the lungs, leading to a disruption in the body's antioxidant defense function, causing a persistent oxidative stress response (Chamitava et al., 2020). This will disturb the repair and clearance of damaged cells in the lungs, as well as the destruction of airway structures (Chamitava et al., 2020). It can also promote the expression of inflammatory factor secretion by regulating redox-sensitive transcription factors and chromatin, further stimulating the body's inflammatory response (Chamitava et al., 2020).

Nagata (2018) reported damaged cells cannot be repaired in time when it is under persistent inflammatory responses, while immune cells and structural cells persistently undergo apoptosis, many apoptotic cells accumulate in the lungs, leading to secondary necrosis, further releasing necrotic cell fragments. This, in

turn, leading to a loss of control in the immune system, launch the inflammatory response, and aggravate the disease progression via "damage-associated molecular patterns" (DAMPs). The timely clearance of apoptotic cells is target for effectively controlling the inflammatory response in the lungs. The recognition and removal of apoptotic cells is mainly mediated by macrophages. Zheng and coworker (2021) suggest that the degree of accumulation of apoptotic cells in the lungs is positively correlated with the efferocytosis function of macrophages. Efferocytosis is crucial in suppressing the chronic inflammatory response of COPD.

Macrophages exert their physiological functions through phagocytosis, among which the process of clearing apoptotic cells (ACs) is referred to as efferocytosis. Billions of cells will get apoptotic daily in human body while phagocytic cells will clear AC efficiently and rapidly to maintain homeostasis within the body. Therefore, efferocytosis plays a crucial role in tissue homeostasis, embryonic development, immunity, and the resolution of inflammation (Zheng et al., 2021).

When efferocytosis is impaired, many apoptotic cells cannot be effectively cleared, leading to the release of pro-inflammatory cellular contents and a persistent inflammatory response. Elliott and coworker (2017) suggest that when efferocytosis occurs, it also promotes tissue repair and initiates anti-inflammatory signaling cascades, releasing anti-inflammatory cytokines, and

suppressing the inflammatory response. Under the stimulation of the inflammatory response, the number of macrophages in the lungs increases, polarizes, and promptly clears apoptotic cells, thereby alleviating the inflammatory response and maintaining the balance of the internal environment. Although an increase in macrophages can be observed in the airways, alveolar regions, bronchoalveolar lavage fluid (BALF), sputum and other respiratory secretions of COPD patients, the persistent inflammatory response leads to a dysfunction in the efferocytosis of alveolar macrophages, causing a continuous accumulation of apoptotic cells in the body, further inducing lung disease. Therefore, regulating the efferocytosis function of alveolar macrophages is important in elucidating the mechanism of chronic inflammatory responses in the lungs, promoting the progression of clinical treatment, and the research and development of drugs (Jubrail et al., 2017).

PPAR γ is involving in many processes, including efferocytosis. PPAR γ can only be activated when bound to its corresponding ligand. Once activated, PPAR γ forms a heterodimer, recruits related co-factors, and binds to the promoter region of specific genes in the PPAR response element (PPRE), thereby regulating phagocytosis-related target genes. At the same time, PPAR γ can also directly activate specific genes, such as CD36. Upon activation, macrophage PPAR γ can upregulate cell efferocytosis-related surface receptors and bridging molecules such as CD36, Gas6, and MFG-E8, thereby enhancing cell phagocytic

ability, promoting macrophage polarization towards the M2 type, and inhibiting inflammation. For instance, Xian and coworker (2017) point that a cell surface receptor, low-density lipoprotein receptor 1 (LRP1), which is proven to be necessary for efferocytosis, also activates the PPAR γ pathway, leading to cholesterol efflux. PPAR γ has multiple functions and is considered nodes between inflammatory and metabolic signals. Mehrotra and Ravichandran (2022) pointed out that the nuclear receptor PPAR γ has multiple roles and is considered a node between inflammatory and metabolic signals.

Nrf2 is a member of the Cap'n'Collar (CNC) transcription factor family. Its bZIP structure is part of the nuclear receptor family and is one of the keys signaling pathways in regulating inflammatory responses. Upon activation by inflammatory factors, Nrf2 dissociates from its cytoplasmic inhibitor Keap1 and forms a heterodimer with the small Maf protein in the nucleus. This heterodimer then activates the antioxidant protein HO-1 through the antioxidant response element (ARE), which can inhibit the transcription of pro-inflammatory M1-type macrophage genes (Sidhaye et al., 2019). At the same time, it can increase the expression levels of M2-type genes involved in anti-inflammatory responses and tissue repair. Furthermore, Nrf2 can effectively stimulate the recruitment of macrophages and the phagocytosis of apoptotic cells (Yan et al., 2018).

COPD is classified under the categories of "Lung syndrome" and "dyspnea

Syndrome" in Traditional Chinese Medicine (TCM). The "Lingshu · Distention Theory" states: "Those with lung distention experience a sensation of emptiness and fullness, accompanied by panting and coughing". Based on the TCM philosophy in "JinKuiYaoLue": "Coughing and gasping for breath indicates lung distention, the individual patient, and their eyes appear as if they are about to pop out". These descriptions align with the clinical symptoms of COPD. Li Jiansheng (2011a) pointed out that the primary pathogenesis of COPD is "deficiency of vital energy and cumulative damage". The main mechanism of disease onset is chronic lung deficiency, delayed treatment, retention of phlegm and turbidity, obstruction of lung qi, and abnormal ascension and descent of lung qi. Over time, the vital energy becomes deficient, the exterior defense is not solid, and external pathogens easily invade repeatedly, inducing the onset of the disease (Li Jiansheng, 2011a). The pathological changes are characterized by a deficiency in the root and excess in the branch (Li Jiansheng, 2011a).

Bufei Yishen prescription decoction is composed of 12 medicinal herbs including Ginseng Root 9g, Mongolian Milkvetch Root 15g, Babury Wolfberry Fruit 12g, Common Macrocarpium Fruit 9g, Chinese Magnoliavine Fruit 9g, Short-horned Epimedium Herb 9g, Chekiang Fritillary Bulb 9g, Cultibated Purple Perilla Leaf 9g, Red Paeoniae Trichocarpae 12g, Earthworm 12g, Tangerine Peel 9g, Liquorice Root 6g (Chinese Medicinal Material Images Database, 2016). It has the functions of tonify lung replenish kidney, activate

blood, resolve phlegm, dispel stasis (WHO International Standard Terminologies on Traditional Medicine in the Western Pacific Region, 2007).

Despite the availability of bronchodilators, inhaled corticosteroids, and long-acting anticholinergic drugs among other medications, the treatment of COPD remains challenging. Some patients may exhibit poor responsiveness to treatment, and long-term drug use may be associated with side effects (GOLD, 2023).

Bufei Yishen prescription was reported as a potential medication for COPD as a treatment way in alternative of existing drugs. The results of a multicenter, randomized, double-blind, active-controlled trial study by Li Jiansheng (2011b) showed that Bufei Yishen prescription can significantly improve lung function, improve clinical symptoms, cough, expectoration, enhance immunity, and reduce the number of acute attacks of COPD. Zhang yile and coworker (2021) suggest that Bushen Yifei decoction combined with salmeterol xinafoate and fluticasone propionate powder for inhalation is effective and safe in treating COPD in stable stage.

Moreover, research by Li Suyun (2003) suggests that this formula can reduce the level of extracellular matrix, regulate collagen metabolism, alleviate airway remodeling. Study by Tian Yange and coworker (2018) suggest that the formula

reduce adhesion factors, inhibit inflammatory reaction and the secrete of inflammatory intermediate matter, thereby alleviating chronic airway inflammation during the remission period of COPD.

In summary, during the development of COPD, the efferocytosis function of macrophages decreases, apoptotic cells cannot be cleared in a timely manner, which enhances the inflammatory response and accelerates the progression of COPD. The PPAR γ and Nrf2 pathways are involved in regulating the efferocytosis function of macrophages, and Bufei Yishen prescription can improve COPD by regulating these related pathways. In this experiment, mice with COPD were used as experimental subjects and treated with Bufei Yishen prescription. The efficacy of Bufei Yishen prescription in treating COPD was evaluated through lung function, lung pathology, and inflammatory factors. The mechanism of Bufei Yishen prescription's therapeutic effect was explored through the efferocytosis ability of alveolar macrophages, apoptosis of alveolar epithelial cells, phenotyping of alveolar macrophages, and the expression of the PPAR γ and Nrf2 pathways. This study provides an experimental basis and rationale for scientific research and clinical application.

CHAPTER 2.0: LITETATURE REVIEW

2.1 The Epidemiology of COPD

COPD had led to high mortality rate worldwide in leading to heavy social burden. This is in need to enhance the prevention and effectiveness of treatment. High exposure to harmful particles usually precipitates the disease, leading to abnormal airway and alveolar conditions. Although the primary pathological changes in COPD occur in the airways and alveoli, pathological alterations are also common in lung parenchyma and pulmonary capillaries (GOLD, 2023).

While the incidence of COPD increases in individuals over 40 years of age (Collaborators, 2020), Venkatesan (2022) highlighted the trend of COPD affecting young people. Here, 'young people' refers to between 20 and 50 years. 2023's GOLD also pointed out this. The latest Guide still focuses on clinical symptoms but breaks the traditional understanding that COPD primarily occurs in middle-aged and elderly individuals.

According to research by Soriano and coworker（2018a), it is estimated that in 2019, approximately 210 million people worldwide have COPD, resulting in about 3 million people died and 70 million disability adjusted life Year (DALYs). The highest age-standardized point prevalences were reported in North America,

South Asia, and Australia, while the lowest prevalences were observed in the Asia-Pacific region. The highest age-standardized death rates were in Australia (Soriano et al., 2018a).

Global reports on COPD prevalence are inconsistent, but the overall trend is increasing. As reported by Soriano and coworker (2018b), the relative increase in global COPD prevalence from 1990 to 2017 was 5.9%. From 1990 to 2019, the incidence and prevalence of COPD in China increased by nearly two-thirds (Yin P, et al. 2022). It is estimated that in 2019, new diagnoses of COPD in China accounted for 24% of the global total, and COPD-related deaths in China accounted for one-third of global cases (Yin P, et al. 2022). Wang and coworker (2018b) pointed that COPD patients, 40 years old and above is about 13% between 2014 and 2015, compared to 8.2% between 2002 and 2004 in China reported by Fang and team (2018). Between 1965 and 1995, the tendency of disease in the United States increased by 16.3%. The study by Marshall and team (2022) across 28 European countries, pointed out that from 2001 to 2019, although COPD probability rates decreased in 23 out of the 28 European countries for men, the rates for women increased by 4.3%. They also noted that while the rate declined by 27.5% for men and 10.4% for women, this decrease was not universal, especially among the female population, highlighting COPD as a significant cause of death. The substantial COPD patient population implies a high number of deaths or disabilities, making COPD a significant challenge

for global public health and a major burden on global medical resources (GOLD, 2023).

The prevalence of COPD varies among different countries. A national health survey in the United States found that the COPD probability of COPD among grown man was 6.2% (Wheaton et al., 2019). However, the prevalence of COPD varied among states, ranging from about 3% in Hawaii to about 13% in West Virginia (Wheaton et al., 2019). An analysis of the geographic distribution of the COPD probability among aged 40 years and above in Europe showed that the prevalence rates in Northern Europe, Western Europe, and Central Europe were 11.5%, 14.2%, and 14.1%, respectively (Blanco et al., 2018). In the Asian region, a cross-sectional survey conducted in China from 2014 to 2015 showed that the highest COPD probability place were in Sichuan province, Gansu province, and Shaanxi province (Wang et al., 2020). In India, the COPD probability of COPD among people aged 30 and over is 7.0% (Verma et al., 2021).

According to a study by Safiri and team (2022), there is an inverse V-shaped relation between the COPD incidence and the DALY for COPD from 1990 to 2019. Fang and team (2018) pointed that Chinese COPD incidence in suburban (14.9%) is higher than in urban (12.2%). The COPD incidence among adult residents in suburban areas of Sichuan Province is also significantly higher than in urban (Jin hang et al., 2021). The prevalence of COPD was reported up to 8.8%

and 10.9% among population with the aged 40 years old and above in Urumqi and Xinjiang province, respectively (Luo qian et al., 2019). However, this distribution does not include all provinces in China. For instance, in Hunan Province, the COPD incidence among individuals aged 40 and above in urban areas is 15.9%, which is higher than the 12.3% in suburban areas (Yin Lei et al., 2020). There are significant disparities in the COPD incidence between different regions and between urban and rural areas, which may be attributed to variations in economic levels, lifestyles, and patterns of population aging (Zha et al., 2019).

The prevalence of COPD varies among different populations, with overall higher rates in males than females (GOLD, 2023). A study by Safiri and team (2022), the number of global COPD patients begins to rise in the 20-29 age group, reaches its peak in the 70-75 age group, and then starts to decline. Although the proportion of females among patients aged 75 and above is higher, males consistently have a higher proportion than females in age groups below 75 years (Safiri et al., 2022). A meta-analysis also showed that worldwide, 14.3% of men over 30 will get COPD, higher than the 7.6% in females (Adeloye et al., 2015). In the population under 40, the number was 3.4% in man and 3.3% in women, while in those over 70, the number was 27.2% and 15.9% (Ntritsos et al., 2018). Similar observations are supported by COPD surveillance data from China. Another study pointed out that in 2014-2015, among the Chinese population aged 40 and above, the number of COPD was 19% and 8.1% in women (Fang et

al., 2018). Yet another study found that the prevalence in males was also higher than in females, such as in the Yucheng District of Chongqing City, where the prevalence in the population aged 40 and above was significantly higher in males (27.7%) than in females (6.8%) (Zhang Yong et al., 2019).

According to Delmas and team (2021), although the under-recognition and under-diagnosis of COPD to some extent affect the accuracy of mortality data, and the accuracy of COPD diagnosis codes registered in health management databases is also uncertain, COPD remains one of the most important causes of death in most countries. The increase in COPD mortality rate is mainly related to the expansion of the smoking population, the aging of the world population (especially in high-income countries), the decrease in mortality rates of other common diseases (such as ischemic heart disease, infectious diseases), and lacking of effective treatment methods. A study by (GBD, 2018) found that the global age-standardized mortality rate of COPD in 2016 was 46.8 per 100,000, and the number is still increasing. In the global disease burden research, it was reported up to 3 million people was died from COPD yearly, which accounting for 6.0% of all-cause deaths (GBD, 2018). With social development, the increasing aging population, high smoking rates, and environmental pollution, the incidence and mortality rates of COPD in China are increasing year by year. Overall, the male mortality rate is higher than that of females, and the rural areas are higher than urban areas. China's cause of death monitoring data in 2022

shows that among the top ten causes of death in Chinese residents, respiratory

diseases (mainly COPD) account for 10.6% of all-cause deaths, ranking fourth

(CCDC, 2022). The proportion of respiratory diseases among all-cause deaths in

the western region is 15.1%, which is higher than the 9.1% in the eastern area

and the 9.0% in the middle area (CCDC, 2022). Every year, there are 1 million

people dying from COPD in China (CCDC, 2022).

2.2 Risk Factors for COPD

From the existing findings, studies inferred both genetic and environmental

factors were influence and related to the development of COPD. Controllable

risk factors include smoking, alcohol consumption, and psychological factors,

while uncontrollable factors include environmental pollution, developmental

abnormalities, and genetic defects. Smoking or exposure to cigarette smoke has

been confirmed as the most significant risk factor (GOLD, 2023).

As early as the last century, a study encompassing 800 subjects over an eight-

year period suggested that approximately 15% of smokers will ultimately

develop COPD (Kurihara et al., 1989). Later, larger-scale studies over extended

periods and with more extensive sample sizes have validated this view (Salvi et

al., 2020). Regardless of whether the research is cross-sectional or longitudinal,

Forced Expiratory Volume in one second (FEV1) of smokers has been observed

to decline faster than that of non-smokers. According to a research report, the

relative risk of COPD in smokers with a smoking history and who continue to smoke is three times higher than in non-smokers (Forey et al., 2011). The risk in getting COPD for those ex-smoker who had quitted for smoking was found 3.5 times higher than non-smokers (Forey et al., 2011). Some researchers speculate that the probability of smokers eventually developing COPD may be even higher, as nearly all smokers will experience a decline in lung function, provided the duration and quantity of smoking is sufficiently high (Forey et al., 2011).

Additionally, changes in the methylation levels of some genetic loci are associated with COPD, such as the methylation of DNA at CpG sites, which could potentially be a critical factor in impaired lung function (Imboden et al., 2019). Moreover, secondhand smoke exposure is a significant factor that cannot be overlooked. Studies have suggested that the amount of exposure to secondhand smoke directly increases the likelihood of developing COPD, regardless of whether the exposed individual is an adult or a child (Diver et al., 2018). A longitudinal follow-up study over 17 years demonstrated that the morality rate from COPD for those exposed to secondhand smoke was approximately twice as high as for those unexposed (He et al., 2012).

While smoking is the primary risk factor for COPD, other risk factors have also been identified over the past few decades (Yang et al., 2021). These include both indoor and outdoor air pollution, dust exposure, harmful gas exposure, repeated

lower respiratory tract infections during childhood, history of asthma, intrauterine growth restriction, and low socioeconomic status (Yang et al., 2021). Long-term inhalation of dust will continuously accumulate in the patient's lungs, causing damage to the respiratory epithelial cilia, which in turn reduces their clearance function, leading to respiratory symptoms and lung function impairment, thereby increasing the risk of COPD (GOLD, 2023). For example, teachers who use chalk and workers in dusty environments such as workshops. Liu and team (2007) have found that harmful gases produced by the burning of agricultural products like wood, crops, and charcoal have led to disease in about 9% of the population in the southern region of China. Lytras and team suggested (2018) that exposure to dust and harmful gases can increase the probability of developing COPD by 1.6 times higher risk compared to individuals not exposed to such environments. Besides the traditionally high-risk occupations such as construction workers and workshop workers that are frequently exposed to high dust and particulate matter, professions such as teachers and nurses have also been found to have an increased risk of COPD (Xie et al., 2021).

Indoor air pollution should not be underestimated, in addition to outdoor air pollution. Insufficient combustion of household fuels like natural gas, coal, and charcoal can generate harmful gases, making indoor air pollution one of the top ten risk factors for COPD (GBD, 2018). However, this factor was not fully ruled out as a lack of long-term, large-scale studies at the population level and

difficulties in quantifying individual exposure levels. As such, further research is needed.

2.3 Pathogenesis of COPD

Airway inflammation is the core mechanism of COPD pathogenesis. The inhalation of cigarette smoke and other harmful gases stimulates macrophages, neutrophils, T lymphocytes, and other cells to differentiate, aggregate in the airways and alveoli, and secrete pro-inflammatory mediators (Barnes, 2016).

In the presence of pro-inflammatory mediators, neutrophils secrete various proteases, such as serine proteases, elastase, and tissue proteases. These proteases can disrupt the alveolar wall, leading to alveolar rupture and restructuring, as well as airway remodeling, initiating a cascade reaction that exacerbates inflammation and contributes to disease progression (Belchamber and Donnelly, 2017). At the same time, these processes can damage epithelial cells and dendritic cells, resulting in small airway injury and structural changes, including degeneration of airway epithelial cells, mucus hyperproduction, and bronchial fibrosis, further exacerbating the inflammatory response (Stampfli and Anderson, 2009; Barnes, 2018). Macrophages play two important roles, including in: on one hand, M1-polarized macrophages exacerbate airway inflammation and remodeling by secreting pro-inflammatory and chemotactic factors; on the other hand, M2-polarized macrophages participate in the

clearance of apoptotic cells and the repair of lung tissue damage, promoting the resolution of inflammation (Puttur et al., 2019).

In biological systems, a delicate equilibrium exists between the beneficial and detrimental effects of reactive oxygen and nitrogen species (ROS and RNS respectively). When this balance tilts in favor of the oxidant species, it leads to a condition known as oxidative stress. Oxidative stress produces a variety of pathological factors such as ROS and RNS, primarily because of metabolic processes (Taniguchi et al., 2021).

These pathological byproducts can induce substantial damage to various macromolecules within the organism. Notably, they have the capacity to interact with and impair key biological molecules such as DNA, proteins, and lipids. The interaction of these reactive species with DNA can lead to mutations, while their interaction with proteins may result in changes in protein function and structure. Lipids, particularly those that make up cell membranes, can undergo peroxidation, compromising the integrity of the membrane (Persson et al., 2017).

The resulting damage from this oxidative stress can cause inflammation and lead to structural changes in the airways, a process known as airway remodeling. This is a significant pathophysiological feature of COPD. The complex interplay between oxidative stress, inflammation, and airway remodeling forms an

integral part of the pathogenesis of COPD and contributes significantly to its development and progression (Bao Haipeng, et al., 2019).

Oxidative stress plays a role in the onset and progression of COPD and interacts with the inflammatory response. Oxidative stress increases the levels of oxidants such as H_2O_2, ROS, and HCIO in the alveoli and blood of COPD patients, while levels of antioxidants such as SOD and GSH are reduced (Taniguchi et al., 2021). This can lead to direct damage to proteins, lipids, and nucleic acids, resulting in cell death and functional impairment. At the same time, oxidative stress can enhance the ability of proteolytic enzymes to hydrolyze matrix proteins, thereby destroying the extracellular matrix, leading to alveolar enlargement, and accelerating the destruction of lung parenchyma and interstation (Persson et al., 2017).

Currently, it is widely believed that the imbalance between proteases and anti-proteases is involved in the pathogenesis of COPD. Studies have shown that the levels of proteases such as matrix metalloproteinases (MMPs) and neutrophil elastase (NE) are elevated, while the levels of antiproteases such as alpha-1 antitrypsin (α1-AT) and tissue inhibitor of metalloproteinase (TIMP) are reduced. This imbalance of protease/antiprotease ultimately results in the destruction of alveolar tissue structure (Bao Haipeng et al., 2019). The extracellular matrix (ECM), composed mainly of collagen, elastin, and fibronectin, serves to

maintain tissue stability and elasticity, as well as facilitate cell migration and control behavior. Neutrophil elastase (NE) and matrix metalloproteinases (MMPs) can degrade nearly all components of the ECM (Zhou et al., 2017). Under the persistent onslaught of inflammation, lung tissue suffers on-going damage and remodeling. Newly formed tissue in an inflammatory environment significantly loses its rigidity and biomechanical properties compared to healthy tissue, ultimately resulting in a decrease in lung elasticity and leading to emphysema (Strange, 2020).

2.4 Related signaling pathway of COPD

Inflammation plays a vital role in the pathogenesis of COPD, leading to architectural changes in lung tissue and impairing lung function. The mechanisms underlying this are complex and multifactorial, involving a host of cells, chemokines, and intricate signaling pathways. These pathways can exist independently but may also interconnect or counteract one another in a dynamic manner, shaping the inflammatory and tissue remodeling responses observed in COPD (Wei Gunzheng et al., 2020).

Toll-like receptors (TLRs) are key pattern recognition receptors (PRRs) within the innate immune system. Lung epithelial cells harbor these pattern recognition receptors on their surface, which become instrumental when the lungs are repeatedly exposed to harmful factors, thereby triggering an inflammatory

response. PRRs comprise TLRs, Retinoic acid-inducible gene I (RIG-I)-like receptors (RLRs), and NOD-like receptors (NLRs) (Vidya et al., 2018). At present, 10 kinds of TLRs have been found in human body, and they play an important role in different diseases (Ji Nan et al., 2022). TLRs is an important barrier against infection. It can identify not only exogenous pathogens, but also endogenous pathogens and their degradation products. TLRs selectively recognizes pathogen-related molecular patterns, including lipopolysaccharide in the outer membrane of Gram-negative bacteria, lipoteichoic acid and peptidoglycan in the cell wall of Gram-positive bacteria, flagellin in bacterial flagella, dsRNA and ssRNA of viruses, etc (Cai Xingxuan et al., 2021). Activated TLRs initiates a series of events involving various protein kinases, resulting in the activation of some transcription factors, such as nuclear factor kappa B, MAPK, interferon regulatory factor, AP1 and so on (Arora et al., 2019). Those transcription factors are transported into the nucleus and bind to DNA, and further transcribe and translate proteins, thereby enhancing innate immune response and initiating adaptive immune response to pathogens. The results showed that the levels of TLR2, TLR4, MyD88 and NF-κ B mRNA were significantly increased in patients with acute exacerbation and stable stage of COPD (Yang Lixia et al., 2020).

NF-κ B is a ubiquitous and multidirectional nuclear transcriptional regulatory protein. The activation of NF-κ B signal pathway is closely related to the

occurrence and development of COPD (Rao Min, Lu Yueming, 2017). Under normal circumstances, NF-κB exists in the cytoplasm and is inactive; its classical activation pathway is to activate TNFR1, which can induce IKK phosphorylation; free NF-κB is activated and quickly transferred to the nucleus, connects with the NF-κB sequence of the target gene, starts the expression of the target gene, and promotes the secretion of immune and inflammatory factors (Shen et al., 2019). Smoking, harmful gases, microorganisms and DAMPs interact with TLRs and complete transmembrane signal transduction, and then regulate the transcription, translation and expression of inflammatory genes through NF-κB pathway to produce and release inflammatory factors such as IL-6, IL-8, COX-2, PGE2. The inflammatory substances produced can not only directly damage cells and the extracellular matrix but also act as endogenous ligands, binding to corresponding receptors on the surface of neutrophils and NK cells. This further leads to the synthesis and release of many inflammatory mediators, followed by the recruitment of inflammatory cells, creating a positive feedback loop. As a result, the pulmonary inflammatory cascade is amplified and prolonged (Wortham et al., 2013). Studies have shown that drugs can down-regulate NF-κB signal pathway, thus reducing or interfering with the inflammatory response of COPD (Li Ya et al., 2021).

Peroxisome proliferator-activated receptors (peroxisomal proliferator-activated receptors, PPARs) belong to the superfamily of type II nuclear hormone

3receptors. PPAR was first isolated from liver cells (hepatocytes) by a group of 9 British scientists, including Issemann and others, in 1990 (Issemann and Green, 1990). Due to lacking of identifiable natural ligands, it was classified as an orphan receptor. However, it was later discovered by Kliewer and Forman (Kliewer et al., 1994) that fatty acids like oleic acid, linoleic acid, and eicosapentaenoic acid could act as natural ligands to activate the PPAR transcription factor. The human PPAR γ gene is located on the short arm of chromosome 3, specifically at region 2, band 5 (3p25) (Zhu et al., 1995). There are three subtypes of PPARs: PPAR α, PPAR β (or δ), and PPAR γ, each of which is encoded by a different gene. Structurally, PPAR γ is divided into six domains (A-F), which include four functional domains. The A/B region at the N-terminus encompasses the activation function (AF-1), while the C region contains the DNA-binding domain (DBD). The D region, known as the hinge region, connects the DBD and the ligand-binding domain (LBD). The E/F region contains the PPAR γ LBD and another activation function (AF-2), which is involved in ubiquitin-dependent degradation and is essential for ligand-induced PPAR γ transcriptional activity, playing a key role in the process from ligand signalling to transcriptional activation (Mansure et al., 2009). PPAR γ, like other members of the nuclear receptor superfamily, requires binding with corresponding ligands for activation. Once activated through ligand binding, PPAR γ forms a heterodimer with the retinoid X receptor (RXR). This heterodimer then recruits a series of specific co-factors, which bind to the

promoter region of specific genes containing peroxisome proliferator response elements (PPRE), thereby regulating gene transcription (Subramani et al., 2013).

Tumor Necrosis Factor-alpha (TNF-α) is a cytokine derived from mononuclear phagocytes, mediating various inflammatory responses and immune reactions. In cases of acute lung injury, activation of PPAR γ can reduce the expression of inflammatory factors such as TNF-α, thereby alleviating lung damage (Liu et al., 2014). Similarly, inhibiting the generation of TNF-α can suppress pulmonary fibrosis (Pilling et al., 2015). Lu and his team (2014) reported that the activation of PPAR γ can inhibit the production of Platelet-Derived Growth Factor-Beta (PDGF-β) mediated by Signal Transducer and Activator of Transcription 6 (STAT6). The potential mechanism is that PPAR γ competes with STAT1 for the limited quantity of CREB-binding protein (CBP) and p300, thus inhibiting the activation of STAT1. Straus and his team (2000) confirmed that, in vitro-cultured macrophages, the use of the PPAR γ ligand 15d-PGJ2 can directly inhibit the expression of NF-κB related genes. This inhibition is achieved through the covalent modification of the cysteine residues of IκB kinase and the DNA binding domain of the NF-κ B subunit. The ligand 15d-PGJ2's direct inhibition of NF-κ B signaling may contribute to the negative regulation of inflammatory responses. Certain in vitro experiments and animal model studies, such as those conducted by Liu and coworker (2013), have shown that the use of the PPAR γ agonist curcumin in a rat model of cerebral ischemic vascular disease can

upregulate the expression of PPAR γ and enhance PPAR γ-PPRE binding activity. This results in a reduction of inflammatory mediators such as NF-κ B, IL-1β, TNF-α, PGE2, NO, COX-2, and INOS, thereby playing a role in inhibiting the inflammatory response. The role of PPAR γ in the negative regulation of inflammatory responses holds significant clinical therapeutic potential. As research continues to deepen our understanding of this regulatory mechanism, PPAR γ is increasingly being recognized as a promising target for anti-inflammatory interventions. However, the inflammatory response is a complex system, and while some mechanisms involving PPAR γ have been elucidated, a more comprehensive understanding of these mechanisms is still needed.

Nuclear factor erythroid 2-related factor 2 (Nrf2) is a crucial regulator broadly present in tissues, playing a key role in controlling cellular oxidative damage. The antioxidant response element (ARE) is a specific DNA promoter binding sequence that can initiate the expression of antioxidant enzyme genes. The Nrf2/ARE pathway, also known as the antioxidant pathway, plays a critical role in cellular defense against oxidative stress. Nuclear factor erythroid 2-related factor 2 (Nrf2) is a modular protein that contains seven Nrf2-ECH homology domains (Neh1-7), which contribute to the regulation of gene transcriptional activity and stability (Zhang et al., 2021).

The C-terminal Neh1 domain of Nrf2 contains a CNC basic leucine zipper (bZIP)

motif. Nrf2 binds to small musculoaponeurotic fibrosarcoma (sMaf) proteins in the cell nucleus through this CNC-bZIP motif, forming heterodimers, which subsequently bind to the antioxidant response element sequences (AREs) (Meng et al., 2022).

Kelch-like ECH-related protein 1 (Keap1) can bind to the DLG and ETGE motifs of the Neh2 structural domain, which is located closest to the N-terminus (Baird and Dinkova-Kostova, 2011). The Neh3 domain located at the C-terminal region aids transcriptional activation of Nrf2 by binding to chromatin structural domains (Baird and Dinkova-Kostova, 2011).

The Neh7 domain interacts with and modulates retinoid X receptor alpha (RXRα), which in turn influences the regulation of Nrf2 downstream targets. This complex interplay of interactions and regulatory functions underscores the key role of the Nrf2/ARE pathway in maintaining cellular redox homeostasis (Nioi et al., 2005).

Keap1 acts as an adapter for Cul3-Rbx1 mediated ubiquitination of Nrf2. Under homeostatic conditions, the Keap1-Cul3-Rbx1 E3 ubiquitin ligase complex ubiquitinates Nrf2, targeting it for proteasomal degradation, thus keeping the level of Nrf2 in the cells low. However, under conditions of oxidative stress, the interaction between Keap1 and Nrf2 is disrupted, thereby stabilizing Nrf2 and

allowing it to activate transcription of antioxidant response element (ARE)-driven genes. This process is integral for the maintenance of cellular redox balance and protection against oxidative damage. under conditions of oxidative stress, the cysteine residues of Keap1 can undergo modification, which disrupts the ability of Keap1 to facilitate Nrf2 degradation. As a result, Nrf2 becomes stable and accumulates in the cell nucleus. The stabilization of Nrf2 under these conditions allows for the transcription of genes encoding antioxidant proteins and phase II detoxification enzymes, thereby contributing to the maintenance of cellular redox homeostasis and the protection of cells against oxidative damage (Suzuki and Yamamoto, 2015).

In addition to the above, the activation of Nrf2 also involves protein kinase pathways (Meng et al., 2022). Nrf2 is positively regulated via phosphorylation by multiple kinases, including phosphatidylinositol 3-kinase (PI3K), protein kinase C (PKC), c-Jun, N-terminal kinase (JNK), and extracellular signal-regulated kinase (ERK). Furthermore, p38 mitogen-activated protein kinase (MAPK) has been reported to exert both positive and negative regulatory effects on the Nrf2 pathway (Li et al., 2018). These kinases are key mediators in signal transduction pathways that respond to various physiological stimuli and stress signals, and their roles in Nrf2 regulation further emphasize the integral function of Nrf2 in cellular stress response and homeostasis. In a cellular stress environment, p62 protein increases and binds to Keap1, which prevents Keap1-

mediated Nrf2 degradation. Therefore, Nrf2 can be stable and accumulate in the nucleus, which will further increase the expression of its downstream target genes (Zhang et al., 2021).

Once accumulated in the nucleus, Nrf2 can bind to the sMaf protein and form a heterodimer, which can bind to the antioxidant response element (AREs) in the gene promoter region (Kojima et al., 2019). In this way, Nrf2 upregulates the expression of a range of antioxidant and cytoprotective genes, including superoxide dismutase (SOD) and heme oxygenase-1 (HO-1) (Zhou et al., 2016). These proteins have the functions of anti-oxidation, anti-inflammation, and metabolic regulation, thus helping to maintain the health and overall homeostasis of cells (Sun et al., 2020).

Many studies have proved that the expression level of NRF2 is directly related to the susceptibility and severity of COPD disease. A study involving Nrf2 knockout mice conducted by Cho and Kleeberger (2014) unveiled some compelling findings. This study observed an augmented susceptibility in the knockout mice to inflammation and epithelial cell injury within the lungs when compared to their wild-type counterparts. Another study also found (Rangasamy et al., 2004) that Nrf2-deficient mice were more susceptible to cigarette smoke and developed more severe emphysema. The researchers found that Nrf2 deficiency leads to a variety of respiratory diseases, including respiratory

infection, acute respiratory distress syndrome (ARDS), COPD, bronchial asthma, idiopathic pulmonary fibrosis (IPF) and lung cancer, and activation of Nrf2 has a protective effect on these lung diseases (Cho and Kleeberger, 2014).

It is worth noting that the Nrf2 and PPAR γ signaling pathways often coordinate and synergize in their antioxidant and anti-inflammatory effects, regulating each other by enhancing their respective expression. The promoter regions of PPAR γ contain ARE (antioxidant response element) domains, which can be directly transcriptionally regulated by Nrf2. The protective effect of acute lung injury in mice requires Nrf2-mediated regulation of PPAR γ expression. Additionally, PPAR γ agonists can induce the transcription of a set of antioxidant genes, such as GST, HO-1, and CD36 genes, because these genes are also regulated by Nrf2 as its target genes. These findings strongly suggest that PPAR γ can also directly regulate the Nrf2 pathway. Further research has revealed that PPAR γ can directly bind to the promoter region of Nrf2 and exert a positive regulatory effect on its expression. Studies involving PPAR γ knockout mice have shown a decrease in Nrf2 expression, indicating the involvement of PPAR γ in the regulation of Nrf2 (Cho et al., 2010; Lee, 2017).

2.5 COPD and Efferocytosis

Apoptosis, also known as programmed cell death, is a major form of cell death in physiological and pathological processes such as tissue and organ

development, cellular renewal, and disease progression. In the human body, billions of cells undergo apoptosis every day. The clearance of apoptotic cells by phagocytes, primarily macrophages, through a process called efferocytosis, is an essential step in maintaining tissue homeostasis (Boada-Romero et al., 2020).

The process of eliminating apoptotic cells by phagocytes is efferocytosis (Doran et al., 2020). Since the pioneering work by Henson and Bratton (2013), which first demonstrated that efferocytosis can generate an active anti-inflammatory response, the relationship between cell apoptosis, efferocytosis, and inflammatory reactions has been a subject of considerable interest. The maintenance of homeostasis depends on the apoptosis of senescent cells and the production of new cells. The body clears about 1% of its body weight every day to maintain homeostasis (Doran et al., 2020).

Under the efficient operation of cell efferocytosis, there are few free apoptotic cells in the inner ring (Trzeciaketal., 2021). A complete and efficient efferocytosis process plays a crucial role in the timely clearance of apoptotic cells from the body, contributing to the maintenance of normal physiological homeostasis and the restoration of homeostasis during disease states (Trzeciaketal., 2021).

This vital role of efferocytosis has been highlighted in the study by Ge and team

(2022). When efferocytosis is impaired, many apoptotic cells cannot be promptly cleared and accumulate within the body. This can lead to secondary necrosis, where the cellular membrane ruptures and releases cellular contents, including damage-associated molecular patterns (DAMPs). The presence of these cellular content's triggers inflammation and immune responses, contributing to the development of chronic inflammatory diseases and autoimmune disorders (Morioka et al., 2019). Following the initiation of apoptosis, cellular morphological changes occur which involve the externalization of phosphatidylserine (PtdSer), signaling an "eat me" message to the surrounding environment. The distribution of phospholipid molecules between the inner and outer bilayers of the cell membrane differs.

In healthy, live cells, ptdSer and phosphatidylethanolamine predominantly localize to the inner leaflet of the bilayer, while phosphatidylcholine and sphingomyelin are mostly situated within the outer leaflet (Sakuragi et al., 2019). In contrast, in apoptotic cells, PtdSer mainly surfaces on the cell exterior. PtdSer can directly bind to various phosphatidylserine receptors on the surface of phagocytic cells and be recognized. Following the recognition of the "eat me" signal from apoptotic cells, phagocytic receptors on the surface of macrophages, such as T-cell immunoglobulin and mucin-domain containing-4 (TIM-4), Brain-specific angiogenesis inhibitor 1 (BAI1), and Tyro3, Axl, and Mer (TAM) receptors, gather towards the apoptotic cells. Subsequent to this, cytoskeletal

rearrangements occur. The engulfment of apoptotic cells is then mediated by soluble bridging molecules including C1q, C3b, mannose-binding lectin (MBL), Milk Fat Globule-EGF Factor 8 Protein (MFG-E8), and Growth Arrest-Specific 6 (Gas6) (Roszer, 2017, Grabiec and Hussell, 2016, He et al., 2011).

In some circumstances, the absence of phagocytic cells in the vicinity of certain tissues necessitates the recruitment of these cells to the site of apoptotic cells via "find me" signals. To date, four representative "find me" signals have been identified: lysophosphatidylcholine (LPC), sphingosine-1-phosphate (S1P), the chemokine CX3CL1 (fractalkine), and nucleotides ATP and UTP (Elliott and Ravichandran, 2016). These apoptotic signaling molecules are transported to macrophages planted in their vicinity via extracellular fluid, or through the blood circulation to monocytes in tissues such as the bone marrow and spleen.

Following this, these signals are recognized by their respective receptors on the surface of the phagocytic cells: the G2A family of G-protein-coupled receptors (G2A), the sphingosine-1-phosphate receptor (S1PR), the chemokine receptor CX3CR1, and the P2Y family of G-protein-coupled receptors (P2Y). Consequently, phagocytic cells are chemotactically directed to the tissue area where the apoptotic cells are located, thus completing the recruitment process (Park and Kim, 2017). Simultaneously, apoptotic cells also secrete "keep out" signals to repel the recruitment of other inflammatory cells such as granulocytes,

thereby achieving the goal of selectively chemotaxing monocytes and macrophages.

Lactoferricin is currently the only well-understood "keep out" signal (Bournazou et al., 2009). Although PtdSer is one of the significant markers of apoptotic cells, a minority of live cells under certain physiological conditions may also display externalized PtdSer. These live cells primarily suppress macrophage-mediated clearance of themselves via the interaction between "do not eat me" signals on their surface, such as CD47 and CD31, and the corresponding receptor molecules on the macrophage surface (Lemke, 2019). After the "eat me" signal binds to the receptor on the surface of the phagocytic cell, the engulfment of the apoptotic cell is mediated by the activation of the RHO family of small GTPases (Lemke, 2019).

For instance, when PtdSer on the surface of apoptotic cells binds with the phagocytic receptor ADGRB1, it promotes the assembly of the engulfment and cell motility protein 1 (ELMO1) and the dedicator of cytokinesis protein 1 (DOCK180) complex. Subsequently, the small GTPase RAC1 is activated (Szondy et al., 2014). The activated RAC1 promotes the aggregation of actin in phagocytic cells and the rearrangement of the cytoskeleton, forming a "phagocytic cup" around the apoptotic cell. The engulfment of apoptotic cells results in the formation of phagosomes (Szondy et al., 2014, Tan Haipeng, 2020).

The fusion and acidification of lysosomes with these phagosomes result in the formation of phagolysosomes. Once mature, the phagolysosomes begin to degrade the internalized apoptotic cells. Multiple metabolic signaling pathways and auto degradation pathways are activated to digest or redistribute excessive intracellular nucleic acids, proteins, and lipids.

Alveolar macrophages are the most abundant and functionally significant professional phagocytes in lung tissue. Current understanding suggests that a dysfunction in the efferocytosis role of alveolar macrophages is a major factor contributing to the exacerbation of COPD (Zheng et al., 2021). Alveolar macrophages are the most numerous and most functionally significant phagocytic cells within lung tissue. Presently, it is believed that the impairment in the function of efferocytosis of alveolar macrophages is a principal cause in the aggravation of COPD (Zheng et al., 2021).

In patients with COPD, both the clearance of bacteria by macrophages and their efferocytosis function, which is the process of removing cell debris and dead or apoptotic cells, are diminished. This leads to an accumulation of necrotic material in the lungs, which in turn perpetuates inflammation and affects the progression of the disease (McCubbrey and Curtis, 2013). Macrophages, under the influence of various local microenvironment stimuli, eventually differentiate into either classically activated macrophages (also known as M1) or alternatively

activated macrophages (M2).

In healthy lungs, most alveolar macrophages are neither M1 nor M2. However, with the progression of disease, macrophage polarization occurs, and an imbalance in the polarization of M1/M2 macrophages may have detrimental effects on the onset and progression of COPD. M1 macrophages exert autoimmunity by producing reactive oxygen species (ROS) and nitric oxide (NO), and they enhance the function of TH1 cells by secreting pro-inflammatory mediators such as interleukin-12 (IL-12) and tumor necrosis factor-alpha (TNF-α).

M1 macrophages can strengthen the phagocytosis of pathogenic microorganisms, antigen presentation, and the secretion of matrix metalloproteinases (MMPs), thereby exacerbating tissue damage (Biswas and Mantovani, 2010, Hanania et al., 2012). On the other hand, M2 macrophages primarily produce anti-inflammatory cytokines such as interleukin-10 (IL-10) and lesser amounts of pro-inflammatory cytokines such as IL-12 (Italiani and Boraschi, 2014). They suppress T cell proliferation and activity, activate tissue repair programs, and inhibit immune responses (Gordon and Martinez, 2010).

Research shows that smoking can cause M1 macrophages to release a variety of inflammatory mediators, such as tumor necrosis factor-alpha (TNF-α) and

interleukin-8 (IL-8). These factors participate in the formation of COPD and can damage lung structure and promote inflammatory responses (Sarir et al., 2010). In the research conducted by He and team (2017a), it was found that with the development of smoking and COPD, the proportion of M1 macrophages increases with the severity of the disease. At the same time, it was found that smoking is a crucial factor in the polarization of M1 macrophages. The increase in M2 macrophages may reflect a deficiency in the normal process of eliminating inflammation and repairing the stability of the pulmonary environment.

Earlier literature reported, smokers were found more polarization of M2 macrophages and individuals with COPD (Bazzan et al., 2017). The polarization level of M2 macrophages in the lungs of smokers is higher than that in non-smokers.

It is worth noting that some reports suggest that upon activation, the PPAR γ receptor can promote the polarization of macrophages towards M2 through its interaction with the JAK1-STAT6 pathway (Odegaard et al., 2007, Szanto et al., 2010). The specific mechanism remains a subject for further research. PPAR γ is also involved in macrophage efferocytosis (Croasdell et al., 2015). The deficiency of PPAR γ can decrease the rate at which macrophages clear apoptotic cells. Nrf2 plays a similar role. Chen Qixian and colleagues (2018) found through animal experiments that the activation of the Nrf2/ARE pathway

reduces the decrease in the phagocytic capacity of lung macrophages caused by

cigarette smoke and provides a protective effect against oxidative stress. See

figure 1.
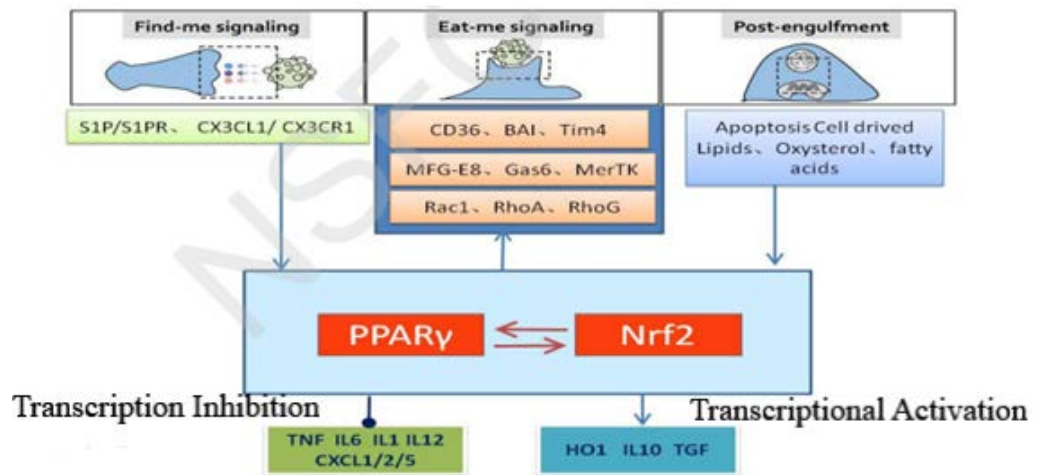
Figure 1. The Regulatory Role of the PPARγ/Nrf2 Signaling Pathway in

Macrophage efferocytosis

2.6 COPD and Bufei Yishen Prescription

COPD falls within the category of "Lung syndrome" and "dyspnea Syndrome"

in TCM (WHO, 2022). In the acute exacerbation stage, the pathogenesis

primarily involves "syndrome of phlegm turbidity obstructing the lung" and

"phlegm syndrome", accompanied by "both qi and yin deficiency" (Li Jiansheng,

2011; WHO, 2022). The pathological changes are characterized by "interior

deficiency" with excessive "exterior symptoms" (Li Jiansheng, 2011; WHO,

2022).

Lung qi deficiency is the root cause of the occurrence and progression of COPD, with "blood stasis" and "phlegm turbidity" as the superficial symptoms. The treatment should address both root cause and superficial symptoms, primarily by replenishing the "deficiency of Lung qi" and treating "phlegm turbidity" and "blood stasis" (Wang Chuanbo et al., 2013; WHO, 2022).

Based on the main clinical manifestations of COPD, modern physicians categorize it as "pulmonary distension" and other related terms. The term "pulmonary distension" first appeared in the book "Ling Shu: Zhubing" and described it as "hollow fullness accompanied by wheezing and coughing." During the Eastern Han Dynasty, Zhang Zhongjing mentioned in the book "Shang Han Za Bing Lun" in his work "Jin Kui Yao Lue" that the course of pulmonary distension is prolonged. Factors such as wind and cold can worsen the condition, and recurrent and persistent respiratory symptoms, such as cough, are important causes of pulmonary distension.

During the period of the Southern and Northern Dynasties and Jin Dynasties, various physicians further deepened their understanding of the pathogenesis of pulmonary distension. They believed that both deficiency and excess patterns coexist in pulmonary distension and emphasized the important role of blood stasis in its development. The book "Zhen Jiu Jia Yi Jing" states that the treatment principle for pulmonary distension is to "tonify deficiency and purge

excess". In the development of medical knowledge during the Sui, Tang, and Five Dynasties, important insights and contributions were made regarding the staging of pulmonary distension. The theory of "pulmonary deficiency with cold invasion" was proposed, and it was recognized that excessive lung qi and re-exposure to external cold are among the causes of pulmonary distension.

During the Sui Dynasty, Chao Yuanfang's "Zhu Bing Yuan Hou Lun" described the pathogenesis of pulmonary distension as follows: "It is formed by the invasion of subtle cold on lung deficiency, where cold attacks the qi, obstructing its dispersion. The stomach counterflows and gathers into the lungs, resulting in distension and fullness of the lungs. The rebellious qi cannot descend, hence causing cough and counterflow." "When the lungs are weak and damaged by slight cold, it leads to coughing. As one coughs, the qi stagnates within the lungs, causing them to swell. This swelling then results in the reversal of qi. Given the intrinsic deficiency of the lungs and the insufficiency of qi, the lungs become an easy target for pathogens, leading to obstructions and congestion that prevent smooth circulation. This is the cause of cough, reverse flow of qi, and shortness of breath." "Pulmonary deficiency" is considered the fundamental factor in the development of pulmonary distension, while "subtle cold invasion" acts as a triggering factor that exacerbates the condition. The understanding of staging of pulmonary distension is reflected in the notion that "when the pathogenic factors are dormant, the qi remains calm; when the pathogenic factors are active, the qi

rushes upwards."

Physicians Sun Simiao and Wang Tao of the Tang and Song dynasties summarized and elaborated on the pathogenesis of pulmonary distension based on previous theories. They also described the staging of pulmonary distension. The "Tai Ping Sheng Hui Fang" states: "When phlegm and fluid accumulate and stagnate, causing wheezing and shortness of breath, constant coughing day and night." It indicates that phlegm and fluid stagnation are the reasons for the inability to lie down in cases of pulmonary distension.

During the Yuan Dynasty, Zhu Zhenheng further developed the understanding of the pathogenesis of pulmonary distension and proposed the concept that "phlegm, accompanied by stasis of blood, obstructs qi and causes disease." The treatment approach should focus on "nourishing the blood to promote qi flow and clearing fire from the liver to resolve phlegm."

In the Ming Dynasty, physician Zhao Xianke's "Yi Guan, Chuan Lun" supplemented the clinical manifestations of pulmonary distension, including "early-onset shortness of breath, distension and fullness in the flanks, and a large but weak left pulse." Li Zhongzi in "Yi Zong Bi Du" pointed out, "Even though recovery is achieved today, it should not be taken for granted. Ginseng and Astragalus should be used to nourish and support the vital energy, facilitating the

clear and solemn qi to descend."

According to TCM, the main pathogenesis of COPD involves the upward reversal of lung qi, dysfunction of lung dispersing and descending, qi stagnation in the lung, and distension and fullness of lung qi. The disease mechanism is primarily attributed to long-standing lung deficiency, chronicity with inadequate treatment, impairment of lung dispersing and descending functions, retention of phlegm and turbidity, obstruction of lung qi, and abnormal lung qi ascending and descending, which results in stagnation in the lung. The pathological factors of COPD mainly involve phlegm turbidity, water accumulation, and blood stasis, which can coexist or transform into one another. Thus, the pathological changes manifest as a combination of deficiency and excess, with phlegm turbidity, water accumulation, and blood stasis representing the excess aspect, while lung, spleen, and kidney deficiencies are the underlying deficiency factors (Yu Shupeng, 2017; Pan Xia, 2020; Li Yuyu, 2016).

In TCM, the lung corresponds to the skin and hair, governs qi, and manages respiration. When lung qi is impaired, external defenses are weakened, rendering the body susceptible to recurrent external pathogenic attacks, triggering the onset of the disease. Hence, during the progression of COPD, the acute phase is primarily characterized by excess symptoms, whereas the stable phase is marked by deficiency symptoms. This aligns with the tenet in "Zhu Bing Yuan Hou Lun,

Shang Qi Ming Xi Hou", which states: "The lung governs qi. When pathogens invade the lungs, the lungs become distended. When distended, the lung meridian is impeded, causing difficulty in the qi pathway, hence the ascension of Qi and the symptom of wheezing." Dan Xi Xin Fa Ke Sou": "When the lungs are distended, coughing ensues, and the patient cannot sleep, either on the left or the right side. This is the disease of phlegm and blood stasis obstructing qi." In terms of treatment, depending on the urgency of the disease manifestation, methods such as eliminating pathogenic factors, promoting lung qi, descending qi, resolving phlegm, strengthening the spleen, and nourishing the kidneys are adopted.

Modern TCM generally adheres to this line of thought in treatment and has also developed upon this foundation. Chen Jingjing and Zhang Nianzhi (2019), through reviewing literature, believe that the disease is fundamentally caused by qi deficiency, with phlegm-stasis as a manifestation. The interaction between phlegm-dampness and blood stasis is a key pathological link in the pathogenesis of COPD. Following the "nourishing the root to cultivate the origin" principle, they propose therapeutic methods of enhancing qi to strengthen the body's foundation and promoting blood circulation to resolve phlegm.

In TCM, "Zheng Xu" refers to the deficiency and insufficiency of qi, yin, and yang in the lung, spleen, and kidney, which leads to the inability to resist external

pathogenic factors. The symptoms of COPD, including decreased lung function and immune function, align with the theory of "Zheng Xu." TCM concept of "Ji Sun" refers to the accumulation of pathogenic factors such as phlegm turbidity, blood stasis, and water retention. The excessive mucus secretion, lung fibrosis, bronchial narrowing, and symptoms of pulmonary emphysema in COPD correspond to this theory.

Based on this, the treatment principle of "Fu Zheng Qu Ji" is proposed. "Fu Zheng" focuses on nourishing the lung, kidney, qi, yin, and yang, improving immune function and lung function. "Qu Ji" aims to promote blood circulation, resolve blood stasis, dissolve phlegm, disperse nodules, and alleviate symptoms of lung emphysema and lung tissue damage.

Bufei Yishen prescription decoction is composed of 12 medicinal herbs including tonifying herbal medicines: Ginseng Root 9g, Mongolian Milkvetch Root 15g, Babury Wolfberry Fruit 12g, Common Macrocarpium Fruit 9g, Short-horned Epimedium Herb 9g, Chinese Magnoliavine Fruit 9g; Phlegm-dispelling herbal medicines: Chekiang Fritillary Bulb 9g, Cultibated Purple Perilla Leaf 9g, Tangerine Peel 9g; Blood-activating herbal medicines: Red Paeoniae Trichocarpae 12g, Earthworm 12g, , Liquorice Root 6g (Chinese Medicinal Material Images Database, 2016). It has the functions of tonify lung replenish kidney, activate blood, resolve phlegm, dispel stasis (WHO 2022).

In this prescription, Ginseng serves as the monarch herb to nourish the primal qi, while Zhi Huangqi supplements qi, raises yang, and stabilizes the exterior. Jiu Zhuru, Gouqizi, Cu Wuweizi, and Zhi Yinyanghuo nourish both the lung and kidney yin and yang. Zhe Beimu, Chao Zisuzi, and Chishao help transform phlegm and disperse nodules, while Chishao and Dilong promote blood circulation, resolve stasis, and activate meridians. Aidi Cha (Lowland Tea) is included to relieve cough and alleviate wheezing.

When these herbs are combined, the prescription primarily focuses on "Fu Zheng" (supporting the body's righteous qi) while "Qu Ji" (dispelling accumulation) serves as an auxiliary function. Together, they contribute to the nourishment of the lungs and kidneys, blood circulation, resolution of stasis, transformation of phlegm, dispersal of nodules, relieving cough, and alleviating wheezing.

Clinical studies have found that Bufei Yishen prescription can improve lung function, alleviate clinical symptoms, improve quality of life, delay disease progression, and reduce the frequency of COPD exacerbations in patients (Li et al., 2012; Li et al., 2013b; Li et al., 2016).

Experimental research has shown that Bufei Yishen prescription can modulate oxidative stress and airway inflammation in COPD animal models through

multiple pathways. It can suppress the secretion of inflammatory factors such as IL-4, IL-6, and TNFα, improve lung pathology and function, and ameliorate side effects such as muscle atrophy, fatigue, and depression (Li et al., 2016; Li et al., 2021b; Wu et al., 2020). The efficacy of the Bufei Yishen prescription in treating stable COPD is significant.

Results from in vitro studies revealed that the BuFei YiShen formula in the blood serum had a certain regulatory effect on inflammatory factors and metalloproteinases induced by lipopolysaccharides and/or cigarette smoke extract (Wu Yaosong et al., 2013; Chen Yulong et al., 2013). It also reduced the levels of reactive oxygen species and elastase (Qin Yanqin et al., 2016).

Li Jiansheng et al (2015) employed a systematic pharmacological approach, integrating transcriptomics, proteomics, and metabolomics, to identify 216 active compounds in the BuFei YiShen prescription related to the treatment of COPD. They predicted a total of 195 potential therapeutic targets and analyzed the underlying mechanisms of action (Li Jiansheng, 2015).

Building upon this, key pathological processes were assessed using cellular inflammation models and hypoxia models to evaluate the pharmacological activities of key effective components, including anti-inflammatory effects, regulation of oxidative stress, and improvement of endothelial damage (Li

Jiansheng, 2016). Additionally, the proportions of these effective components were determined through orthogonal design experiments (Li Jiansheng, 2016). Based on the COPD rat model and considering efficacy, safety, and cost-effectiveness, a refined selection process identified representative components from qi tonifying herbal medicines, including Panax ginseng extract, Astragaloside IV; from Kidney-tonifying herbal medicines, Epimedium brevicornum glycoside; from Phlegm-dispelling herbal medicines, Citrus reticulata peel extract; and from Blood-activating herbal medicines, Paeoniflorin. These components were combined to form the preliminary BuFei YiShen prescription, which was evaluated for its therapeutic effects on COPD mice (Li Jiansheng, 2016).

Finally, it was optimized to form the BuFei YiShen prescription consisting of ginsenoside Rh1, Astragaloside IV, Icariin, Citrus reticulata peel extract, and Paeoniflorin (Li Jiansheng, 2018). Patent number: 201811115372.3.

The substance basis for the pharmacological effects of traditional Chinese medicine is generally not a single or two monomers but a combination of multiple components working synergistically. The same component may have different effects on different research subjects (Tao Li et al., 2013). The study has shown that the effective components of ginseng and red peony, such as ginsenosides and paeoniflorin, can reduce the levels of inflammatory factors in

the LPS-induced co-culture inflammation model of alveolar epithelial cells/macrophages (Qin Yanqin et al., 2017). The study found that ginsenoside Rh1 improves lung tissue pathology, inhibits the expression of pro-inflammatory factors, and regulates immune responses in a mouse model of asthma (Zhang Chunjing et al., 2018). Ginsenoside Rg1 possesses extensive antioxidant and anti-inflammatory properties (Gao Y et al., 2017). Icariin can inhibit TNF-α/IFN-γ-induced human keratinocyte inflammatory response by regulating the P38/MAPK pathway (Kong Lingwen et al., 2015). The study found that icariin has a protective effect on LPS-induced acute lung injury, and it is associated with the regulation of the PI3K/Akt and NF-κB pathways (Xu Changqing et al., 2010). Both in vivo and in vitro experiments have shown that Citrus reticulata peel extract has a significant anti-inflammatory effect and effectively improves inflammation and extracellular collagen deposition induced by high glucose (Liu Zhenzhou, et al., 2019; Li Weifeng et al., 2018). Paeoniflorin can reduce the expression of inflammatory factors in vascular endothelial cells, decrease the adhesion between endothelial cells and monocytes, and alleviate asthma in mice by regulating the TLR4/NF-κB MAPK signaling pathway (Liu Yarong et al., 2018; Tang Yongjun et al., 2018).

Clinical research evidence showed that BuFei YiShen prescription has good effects in improving symptoms and signs, reducing acute exacerbations, improving lung ventilation function, enhancing exercise capacity, and improving

quality of life in treating COPD (Haifeng et al., 2015; Li JIansheng et al., 2014; Li Jiansheng et al., 2013). Based on the results of randomized controlled clinical studies for COPD treatment, it has been demonstrated that the Bufei Yishen prescription can significantly improve lung function, alleviate clinical symptoms such as coughing, phlegm, shortness of breath, and chest tightness, enhance immunity, and reduce the frequency of acute COPD exacerbations.

Furthermore, this prescription can lower extracellular matrix levels, regulate collagen metabolism, alleviate airway remodeling, and decrease adhesion factors, inhibiting the activation of inflammatory cells and the release of inflammatory mediators, thus reducing chronic airway inflammation during the stable phase of COPD (Li Suyun et al., 2003, Li Suyun et al., 2003).

Additionally, Bufei Yishen prescription can reduce PGE2, elevate SOD3 and PPAR γ expression, significantly improve the oxidative stress state of COPD, decrease MMP-2, MMP-9, and TIMP-1 mRNA in COPD lung tissue, and significantly correct lung collagen and protease markers (Tian Yange et al., 2018, Tian Yange et al., 2013).

It is also worth noting that Bufei Yishen prescription can regulate the Nrf2 signaling pathway to improve lung inflammation in COPD, but the specific mechanism is not yet clear (Zhang Lanxi et al., 2020).

However, the pathogenesis of COPD involves a wide range of factors, and the target and mechanisms of action of the Bufei Yishen prescription require further in-depth research.

In summary, Bufei Yishen prescription can alleviate the inflammatory response and oxidative stress in COPD, and can regulate multiple signaling pathways, including PPAR γ. It can also inhibit the secretion of macrophage inflammatory factors induced by lipopolysaccharides or cigarette smoke and activate the PPAR γ signaling pathway (Li Chenxu, 2020).

The efferocytosis function of macrophages plays a crucial role in terminating inflammatory responses, and impairment of macrophage efferocytosis is observed in COPD. Oxidative stress and cigarette smoke are the main factors contributing to this impairment (Li Chenxu, 2020).

PPAR γ and Nrf2 signaling pathways are key regulators of oxidative stress and inflammatory responses. They are closely associated with the occurrence and progression of COPD and regulate macrophage efferocytosis function. Furthermore, there is an interplay between PPAR γ, Nrf2 signaling pathways, and macrophage efferocytosis in COPD.

Based on this, we hypothesized that the disturbance of PPAR γ, Nrf2 signalling pathway are an important mechanism of COPD macrophage efferocytosis, and Bufei Yishen prescription may play a role in the treatment of COPD by regulating PPAR γ / Nrf2 signal pathway crosstalk regulation. Based on this, further research can be conducted to elucidate the molecular mechanisms of Bufei Yishen prescription in the treatment of COPD by regulating the PPAR γ and Nrf2 signaling pathways to improve macrophage efferocytosis function. In this experiment, COPD mice can be used as the experimental subjects to evaluate the therapeutic efficacy of the Bufei Yishen prescription through assessments of lung function, lung pathology, inflammatory factors, etc.

Additionally, the efferocytosis capacity of alveolar macrophages, apoptosis of alveolar epithelial cells, phenotypic changes of alveolar macrophages, and the expression of the PPAR γ/Nrf2 pathway can be investigated to explore the mechanisms underlying the therapeutic effects of Bufei Yishen prescription. This research will provide a basis and evidence for further scientific and clinical applications.

CHAPTER 3.0：Material and Methodology

3.1 Experimental materials
3.1.1 Experimental animals

SPF-grade C57BL/6 mice, 120 in total, with an equal distribution of males and females, aged 6-8 weeks, weighing 18-20g. The animals were provided by Jinan Pengyue Experimental Animal Breeding Co., Ltd. (License number: SCXK (Lu) 20140007). This study was approved by the Ethics Committee for Animal Welfare of the Henan University of Traditional Chinese Medicine. Number: DWLL2018030047.

3.1.2 Cigarettes

Red Flag Canal brand filtered cigarettes (flue-cured tobacco cigarettes) produced by Henan Zhongyan Industrial Co., Ltd. The cigarettes have a tar content of 10mg, nicotine content in smoke of 0.8mg, and carbon monoxide content in smoke of 12mg.

3.1.3 Cells

LLC cells, purchased from the Kunming Cell Bank of the Chinese Academy of Sciences. The cell bank number is KCB20781YJ.

3.1.4 Major experimental instruments

Table 1.1: Major experimental instruments

Experimental instruments Name	Brand
IVC- II animal rearing cage	Feng's Experimental Animal Equipment Co., Ltd.
Electronic balance	Shanghai Jingke Tianmei Scientific Instrument Co., Ltd.
Non-restraint small animal pulmonary function measurement system	BUXCO, Inc. (United States)
M2145 automatic microtome	Leica GmbH (Germany)
Enzyme-linked immunosorbent assay (ELISA) reader	BIO-TEK Instruments, Inc.
High-speed centrifuge	Thermo Fisher Scientific Inc. (United States)
Thermostatic incubator	Shanghai Jinghong Experimental Equipment Co., Ltd.
Vortex mixer	Changzhou Guotai Experimental Equipment Research Institute
Pipette	Eppendorf AG (Germany)

Thermostatic water bath	Shanghai Jinghong Experimental Equipment Co., Ltd.
Ultra-low temperature freezer	REVCO Value (Thermo Fisher Scientific Inc., United States)
OLYMPUS-DP70 microscope and microscopy imaging system	Olympus Corporation (Japan)
Micropipette	Eppendorf AG (Germany)
Super clean workbench	Sujing Group Antai Company
Carbon dioxide incubator	Thermo Fisher Scientific Inc. (United States)
Centrifuge machine	Thermo Fisher Scientific Inc. (United States)
Inverted microscope	Leica GmbH (Germany)
LDZM vertical pressure steam sterilizer	Shanghai Shen'an Medical Equipment Factory
Decolorizing shaker	Changzhou Guotai Experimental Equipment Research Institute

600L liquid nitrogen biological container	CBS Corporation (now Viacom CBS Inc.)
Vacuum pump	Henan Gongyi Yingyu Huazhong Instrument Factory
Flow cytometry	BD (Becton and Dickinson Company)

3.1.5 Major Experimental reagent

Table 1.2: Major Experimental reagent

Experimental reagent Name	Brand	Batch/Lot Number
Mouse IL-4 ELISA Kit	BoShiDe Biotech Co., Ltd.	12715961010
Mouse TNFα ELISA Kit	BoShiDe Biotech Co., Ltd.	24115991010
Phosphate buffer (PBS)	Beijing Solarbio Science & Technology Co., Ltd.	20191116
DMSO (dimethyl sulfoxide)	Beijing Solarbio Science & Technology Co., Ltd.	20190124
neutral formaldehyde	Yantai Shuangshuang Chemical Co., Ltd.	20180501
physiological saline	Henan Kelun Pharmaceutical Co., Ltd.	C119060401-2

Filtered cigarettes	Henan Zhongyan Industrial Co., Ltd.	MKCD9167
1640 Medium	Beijing Solarbio Science & Technology Co., Ltd.	20181130
DMEM (Dulbecco's Modified Eagle Medium)	Beijing Solarbio Science & Technology Co., Ltd.	20190924
Trypsin-EDTA digestion solution	Beijing Solarbio Science & Technology Co., Ltd.	20191024
fetal bovine serum	GEMINI	A79E00G
0.4% Trypan Blue	Beijing Solarbio Science & Technology Co., Ltd.	20180803
4% tissue cell fixative	Beijing Solarbio Science & Technology Co., Ltd.	20191118
Annexin V-FITC/PI	Hangzhou Lianke Biotechnology Co., Ltd.	A80010633
apoptosis kit	Hangzhou Lianke Biotechnology Co., Ltd.	A80010633
PKH26 Cell Linker Kit	Mackon Biotech Co., Ltd.	1012X18469

Terminal deoxynucleotidyl transferase dUTP nick end labeling	Bausch Biotechnology Co., Ltd.	14I07G11H2125
Anti-CD68 Antibody	Beijing Biocoen Biotechnology Co., Ltd.	AH10298081
Anti-NOS2/INOS Antibody	Beijing Biocoen Biotechnology Co., Ltd.	AH04138902
CD163 Antibody	Beijing Biocoen Biotechnology Co., Ltd.	AH12066875
Nrf2 Antibody	Beijing Biocoen Biotechnology Co., Ltd.	AI06112504
PPAR γ Antibody	Beijing Biocoen Biotechnology Co., Ltd.	AD03031245
Rabbit IgG Immunohistochemistry Kit	Bausch Biotechnology Co., Ltd.	13I10C26H1622
ML385	GLPBIO	QC19254
Dimethyl fumarate	MedChemExpress (MCE)	14148
GW9662	Med Chem Express (MCE)	HY-16578

| Pioglitazone | Med Chem Express (MCE) | 33584 |

3.2 Experimental method
3.2.1 Mice Feeding

The mice were housed in individual cages with a maximum capacity of 5 animals per cage as per the standard mice husbandry guidelines. The cages were maintained on a weekly basis, with water and bedding material being changed every week. The diet was replenished every two days. Temperature and humidity of the animal housing environment were monitored daily at 8 AM and 6 PM. Mice were housed in a specific pathogen-free facility with ad libitum access to food and water for one week prior to the formal experiment. The behavior and overall health status of the mice were observed and recorded during every check. The mice feed was purchased from the Henan Medical Experimental Animal Center.

3.2.2 Mice modeling

After one week of acclimatization and when the mice were in a stable condition, they were numbered, and 12 mice were randomly selected for the blank control group (CT) using a random number table method. The remaining mice (108 mice) were utilized to establish a COPD model using a cigarette smoke exposure method (Li Ya et al., 2012). The experimental setup included a

smoking rack (175×60×160 cm), Red Flag Canal brand cigarettes, and PE plastic film. The modeling process lasted for 8 weeks, with smoking conducted on 6 days per week. Each day, the mice were exposed to cigarette smoke twice, with a 3-hour interval between exposures (Li Ya et al., 2012).

During the smoke exposure, the mice cages were placed on the smoking rack and sealed with PE plastic film. A total of 25 cigarettes were ignited, and the smoke was allowed to fill the chamber for 40 minutes. A thermometer was placed on the smoking rack to monitor the temperature, which was maintained at 26℃ throughout the exposure period. After the smoke exposure, the mice were kept stable for 30 minutes and then returned to the animal facility (Li Ya et al., 2012).

3.2.3 Preparation of Mice Drug

The preparation of Nrf2 agonist (Dimethyl fumarate): the dosage of Dimethyl fumarate was 50 mg/kg/day, and 100mg Dimethyl fumarate was dissolved with 0.8 mL DMSO every week. After being fully dissolved, the volume was fixed to 16 mL. The final concentration of Dimethyl fumarate was 6.25 mg/mL, stored at 4 ℃.

Preparation of specific Nrf2 inhibitor (ML385), formula :$C_{29}H_{25}N_3O_4S$:   the dosage of ML385 was 30 mg/kg/day, the 64mg ML385 was dissolved with 320

μl DMSO per week, and the final concentration was 4 mg/ml (volume fraction of DMSO < 5%) at 4 °C.

PPAR γ agonist (Pioglitazone): the dosage was 10 mg/kg/day, the 20 mg Pioglitazone was dissolved with 320ul DMSO, then the volume was fixed to 16 mL with normal saline, and the final concentration was 1.25mg/ml (volume fraction of DMSO < 5%), stored at 4 °C.

PPAR γ inhibitor (GW9662), formula :$C_{13}H_9ClN_2O_3$: the dosage was 1 mg/kg/day, the 6 mg GW9662 was dissolved with 1.44ml DMSO, then the volume was fixed to 48 mL with normal saline, and the final concentration was 0.125mg/mL (volume fraction of DMSO < 5%), stored at 4 °C.

Bufei Yishen prescription decoction: Ginseng Root 9 g, Mongolian Milkvetch Root 15 g, Babury Wolfberry Fruit 12 g, Common Macrocarpium Fruit 9 g, Short-horned Epimedium Herb 9 g, Chinese Magnoliavine Fruit 9 g, Chekiang Fritillary Bulb 9 g, Cultibated Purple Perilla Leaf 9 g, Tangerine Peel 9 g, Red Paeoniae Trichocarpae 12 g, Earthworm 12 g, Liquorice Root 6 g (Chinese Medicinal Material Images Database, 2016).

The dosage was 5.34 g/kg/day, which was prepared once a week. Bufei Yishen prescription was prepared in advance by weighing 10g each time, and it was

dissolved in physiological saline of 20 mL. At this time, the final concentration of the Bufei Yishen prescription was 0.5 g/mL, and then stored in the refrigerator at 4 ℃.

After weighing the body weight every Monday, the weekly dosage for the current week was calculated using the equivalent dose conversion formula.

$D_{mice} = D_{human} \times (HI_{mice} / HI_{human}) \times (W_{mice} / W_{human})^{2/3}$. D: dosage, HI: Human to Mice Index, W：weight (Tian Yange, 2015).

Provided and identified by the National Traditional Chinese Medicine Administration Level Three Laboratory for Chinese Medicine Preparations, First Affiliated Hospital of Henan University of Traditional Chinese Medicine.

3.2.4 Mice administration

After the establishment of the model, the mice were randomly divided into model group (M, 12 mice), PPAR γ agonist group (PA, 12 mice), PPAR γ inhibitor group (PI, 12 mice), Nrf2 agonist group (NA, 12 mice) and Nrf2 inhibitor group (NI, 12 mice). Bufei Yishen prescription group (BYF, 12 mice), Bufei Yishen prescription combined with PPAR γ inhibitor group (BPI, 12 mice), Bufei Yishen prescription combined with Nrf2 inhibitor group (BNI, 12 mice), Bufei Yishen prescription combined with PPAR γ and Nrf2 inhibitor group (BPNI, 12 mice)

There were 12 mice in each group. Mice in each group were given corresponding drugs once a day, 6 times a week for 4 weeks.

Gavage method: Hold the tail of the mouse with one hand, and with the other hand, pinch the skin on the back of its neck with the thumb and forefinger to stretch the head and neck, aligning the head, neck, and body in a straight line. Connect a 1 mL syringe to the mouse gavage needle and pass the tip of the gavage needle sequentially over the upper jaw and throat, applying slight pressure towards the tongue to ensure smooth passage with or without resistance, and slowly administer the drug solution (Xu Yifan, 2022).

The control group (CT) and the model group of mice were administered gastric gavage and intraperitoneal injection of physiological saline. The Nrf2 agonist group (NA) was administered Dimethyl fumarate via oral gavage and physiological saline via intraperitoneal injection. Nrf2 inhibitor group (NI) was administered physiological saline via oral gavage and ML385 via intraperitoneal injection. PPAR γ agonist group (PA) was administered physiological saline via oral gavage and Pioglitazone via intraperitoneal injection. The PPAR γ inhibitor group (PI) was administered physiological saline via oral gavage and GW9662 via intraperitoneal injection. Bufei Yishen prescription group (BYF) was administered Bufei Yishen prescription via oral gavage and physiological saline via intraperitoneal injection. Bufei Yishen prescription combined with PPAR γ

inhibitor group (BPI) was administered Bufei Yishen prescription via oral gavage and GW9662 via intraperitoneal injection. Bufei Yishen prescription combined with Nrf2 inhibitor group (BNI) was administered Bufei Yishen prescription via oral gavage and ML385 via intraperitoneal injection. Bufei Yishen prescription combined with PPAR γ and Nrf2 inhibitor group (BPNI) was administered Bufei Yishen prescription via oral gavage and GW9662, ML385 via intraperitoneal injection.

After 4 weeks of drug administration, samples were collected. Prior to sample collection, a 12-hour fasting period was observed, with ad libitum access to water. Physiological saline via oral gavage: male mice 0.25 mL/times, female mice 0.2 mL/times.

3.3 Physical Overview

The coat color, mental status, diet and breathing of the experimental mice were observed twice a day in the morning and evening, and the body weight of each experimental group was weighed every Monday.

3.4 Lung Function Examination

The changes in non-invasive pulmonary function in mice were assessed using a whole-body plethysmograph (WBP), with measurements taken at 0, 4, 8, and

12 weeks, respectively. Relevant parameters were collected and processed by a computer. Before conducting the test, the instrument's parameters were calibrated, and then the experimental mice were placed in the plethysmography chamber. Once the mice's breathing became stable, the test was initiated, with each mouse being tested for 4 minutes

Subsequently, the respiratory curve was displayed, and the software analyzed the graph to calculate the final values for tidal volume (TV), expiratory volume per minute (minute volume, MV), peak expiratory flow (peak expiratory flow, PEF), and 50% tidal expiratory flow (expiratory flow at 50% expired volume, EF50).

3.5 Pathological changes of lung tissue

When collecting specimens, 10% neutral formalin was perfused into the left lungs of mice in each experimental group. Subsequently, lung tissues were fully immersed in EP tubes containing 10% neutral formalin for fixation for 72 hours. After 72 hours, paraffin blocks were prepared following the procedure below: dehydration in a graded series of alcohols (70%-80%-90%-95%I-95%II-100%I-100%II), clearing in xylene (I and II), impregnation in paraffin (I-III), embedding. Once the paraffin blocks were successfully prepared, they were cut into 4μm thick sections using a microtome.

To ensure the sections adhere tightly, the sections were placed in a slide warmer at 58°C for 60 minutes. Hematoxylin-eosin staining (HE) was performed following the standard procedure. After successful preparation of the sections, lung tissue histopathological changes in alveoli, airways, and bronchi of mice in each experimental group were observed under a microscope.4.4 Detection of inflammatory factors in lung homogenate.

3.6 Measurement of inflammatory factors in lung homogenate
3.6.1 Preparation of experimental materials

Before the start of the experiment, prepare the ice box, PBS, liquid pipette, gun head, 4 mL EP tube, 1.5 mL EP tube, surgical scissors, pre-cooling cryogenic centrifuge.

3.6.2 Preparation of lung tissue homogenate

The right lung lobe tissues of mice in each group were removed from the refrigerator at-80 °C, placed in an ice box, marked with 4 mL and 1.5 mL EP tubes, and transferred to the corresponding centrifuge tubes, respectively, washed with 3 mL saline for 1-2 times, and then transferred to the corresponding 1.5 mL centrifuge tubes. The tissues were shredded with ophthalmic scissors, 2 small steel balls and 360 μL 4 °C precooled PBS were added respectively and placed in the tissue crusher to break 10min. After the above operations were completed, the samples of each group were centrifuged with a cryogenic

centrifuge for 10 min and 1200g. After centrifugation, the supernatant was collected and stored at-20 ℃.

3.6.3 ELISA method (IL-4 and TNFα in lung homogenate)

a) Prepare the icebox, take out the samples of each experimental group from the -20℃ refrigerator, and place them in UP water for rapid thawing. After thawing, swirl and mix the samples well.

b) Standard treatment: Prepare the standard according to the instructions and dilute it to 7 concentrations.

c) Dilute samples: Dilute TNF α and IL-4 samples according to the instructions.

d) Sample addition: Add the standard sample and diluted sample to the plate, 100 μL per well. Only add sample diluent to the zero well. Place in a 37℃ constant temperature incubator and incubate for 90 minutes.

e) Add antibody working solution: Quickly dry the liquid in the enzyme plate, add diluted TNF α and IL-4 antibody working solution, 100 μL per well (except the zero well), and incubate for 60 minutes at 37℃.

f) Wash the plate three times: Add 320 μL of detergent to each well, soak for 90 seconds each time, and pat the washing liquid in the enzyme plate to dry.

g) Add diluted ABC working solution sequentially: 100 μL per well (except the zero well).

h) Wash the plate: Add 320 μL washing solution per well, rest for 1-2 minutes. After drying, absorb the remaining liquid with absorbent paper. Repeat this

process 5 times.

i) Add chromogenic solution: Preheat the TMB chromogenic solution to 37℃, add 100 μL per well, and incubate for 15 minutes away from light at 37℃.

j) TMB termination solution: Add 100 μL per well, adjust the wavelength of the enzyme meter to 450nm, detect the OD value, draw the standard curve, and calculate the sample concentration.

3.7 The detection of alveolar macrophage efferocytosis function in COPD mice
3.7.1 Preparation of apoptotic pulmonary epithelial LLC cells

a) Prepared and packed common reagents: After routine ultraviolet disinfection and ventilation, entered the cell room, took 1640 medium, PBS, fetal bovine serum, and trypsin from the 4 ℃ refrigerator, and placed them on the super clean table. Prepared the complete culture medium according to the ratio of fetal bovine serum to 1640 (1:9). Packed PBS and trypsin sequentially, sealed them, and stored them in the refrigerator.

b) Resuscitated LLC cells: Before starting the experiment, took out the reagents in advance and allowed them to reach room temperature for 10 minutes. Opened the water bath and set the temperature to 37 ℃. Added 10 mL of 1640 to the petri dish and completed the culturing process. LLC cells were retrieved from the liquid nitrogen tank and quickly transferred to the cell room. Placed the cryopreservation tube into the PE glove and shook it in a water bath to promote the thawing of the cell suspension. During shaking, ensured the orifice of the

cryopreservation tube was upward, and the mouth of the tube was higher than the liquid level to prevent cell suspension contamination. After the cell suspension was dissolved, transferred it to the super clean table, blew the cell suspension evenly, and transferred it to a petri dish. Shook it 5-6 times in a cross pattern, mixed well, marked the cell name, operator name, and date, and observed the cells under an inverted microscope. If there were no issues, continued to culture the cells in a constant temperature and humidity incubator at 37 °C and 5% CO_2. Changed the medium every other day, discarded the old culture medium, added 2 mL room temperature balanced PBS, crossed and shook gently, removed all the PBS with a pipette, repeated 1-2 times, then added 10 mL 1640 to complete the culture. If the cells adhered well and there were no floating cells under the inverted microscope, continued the culture.

c) Subcultured LLC cells: When the cells covered 70-80% of the dish bottom, subcultured them at a 1:4 ratio. Discarded the culture medium, added 2 mL room temperature balanced PBS, washed 1-2 times, digested the cells with 1 mL trypsin, shook evenly in a cross pattern, and observed under an inverted microscope. When the cell boundaries gradually became round and some cells detached from the dish bottom and became suspended, sprayed alcohol on the super-clean table, added 2 mL to finish the culture and stopped digestion, gently blew with the pipette, completely resuspended the cells, transferred to a 4 mL EP tube, leveled it, and centrifuged at 1000 rpm for 5 minutes. Discarded the supernatant, added 2 mL complete culture medium to suspend the cells, took 0.5

mL into a new petri dish, cultured, and stabilized the volume to 10 mL. After three passages, began the follow-up experiment if the cells were growing well.

d) Cryopreserved LLC cells: When the cells covered 70-80% of the dishes and were in good condition, froze the cells. Prepared 1640 medium, fetal bovine serum, DMSO, PBS, and trypsin in advance. After routine digestion, centrifuged the cells at 1000 rpm for 5 minutes. Prepared the cell cryopreservation solution during centrifugation. Each group needed 1 mL cryopreservation solution with a ratio of 1640 medium to fetal bovine serum to DMSO (5:4:1). Prepared the required freezer and labeled it.

e) After centrifugation, resuscitated the cells with the cell cryopreservation solution, transferred the suspension to the frozen tube, balanced for 10 minutes at 4 °C and 20 minutes at -20 °C, then transferred to the refrigerator at -80 °C overnight and stored in the liquid nitrogen tank with proper documentation.

f) LLC cell seeding: When 70-80% of the cells covered the bottom of the plate, collected, centrifuged, resuspended, and counted the cells. Inoculated cells in a 10×10 mm petri dish at 7×10^6 cells/dish, divided into blank and apoptotic groups, and supplemented with complete culture medium to 10 mL, then transferred to the incubator.

g) Induction of LLC cell apoptosis by UV exposure: After 24 hours of seeding, observed the cell state. If the cells were in good condition, induced apoptosis in LLC cells by UV exposure. After routine cleaning, added 20 mL complete medium to the cells. Placed the petri dish into the purple diplomatic instrument,

opened the petri dish cover, set the power to 30000 $\mu J/cm^2$, and the ultraviolet irradiation time to 20 minutes. After irradiation, covered the petri dish, transferred it to the cell chamber, and incubated in the incubator for 1.5 hours. Prepared 50 mL EP tube, cell counting plate, and coverslip in advance during incubation. Placed a coverslip on the counting board, securing it in place with PBS around the edges for subsequent use. Collected and counted the cells in the normal group according to routine operation. Transferred the UV-induced apoptotic LLC cells to the supernatant, collected the supernatants, added 2 mL precooled PBS buffer, gently blew down the cells with a liquid transfer gun, and then collected them into the centrifuge tube. Injected 10 μL cell suspension into the counting area of the counting plate and calculated the number of cells.

h) Flow cytometry for detecting the apoptosis rate of LLC cells: Extracted 5×10^5 cell suspensions from each of the two groups of cells collected in step g), placed them in a 4 mL EP tube, and centrifuged at 1000 rpm for 5 minutes. During centrifugation, took out the precooled sterile ultra-pure water and diluted $5 \times$ Binding Buffer to $1 \times$ Binding Buffer. After centrifugation, moved the EP tube to the super clean table, discarded the supernatant, and fully suspended the cells of each group with 500 μL $1 \times$ Binding Buffer. Then added 5 μL fluorescein FITC-labeled annexin (Annexin V-FITC) and 10 μL propidium iodide (PI) to the centrifuge tube. After gentle mixing, incubated for 5 minutes at room temperature in the dark. Opened and adjusted the flow cytometer, debugged the detection program, let the instrument stabilize for 5 minutes, labeled the flow

tube, transferred cells, and then started the computer to detect the apoptosis rate.

Apoptosis rate = (early apoptosis + number of apoptotic cells in middle and late stage) / total number of cells × 100%

3.7.2 Isolation and seed dish of alveolar macrophages from COPD mice

a) Prepared 10% Formalin Solution: Weighed 10g of formalin hydrate using an electronic balance, transferred it to a 250 mL beaker, added 100mL of UP water to the beaker, stirred vigorously using a magnetic stirrer, transferred the solution to a centrifuge tube, sealed, and stored it at room temperature. Prepared as needed.

b) UV Irradiation of Laminar Flow Hood for 30 minutes, Ventilation for 10 minutes: Prepared medical tape, sterile ophthalmic scissors, forceps, 5mL syringe, 1mL syringe, PBS buffer, sterile foam board, and suture material.

c) Weighed mice from each experimental group and anesthetized them according to their body weight at a dosage of 0.3 mL/100g. After full anesthesia, disinfected the entire body with alcohol, and transferred the mice to the laminar flow hood.

d) Secured the limbs of the mice to the operating table with tape. Used ophthalmic scissors to incise the skin on the neck of the mouse. With forceps, adequately separated the trachea from surrounding tissues. Placed a suture material under the trachea and made a horizontal incision in the shape of "—"

using ophthalmic scissors.

e) Gently inserted the needle of a 5 mL syringe, controlled the depth, and then tied a knot with the suture material to secure it.

f) After fixation, injected 1mL of PBS buffer into the lungs using a 1mL syringe. After successful injection, gently pressed the chest area of the mouse, then slowly withdrew. Repeated this procedure 5 times, ensuring a recovery rate of >80%.

g) After successful collection of bronchoalveolar lavage fluid, centrifuged at 3000rpm for 10 minutes. Used a pipette gun to gently aspirate the supernatant, resuspended the cell pellet in complete medium, transferred to a 35mm dish, and incubated for 2 hours in a cell culture incubator. Washed with PBS 2-3 times, and the collected adherent cells were mouse alveolar macrophages.

h) Counted the collected mouse alveolar macrophages from the previous step, seeded them into a 35mm culture dish at 1×10^6 cells/dish, adjusted the volume to 1.5mL, and continued the culture.

3.7.3 Labeling of LLC apoptotic cells with PKH26 membrane labelled probe

a) Prepared 10 mL EP tubes, fetal bovine serum, and complete culture medium in advance.

b) Following the detection of apoptosis rates in LLC cells collected in Experiment 3.7.1 using flow cytometry, the remaining cells were washed 1-2 times with PBS for evaluating the phagocytic ability of macrophages (transferred

the non-stained LLC apoptotic cells to another centrifuge tube for later use).

c)   Dispensed apoptotic cells into different centrifuge tubes at a quantity of 3×10^7 cells/group.

d)   Started centrifugation after balancing, at 2000 rpm for 5 minutes.

e)   During centrifugation, took two 10 mL EP tubes. Added 1.5 mL Diluent C and 6 μL PKH26 ethanol solution to one tube to prepare $2\times$ PKH26 staining solution. Wrapped it with aluminum foil to avoid light exposure. Mixed thoroughly and set it aside.

f)   After cell centrifugation, carefully transferred the EP tubes to the laminar flow hood, and using a pipette gun, gently aspirated the supernatant along the tube wall (final residual cell volume < 25 μL).

g)   Resuspended cells in 1.5 mL Diluent C, blew gently to mix evenly, and transferred the cell suspension to the $2\times$ PKH26 staining solution. Quickly and gently mixed, incubated at room temperature in the dark for 5 minutes. During incubation, gently flicked and mixed occasionally.

h) After incubation, added an equal amount of fetal bovine serum, mixed quickly and gently to terminate the staining reaction, and continued incubation for 1 minute.

i)   Centrifuged at 2000 rpm for 5 minutes and discarded the supernatant.

j)   Washed the cells with complete medium to remove excess staining solution, repeated 1-2 times. After washing, resuspended the cells in 10 mL complete medium.

3.7.4 Detection of cell efferocytosis of alveolar macrophages by flow cytometry

a)   At the conclusion of the PKH26 staining of LLC apoptotic cells, the mice alveolar macrophages seeded in step 3.7.2 had successfully adhered, with a cell count of 1×10^6.

b)   Added the PKH26-stained LLC apoptotic cells to the culture dish, with a seeding density of 5×10^6 cells per dish (the ratio of mice alveolar macrophages to LLC cells was 1:5). After thorough mixing in a cross pattern, incubated in the cell culture incubator for 1 hour. The final volume in the culture dish was 2.5 mL.

c)   After incubation, transferred the cells to the laminar flow hood, added 20 μL of 0.4% Trypan Blue, mixed in a cross pattern, and incubated for 1 minute.

d)   Discarded the supernatant, washed once with PBS, added 500 μL of trypsin to digest the cells. Collected the cells according to standard procedures when the cell morphology changed.

e)   Transferred the cell suspension to EP tubes using a pipette gun, centrifuged at 3000 rpm for 5 minutes.

f)   Discarded the supernatant after centrifugation, added 1 mL of 4% cell fixation solution, mixed, incubated for 20 minutes, centrifuged at 3000 rpm for 5 minutes, and discarded the supernatant.

g)   During the incubation period, turned on the flow cytometer, adjusted the

voltage, and preheated the instrument.

h)   Centrifuged and discarded the supernatant, resuspended the cells in 500 μL of PBS, and transferred them to labeled flow tubes.

i)   Initiated the machine. Mouse macrophages with phagocytic capabilities could engulf PKH26-labeled apoptotic LLC cells. The flow cytometer could assess the ability of mouse macrophages to engulf apoptotic cells by measuring fluorescence intensity.

3.8 Detection of apoptosis in mice lung tissue by TUNEL method

a)   Removed Endogenous Oxidants: Incubated all tissue sections with 3% H_2O_2 at room temperature for 10 minutes to eliminate endogenous oxidants. After incubation, rinsed with distilled water.

b)   Prepared Proteinase K Working Solution: Diluted Proteinase K in PBS, added it dropwise to the tissue sections, ensuring complete coverage. Incubated at room temperature for 10 minutes, then washed 2-3 times with 0.01 mol TBS.

c)   Added 20 μL of labeling buffer to each tissue section.

d)   For each tissue section, prepared a working solution containing 1 μL of terminal deoxynucleotidyl transferase (TdT) and DIG-d-UTP dissolved in 18 μL of buffer. Applied 20 μL to each tissue section, then incubated in a humid chamber at 37°C for 2 hours. After incubation, washed 2-3 times with 0.01 mol TBS.

e)   Added 50 μL of blocking solution to each tissue section, incubated at room

temperature for 30 minutes, and no washing was required.

f) Applied 50 μL of diluted biotinylated anti-digoxin antibody to each tissue section, incubated at 37°C for 30 minutes. After incubation, washed 2-3 times with 0.01 mol TBS.

g) Applied 50 μL of SABC to each tissue section, incubated at 37°C for 30 minutes, and washed 2-3 times with 0.01 mol TBS.

h) Added DAB chromogenic solution at 60 μL per section, incubated at room temperature. Controlled the reaction time under a light microscope and terminated the reaction by rinsing with distilled water when a brown color appeared.

i) Counterstained with hematoxylin, washed 2-3 times with 0.01 mol TBS, and rinsed 1-2 times with distilled water.

k) Dehydrated, cleared, and mounted the slides.

l) Examined the sections under an optical microscope. The brown areas indicated apoptotic cells. Randomly selected 5 fields at 200x magnification and analyzed with Image Pro Plus 6.0 (IPP 6.0) software to calculate the apoptotic index (AI%).

Apoptotic Index (%) = Number of apoptotic cells / Total number of cells × 100%.

3.9 The expression of macrophage phenotype CD68, INOS, CD163, Nrf2 and PPAR γ in mice lung tissue was detected by immunohistochemical method

a) Removed Endogenous Oxidants: Treated sections were incubated with 3%

H_2O_2 and incubated at room temperature for 10 minutes. Washed 2-3 times with distilled water.

b)   Immersed the sections in 0.01 mol citrate buffer, heated using a microwave for antigen retrieval, and washed with PBS after the slides had cooled.

c)   Added 5% BSA blocking solution, incubated at room temperature for 20 minutes, air-dried after blocking, and no washing was required.

d)   Antibody Dilution: CD68 was diluted at a ratio of 1:300, INOS, CD163 at a ratio of 1:200.

e)   Dropped an appropriate amount of primary antibody according to the grouping, incubated overnight at 4°C, then washed 2-3 times with PBS.

f)   Added secondary antibody, incubated at room temperature for 20 minutes, then washed 2-3 times with PBS.

g)   Sequentially added 50 μL of SABC to each tissue section, incubated at 37°C for 30 minutes, and washed 1-2 times with PBS.

h)   Applied 60 μL of DAB chromogenic solution to each tissue section, incubated at room temperature. Controlled the reaction time under an optical microscope, rinsed with distilled water when a brown color appeared to terminate the reaction.

i)   Counterstained with hematoxylin, washed with PBS after counterstaining, and then rinsed with distilled water.

j)   Performed dehydration, clearing, and mounting.

l)   Data Analysis: Under an optical microscope, brown areas represented

immunohistochemically positive regions. Randomly selected 5 fields at 200×

magnification and used Image Pro Plus 8.0 software for statistical analysis.

3.10 Statistical Analysis

IBM SPSS 26 software counted and analyzed the experimental data, and the

results were expressed as mean ± standard deviation (variance ± s). For the

analysis of animal mortality in each group, the chi-square test was employed.

For repeated measurements of data such as body weight and non-invasive lung

function, repeated measures analysis of variance (RM-ANOVA) was utilized.

The inter-group comparison of continuous data was conducted using one-way

analysis of variance (One-Way ANOVA). If the variance is homogeneous, the

LSD method is used, and if the variance is uneven, the DunnettT3 method is

used. The significant level was $\alpha = 0.05$ ($P<0.05$), indicating that there was

statistical difference. All the graphics in this paper are made by GraphPad Prism

9.5.1.733 software.

Chapter 4.0: Result

4.1 Comparison results among CT, M, PA, NA, PI, and NI groups

4.1.1 Physical Overview

During the 1–8-week modeling period in COPD mice, mice in the CT group exhibited good mental states, were agile in movement, had glossy and smooth fur, maintained normal eating and excretion, and showed normal weight gain. In the M group, mice showed restlessness and agitation starting from the second week, frequently engaged in tearing and fighting. Most mice in this group had bite wounds on their head, neck, abdomen, and tail. By the 6th week of modeling, the level of agitation in mice decreased, gradually leading to symptoms such as dry fur, lethargy, slow movement, reduced food and water intake, and slowed weight gain. The above-mentioned symptoms were alleviated in mice from the PA and NA groups. In the 10th week, two mice in the model group died, and post-mortem examination revealed the presence of pus points in the lungs, suggesting death due to lung abscess.
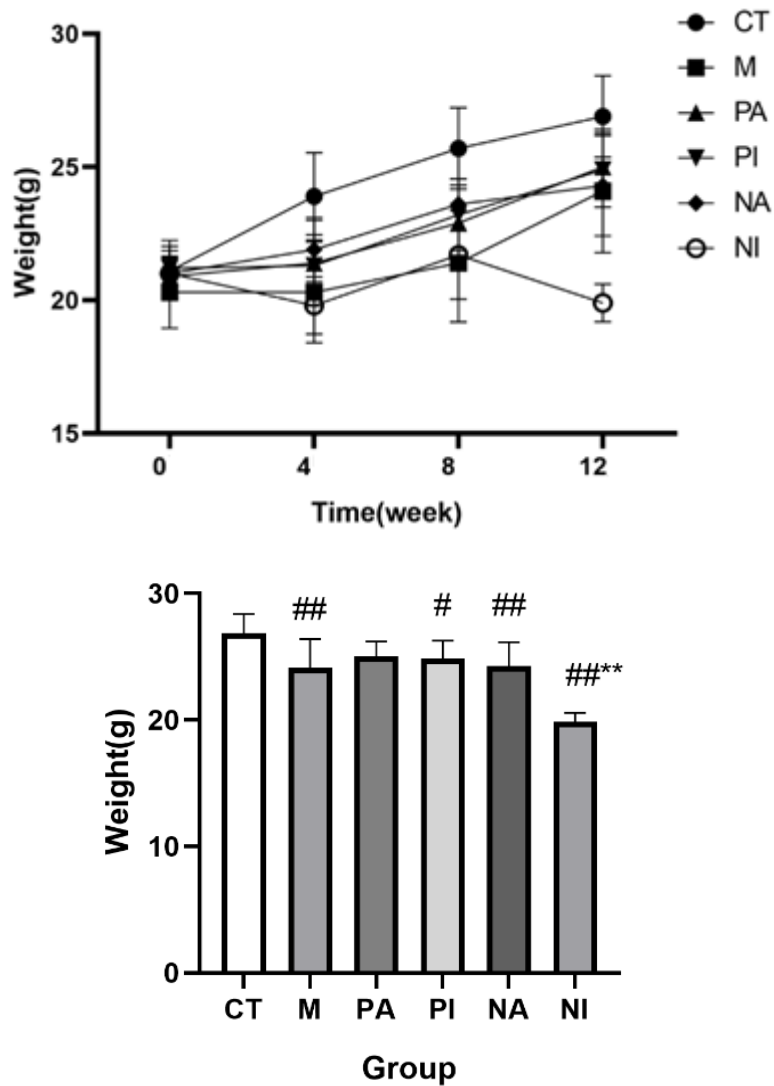
4.1.2 Weight change

The body weight of mice increased over time in all groups. There was a statistically significant difference between groups as determined by one-way ANOVA Following modeling. The M group (24.10 ± 2.32g) exhibited a

significant reduction in body weight compared to the CT group (26.85±1.53g,

P=0). In comparison to the M group, both the PA and PI groups showed no

significant changes (P=0.766, 0.644). The NA group exhibited no significant

changes compared to the M group (P=0.526), while the NI group (19.85±0.71g)

showed a significant decrease (P=0.004). See Table 1.3, figure 1.1.

Table 1.3: Changes of body weight in mice (g, $\bar{x}\pm s$)

	N	0 week	P	4 weeks	P	8 weeks	P	12 weeks	P
CT	12	21.12±0.93		23.92±1.64		25.67±1.53		26.85±1.53	
M	10	20.32±1.35	0.135	20.25±1.90[##]	0	21.40±2.22[##]	0	24.10±2.32[##]	0
PA	12	20.90±0.70	0.229	20.88±0.61[##]	0.422	22.87±1.42[##]	0.087	25.00±1.20	0.766
PI	12	21.20±1.05	0.142	21.32±1.16[##]	0.183	23.20±1.35[#]	0.387	24.92±1.40[#]	0.644
NA	12	21.03±0.56	0.199	21.93±1.21[##]	0.365	23.58±2.08[#]	0.884	24.28±1.88[##]	0.526
NI	12	21.03±0.86	0.199	19.80±1.08[##]	0.568	21.67±1.66[##**]	0.009	19.85±0.71[##**]	0.004

Comparing with the control group, #: P<0.05, ##: P<0.01. Comparing with the model group, **: P<0.01.

Figure 1.1: The change of body weight of mice and the weight of mice at the 12th week

Comparing with the control group, #: P<0.05, ##: P<0.01. Comparing with the model group, **: P<0.01.

4.1.3 Pulmonary function(TV、MV、PEF、EF50)

There was a statistically significant difference between groups as determined by one-way ANOVA Following modeling. Compared to the CT group

(TV:0.39±0.02 mL, MV:179.32±17.70 mL/min, PEF:9.99±0.67 mL/s, EF50:0.49±0.04 mL/s), the M group of mice (TV:0.28±0.03 mL, MV: 120.35±13.01 mL/min, PEF: 5.72±0.38 mL/s, EF50: 0.27±0.05 mL/s) exhibited a significant decrease (P=0) in tidal volume (TV, see tables 1.4, figure 1.2) minute volume (MV, see table 1.5, figure 1.3), peak expiratory flow (PEF, see table 1.6, figure 1.4), and forced expiratory flow at 50% of the forced vital capacity (EF50, see table 1.7, figure 1.5).

When comparing with the M group (TV:0.28±0.03 mL, MV: 120.35±13.01 mL/min, PEF: 5.72±0.38 mL/s, EF50: 0.27±0.05 mL/s), the PA (0.33±0.01 mL, 151.24±9.37 mL/min, 6.84±0.59 mL/s, 0.36±0.05 mL/s) and NA groups (0.36±0.03 mL, 162.15±14.41 mL/min, 7.83±0.96 mL/s, 0.39±0.06 mL/s) showed an increase in TV (P=0.024, 0.046), MV (P=0), PEF (P=0.042, 0.025), and EF50(P=0.002, 0.042). See tables 1.4, 1.5, 1.6, 1.7, figure 1.2, figure 1.3, figure 1.4, figure 1.5.

However, there were no significant differences in TV (P=0.772, 0.327), MV (P=0.962, 0.096), and PEF (P=0.766, 0.084) between the PI and NI groups compared to the M group (P>0.05). See tables 1.4, 1.5, 1.6, figure 1.2, figure 1.3, figure 1.4. Additionally, there was no significant difference in EF50 between the PI group and the M group (P=0.193), while the NI group exhibited a decrease (P=0.042) in EF50. See tables 1.7, figure 1.5.

Table 1.4: Changes of TV in mice (ml，$\bar{x}\pm s$)

	N	0 week	P	4 weeks	P	8 weeks	P	12 weeks	P
CT	12	0.27±0.01		0.36±0.03		0.34±0.03		0.39±0.02	
M	10	0.26±0.02	0.775	0.29±0.01##	0	0.27±0.01##	0	0.28±0.03##	0
PA	12	0.26±0.02	0.626	0.31±0.03##	0.085	0.29±0.02##*	0.025	0.33±0.01#*	0.024
PI	12	0.27±0.01	0.445	0.29±0.03##	0.986	0.28±0.02##	0.173	0.27±0.01##	0.772
NA	12	0.25±0.01	0.203	0.30±0.02##	0.187	0.30±0.01##**	0.001	0.36±0.03*	0.046
NI	12	0.25±0.02	0.102	0.29±0.02##	0.913	0.26±0.01##	0.763	0.27±0.01##	0.327

Comparing with the control group, #: P<0.05, ##: P<0.01. Comparing with the model group, *: P<0.05, **: P<0.01.

Table 1.5: Changes of MV in mice (ml/min，$\bar{x}$±s)

	N	0 week	P	4 weeks	P	8 weeks	P	12 weeks	P
CT	12	133.23±13.09		169.03±31.61		148.64±21.04		179.32±17.70	
M	10	128.49±14.59	0.524	133.82±17.83	0.374	114.04±12.67	0.095	120.35±13.01[##]	0
PA	12	130.26±12.65	0.812	137.31±21.91	1	122.62±11.30	0.952	151.24±9.37[##**]	0
PI	12	129.82±15.02	0.866	130.76±25.72	1	116.37±13.32	1	120.88±4.28[##]	0.962
NA	12	132.09±9.47	0.634	146.56±11.06	0.856	121.73±4.23	0.876	162.15±14.41[#**]	0
NI	12	129.51±9.73	0.897	120.23±7.75	0.732	113.56±6.40	1	107.48±13.72[##]	0.096

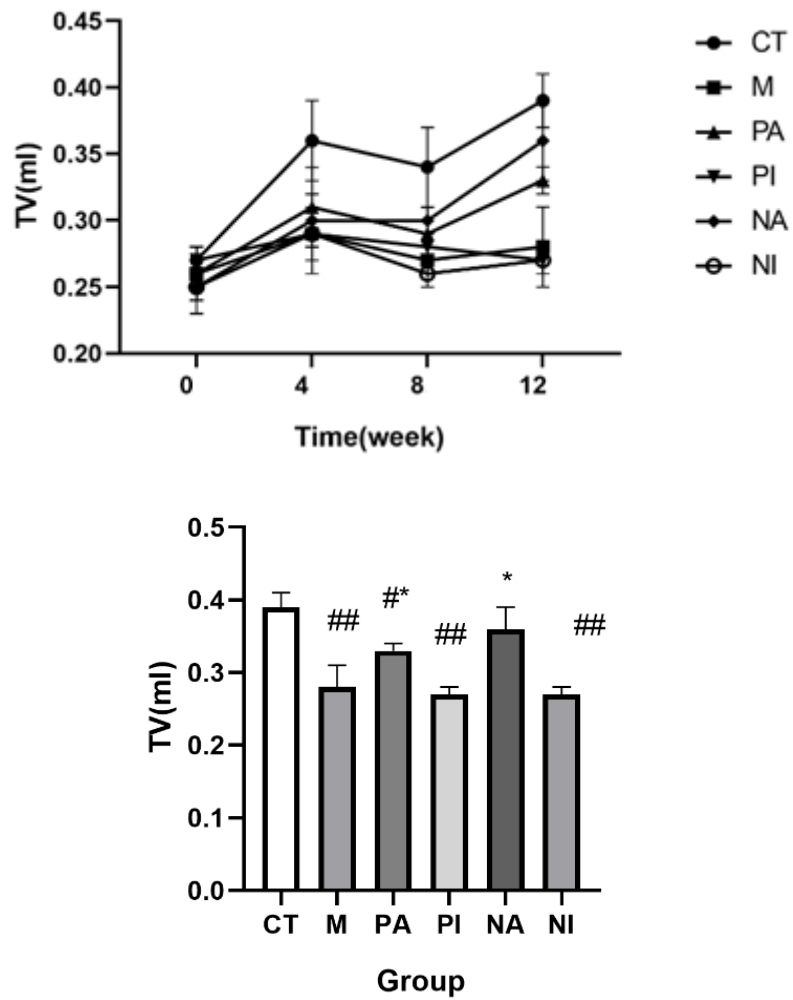Comparing with the control group, #: $P<0.05$, ##: $P<0.01$. Comparing with the model group, **: $P<0.01$.

Table 1.6: Changes of PEV in mice (ml/s，$\bar{x}\pm$s)

	N	0 week	P	4 weeks	P	8 weeks	P	12 weeks	P
CT	12	6.63±0.38		8.86±0.81		7.58±0.92		9.99±0.67	
M	10	7.33±0.88	0.684	6.98±0.33[##]	0	6.19±0.71[##]	0	5.72±0.38[##]	0
PA	12	7.04±0.24	0.466	7.82±0.66[#*]	0.047	6.40±0.32[##]	0.535	6.84±0.59[##*]	0.042
PI	12	6.65±0.55	1	7.32±0.88[##]	0.398	5.83±0.44[##]	0.274	5.43±0.19[##]	0.766
NA	12	6.55±0.29	1	8.40±0.64[**]	0.001	6.17±0.28[##]	0.963	7.83±0.96[#*]	0.025
NI	12	6.41±0.61	1	6.80±0.52[##]	0.643	5.18±0.44[##**]	0.004	5.06±0.27[##]	0.084

Comparing with the control group, #: P<0.05, ##: P<0.01. Comparing with the model group, *: P<0.05, **: P<0.01.

Table 1.7: Changes of EF50 in mice (ml/s，$\bar{x}$±s)

	N	0 week	P	4 weeks	P	8 weeks	P	12 weeks	P
CT	12	0.25±0.01		0.27±0.03		0.29±0.05		0.49±0.04	
M	10	0.27±0.04	0.982	0.23±0.03##	0.006	0.21±0.02##	0	0.27±0.05##	0
PA	12	0.26±0.02	1	0.23±0.02#	0.666	0.23±0.02##	0.214	0.36±0.05##**	0.002
PI	12	0.26±0.03	1	0.22±0.02##	0.767	0.22±0.02##	0.305	0.24±0.02##	0.193
NA	12	0.26±0.01	1	0.25±0.02	0.078	0.22±0.02##	0.442	0.39±0.06##**	0
NI	12	0.26±0.01	1	0.20±0.03##	0.115	0.20±0.02##	0.527	0.22±0.03##*	0.042

Figure 1.2: Changes of TV in mice and TV value of each group at the 12th week.

Comparing with the control group, ##: $P<0.01$. Comparing with the model group, *: $P<0.05$.
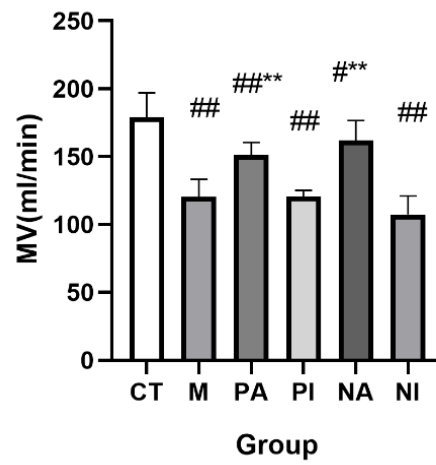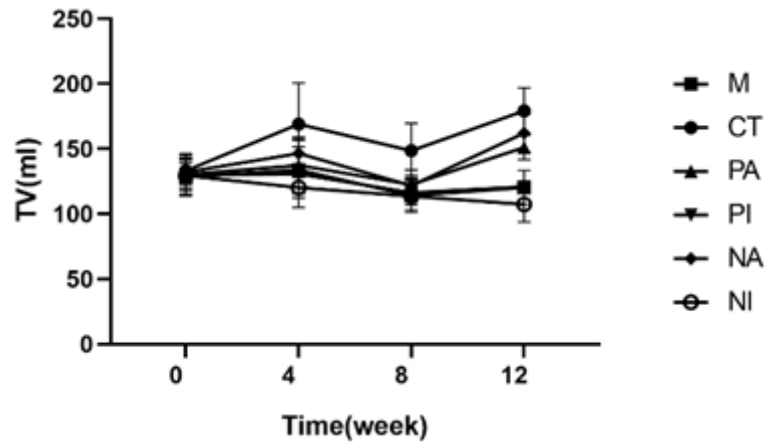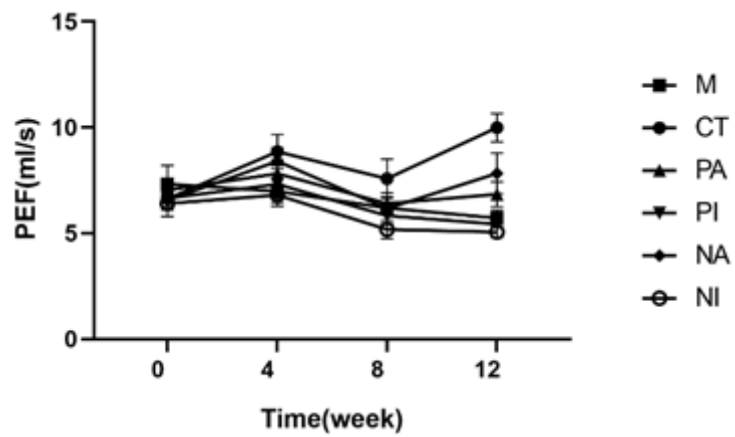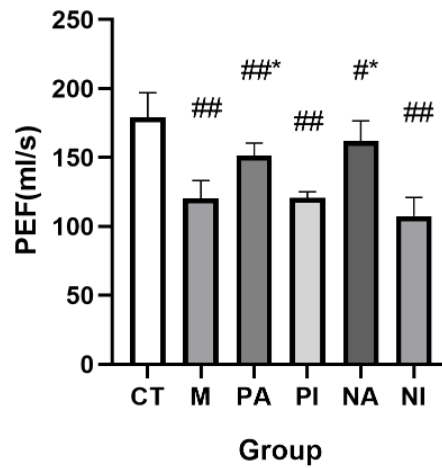
Figure 1.3: Changes of MV and MV value of each group at the 12th week
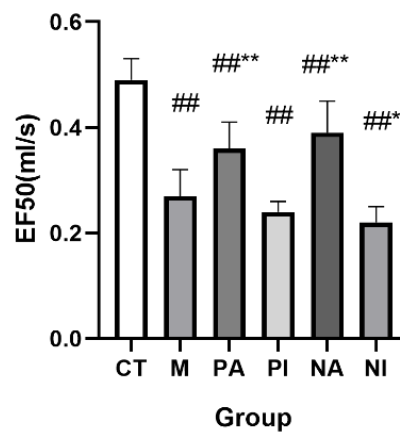
Comparing with the control group, #: P<0.05, ##: P<0.01. Comparing with the

model group, **: P<0.01.

Figure 1.4: Changes of PEF in mice and PEF value of each group at the 12th week
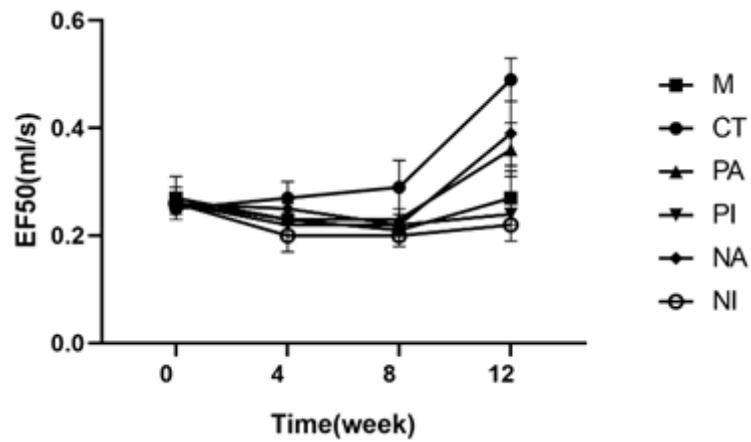
Comparing with the control group, #: P<0.05, ##: P<0.01. Comparing with the model group, *: P<0.05.

**Figure 1.5: Changes of EF50 in mice and EF50 value of each group at the 12th week**

Comparing with the control group, ##: P<0.01. Comparing with the model group, *: P<0.05.

4.1.4 Pathological changes of lung tissues

Pathological images of mice lung tissues show that in the CT group, the alveolar size is relatively uniform, and the alveolar wall structure is relatively intact, with some alveolar walls undergoing rupture and recombination. The thickness of the bronchial wall is normal, with occasional infiltration of inflammatory cells. See figure 1.6 A. In the M group, the alveolar size is uneven, the alveolar wall structure is disrupted, and there is a significant amount of alveolar wall rupture. The bronchial wall is markedly thickened, with pronounced fibrosis in the surrounding tissue. The bronchial lumen is narrow, goblet cell hyperplasia is observed, and there is a considerable infiltration of inflammatory cells. See figure 1.6 B.

Comparatively, in the PA and NA groups, the mice alveoli exhibit more uniform sizes, and the alveolar wall structure is relatively intact. The situation of alveolar rupture and fusion is alleviated. The bronchial wall becomes thinner, and there is some improvement in fibrosis around the bronchi, luminal narrowing, and infiltration of inflammatory cells. See figure 1.6 C, E

In the PI group, there is a slight improvement in the structure of alveoli and

bronchi. In the NI group, bronchial luminal narrowing intensifies, and there is

an increase in the infiltration of inflammatory cells. See figure 1.6 D, F
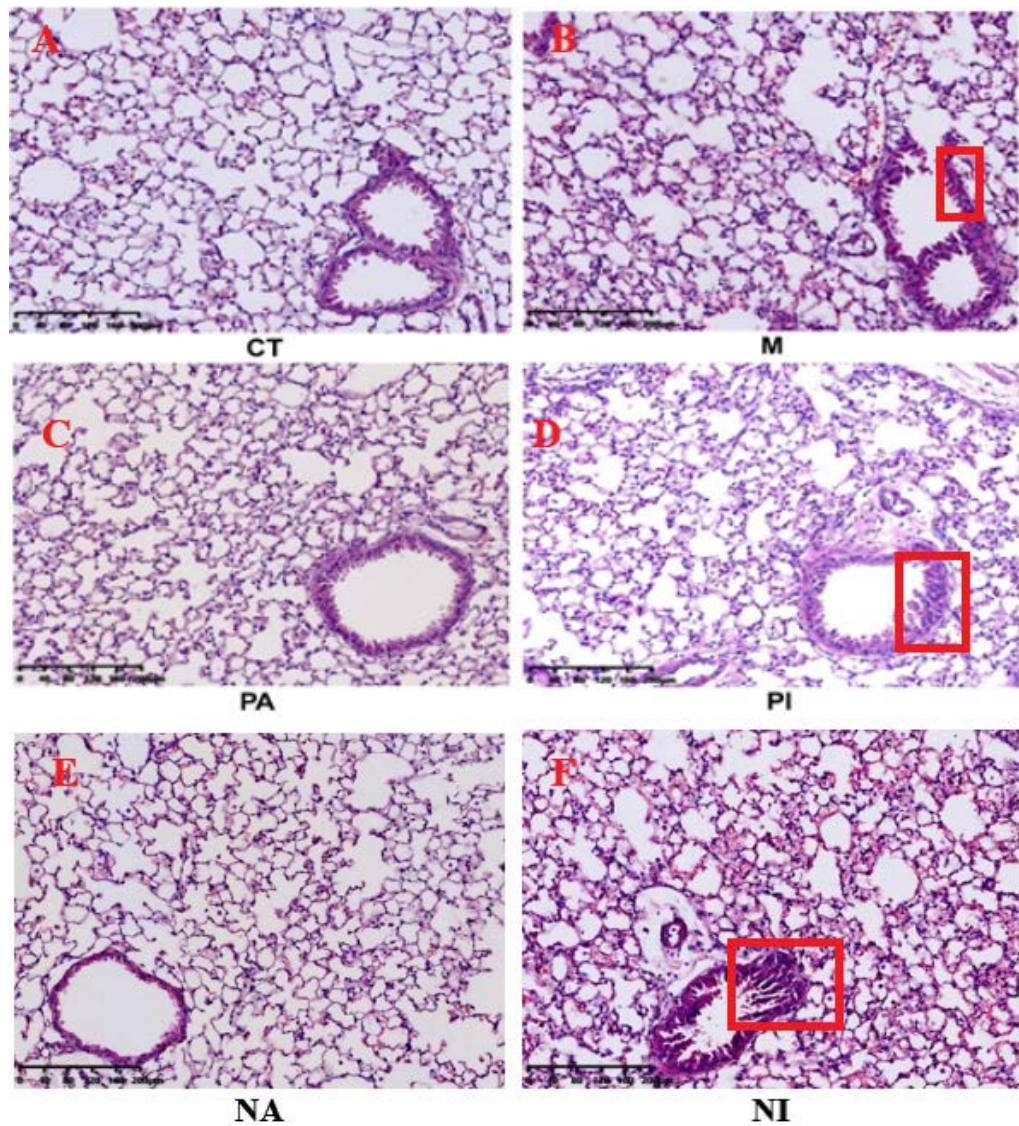
Figure 1.6: Lung Pathology of mice tissues in each group

4.1.5 Determination of TNF α and IL-4 in lung tissue homogenate

There was a statistically significant difference between groups as determined

by one-way ANOVA Following modeling. Compared with CT group (325.99±84.63 pg/mL, 343.24±48.87 pg/mL), the expressions of inflammatory cytokines TNF α and IL-4 in lung tissue homogenate of mice in M group (642.16±146.03 pg/mL, 431.39±50.17 pg/mL) were significantly increased (P=0, P=0). Compared with M group (642.16±146.03 pg/mL, 431.39±50.17 pg/mL), the expression of TNF α and IL-4 in PA group (286.57±44.66 pg/mL, P=0, 237.05±32.05 pg/mL, P=0) and PI group (354.93±88.40 pg/mL, 285.58±50.47 pg/mL) decreased significantly (P=0, P=0). Compared with M group (642.16±146.03 pg/mL, 431.39±50.17 pg/mL), the expression of TNF α and IL-4 in NA group (322.22±52.66 pg/mL, P=0, 270.59±65.95 pg/mL, P=0) and NI group (348.32±49.13 pg/mL, P=0.026, 509.14±131.79 pg/mL, P=0.008) decreased. See Table 1.8, figure 1.7.

Table 1.8: Expression of TNF α and IL-4 in lung homogenate of mice (pg/mL，n=6，$\bar{x}\pm s$)

	TNFα	P	IL-4	P
CT	325.99±84.63		343.24±48.87	0.005
M	642.16±146.03[##]	0	431.39±50.17[##]	0
PA	286.57±44.66[**]	0	237.05±32.05[##**]	0
PI	354.93±88.40[**]	0	285.58±50.47[**]	0
NA	322.22±52.66[**]	0	270.59±65.95[#**]	0
NI	509.14±131.79[##*]	0.026	348.32±49.13[**]	0.008

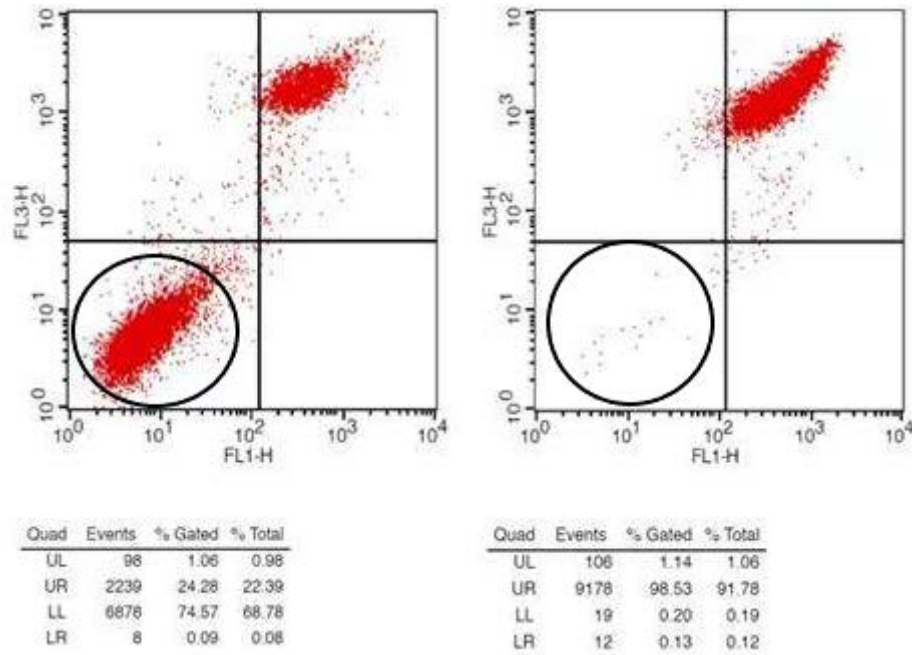Comparing with the control group, ##: P<0.01. Comparing with the model group, *: P<0.05, **: P<0.01.
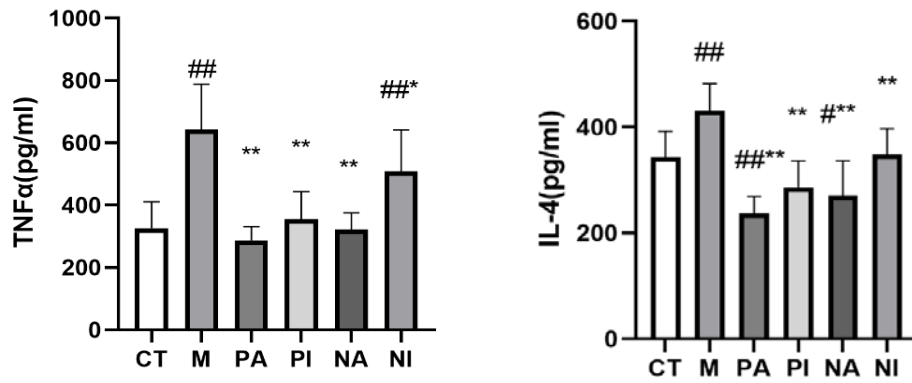
Figure 1.7: Expression of TNF α and IL-4 in lung homogenate of mice

Comparing with the control group, #: P<0.05, ##: P<0.01. Comparing with the model group, *: P<0.05, **: P<0.01.

4.1.6 Detection of cellular efferocytosis function of alveolar macrophages in COPD mice

Through flow analysis of LLC cells, FITC-labelled Annexin V was used to detect apoptotic cells, most of the LLC cells without apoptosis induced by UV irradiation are in normal state, only a few of them are in the late stage of apoptosis, and the apoptosis rate is 24.37%. The apoptosis rate of LLC cells induced by UV irradiation is 98.66% > 90%. See figure 1.8.

Quad	Events	% Gated	% Total
UL	98	1.06	0.98
UR	2239	24.28	22.39
LL	6876	74.57	68.78
LR	8	0.09	0.08

Quad	Events	% Gated	% Total
UL	106	1.14	1.06
UR	9178	98.53	91.78
LL	19	0.20	0.19
LR	12	0.13	0.12

Figure 1.8: LLC cell apoptosis

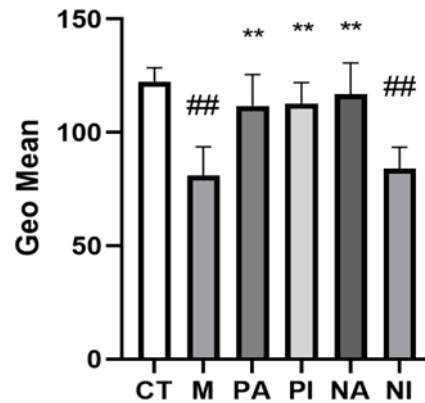There was a statistically significant difference between groups as determined by one-way ANOVA Following modeling. Compared with CT group (122.29±6.29), the efferocytosis ability of alveolar macrophages in M group (81.00±12.70) decreased significantly (P=0). Compared with M group (81.00±12.70), PA (111.65±13.90) and PI groups (112.57±9.52) increased significantly (P=0), NA group (116.75±13.97) increased significantly (P=0), but NI group (84.08±9.41) had no significant change (P=0.641). See Table 1.9, figure 1.9.

Table 1.9: Cell efferocytosis of mice alveolar macrophages (n=6, RFU, $\bar{x}$±s)

	Geo Mean	P
CT	122.29±6.29	0
M	81.00±12.70##	0
PA	111.65±13.90**	0
PI	112.57±9.52**	0

NA	$116.75 \pm 13.97^{**}$	0
NI	$84.08 \pm 9.41^{\#\#}$	0.641

Comparing with the control group, ##: P<0.01. Comparing with the model group,

**: P<0.01.

Figure 1.9: Detection of cell efferocytosis ability of alveolar macrophages

in mice. Comparing with the control group, ##: P<0.01. Comparing with the

model group, **: P<0.01.

4.1.7 Detection of apoptosis in lung tissue of mice model

There was a statistically significant difference between groups as determined by one-way ANOVA Following modeling. Compared with CT group (41.34±1.69%), the apoptosis index of lung tissue in M group (61.68±4.37%) increased significantly (P=0). See Table 1.10, figure 1.10, 1.11 A and B.

Compared with M group, it decreased significantly in PA group (38.78±3.65%, P=0) and NA group (43.40±1.25%, P=0.001). See Table 1.10, figure 1.10, 1.11 B, C, E.
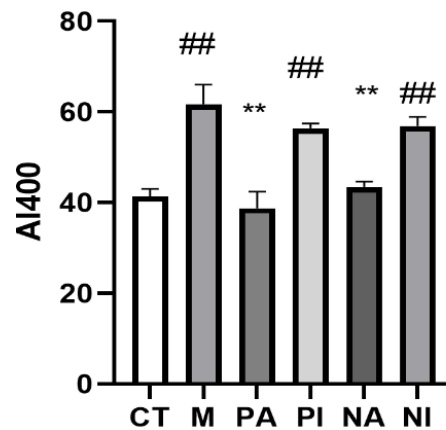
There was no significant change in PI group (56.36±1.06%, P=0.233) and NI group (56.88±2.04%, P=0.353). See Table 1.10, figure 1.10, 1.11 B, D, F.

Table 1.10: Apoptosis index of lung tissue in mice (n=6, %, $\bar{x}$±s)

	AI400	P
CT	41.34±1.69	
M	61.68±4.37[##]	0
PA	38.78±3.65[**]	0
PI	56.36±1.06[##]	0.233
NA	43.40±1.25[**]	0.001
NI	56.88±2.04[##]	0.353

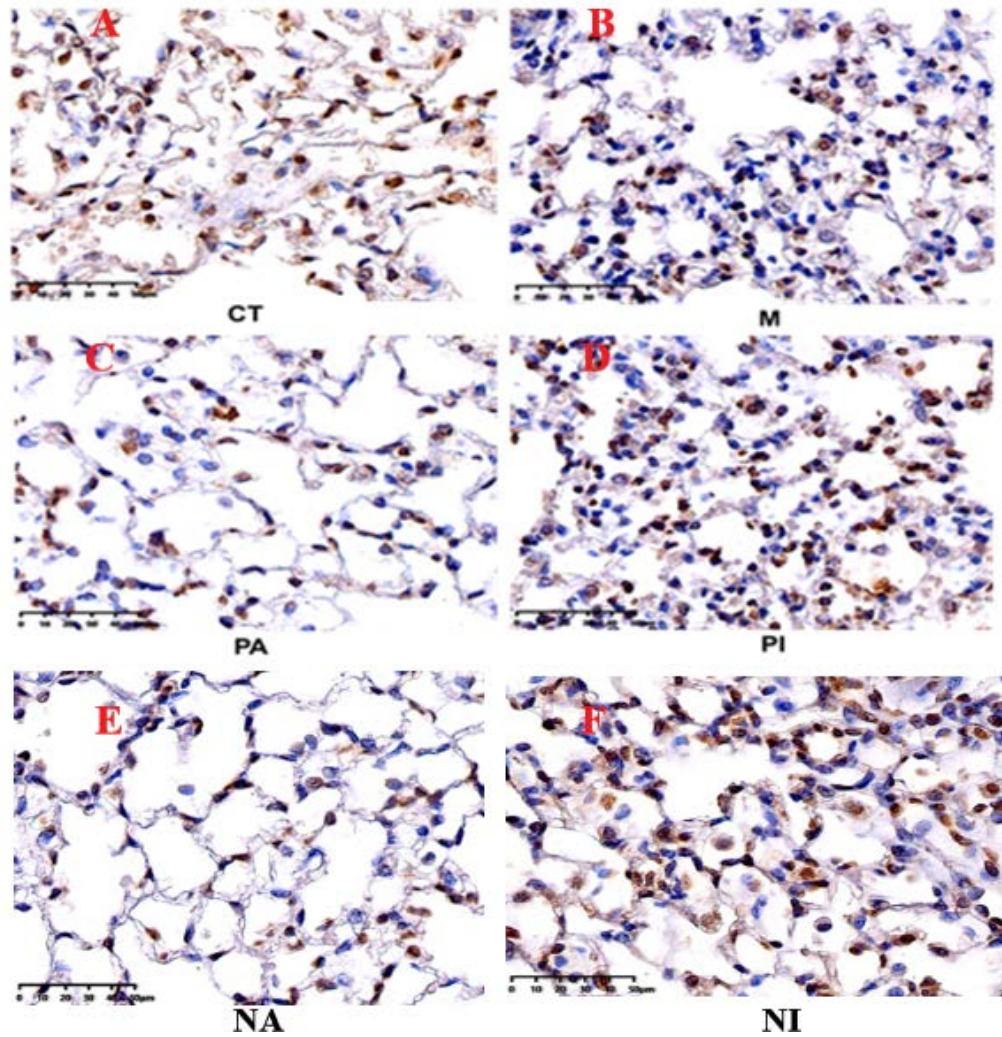Comparing with the control group, ##: P<0.01. Comparing with the model group,

**: P<0.01.

Figure 1.10: Detection of apoptosis in lung tissue of mice

Comparing with the control group, ##: P<0.01. Comparing with the model group,

**: P<0.01.

Figure 1.11: Apoptosis detected by TUNEL method. The brown portion represents apoptotic cells, while the blue corresponds to normal cells.

4.1.8 The expression of CD68, INOS, CD163, PPAR γ, and Nrf2 in alveolar macrophages of mice

Expression of CD68 in alveolar macrophages of mice

CD68 mark alveolar macrophages. There was a statistically significant difference between groups as determined by one-way ANOVA Following modeling. Compared with CT group (9.62 ± 1.29), the expression of CD68 in alveolar macrophages of M group (13.76 ± 0.44) increased significantly

(P=0.003). See Table 1.11, figure 1.12, 1.13 A, B.

Compared with M group (13.76±0.44), the expression in PA group (7.65±0.23) and NA group (7.74±0.49) decreased significantly (P=0). See Table 1.11, figure 1.12, 1.13 B, C, E.
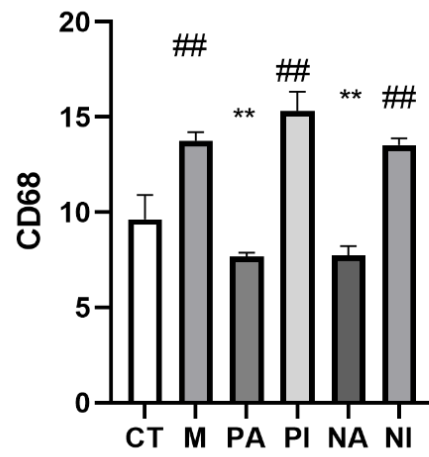
But there was no significant change in PI group (15.32±1.02, P=0.110) and NI group (13.53±0.35, p=0.987). See Table 1.11, figure 1.12, 1.13 B, D, F.

Table 1.11: Expression of CD68 in pulmonary macrophages of mice (n=6, IOD, $\bar{x}$±s)

	CD68	P
CT	9.62±1.29	
M	13.76±0.44[##]	0.003
PA	7.65±0.23[**]	0
PI	15.32±1.02[##]	0.110
NA	7.74±0.49[**]	0
NI	13.53±0.35[##]	0.987

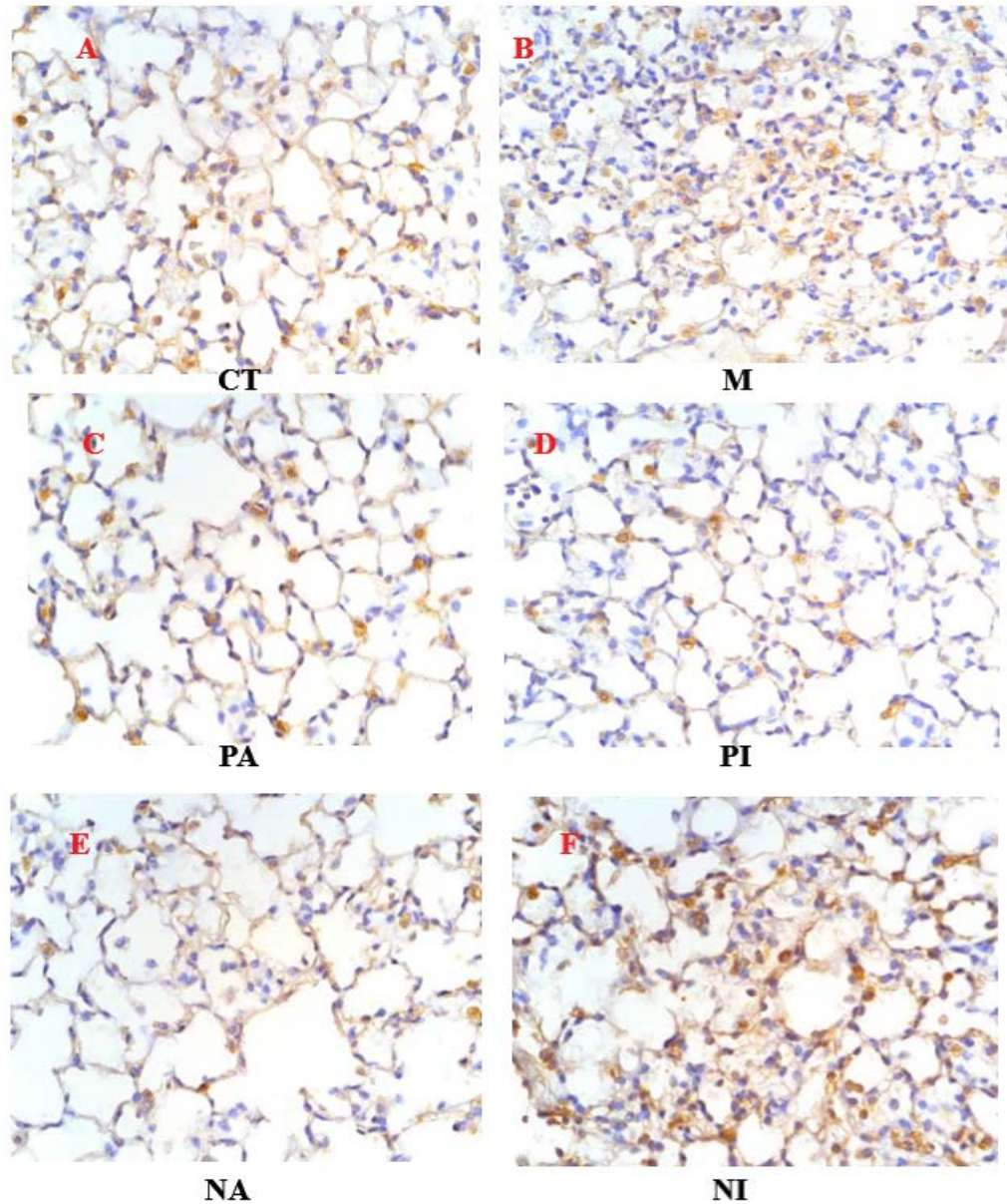Comparing with the control group, ##: P<0.01. Comparing with the model group, **: P<0.01.

Figure 1.12: Expression of CD68 in mice alveolar macrophages

Comparing with the control group, ##: $P<0.01$. Comparing with the model group,

**: $P<0.01$.

Figure 1.13: Expression of CD68 in lung tissue of mice. The brown color indicates immunohistochemical positivity.

Expression of INOS in alveolar macrophages of mice

INOS mark M1 alveolar macrophages. There was a statistically significant difference between groups as determined by one-way ANOVA Following modeling. Compared with CT group (8.58 ± 0.84), the expression of INOS in alveolar macrophages of M group (19.77 ± 2.19) increased significantly ($P=0$).

See Table 1.12, figure 1.14, 1.15 A, B.

Compared with M group (19.77±2.19), the expression in PA group (9.07±0.78) and NA group (9.29±0.68) decreased significantly (P=0), See Table 1.12, figure 1.14, 1.15 B, C, E

There was no significant change in PI group (16.24±0.67, P=0.085) and NI group (15.72±0.38, P=0.051). See Table 1.12, figure 1.14, 1.15 B, D, F.

Table 1.12: Expression of INOS in pulmonary macrophages of mice (n=6, IOD, $\bar{x}$±s)

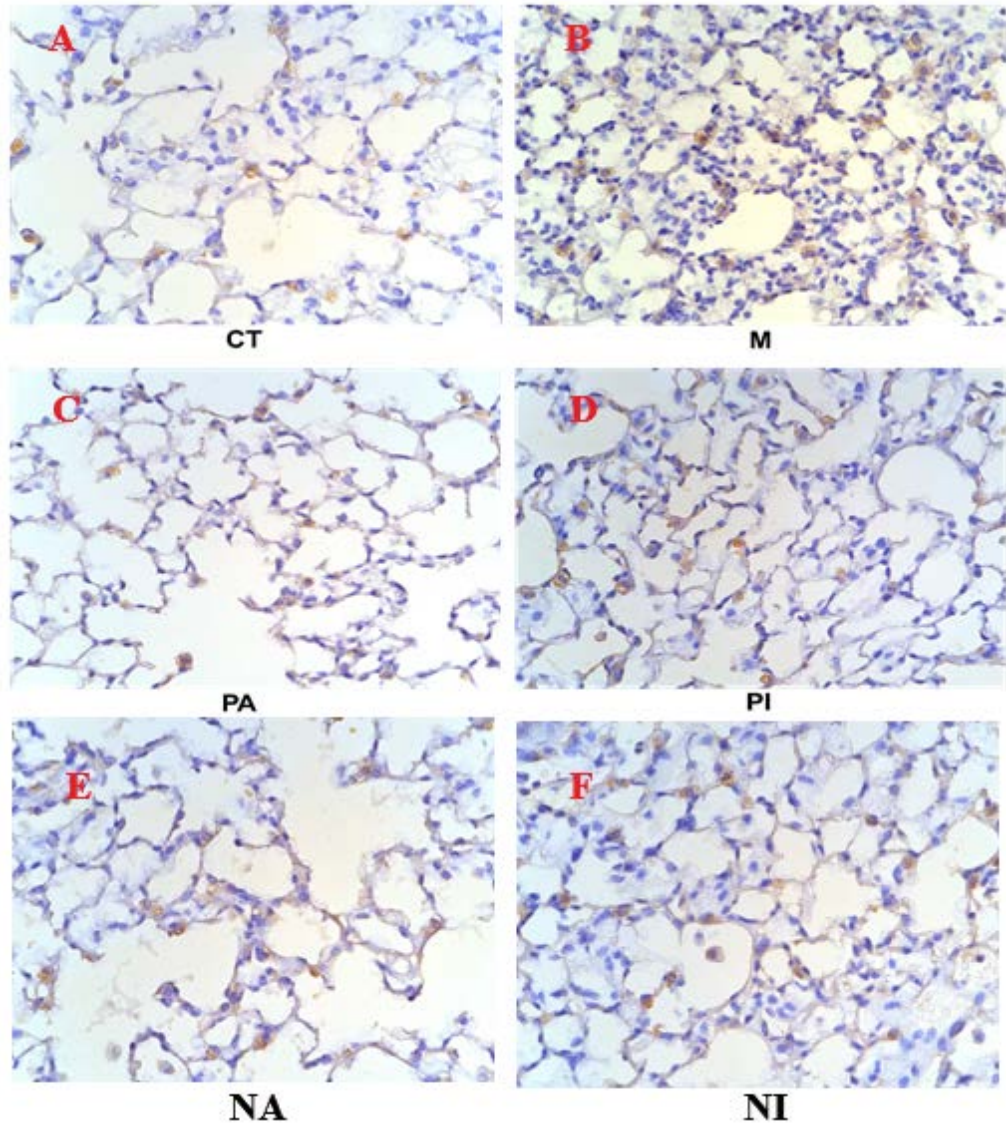|	INOS	P
CT	8.58±0.84	
M	19.77±2.19[##]	0
PA	9.07±0.78[**]	0
PI	16.24±0.67[##]	0.085
NA	9.29±0.68[**]	0
NI	15.72±0.38[##]	0.051

Comparing with the control group, ##: P<0.01. Comparing with the model group, **: P<0.01.
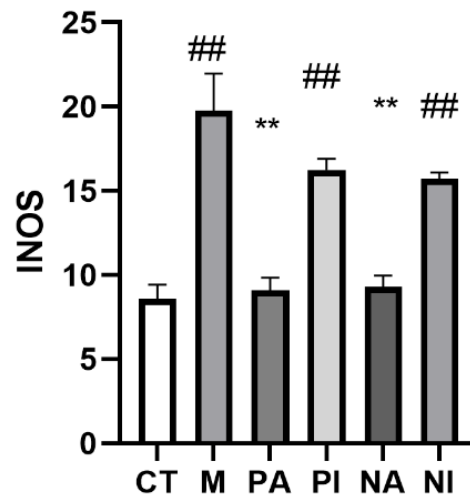
Figure 1.14 Expression of INOS in mice alveolar macrophages

Comparing with the control group, ##: $P<0.01$. Comparing with the model group,

**: $P<0.01$.

Figure 1.15: Expression of INOS in lung tissue of mice. The brown color indicates immunohistochemical positivity.

Expression of CD163 in alveolar macrophages of mice

CD163 mark M2 alveolar macrophages. There was a statistically significant difference between groups as determined by one-way ANOVA Following modeling.

Compared with CT group (9.04±0.39), the expression of CD163 in alveolar macrophages of M group (15.11±0.44) increased significantly (P=0). See Table 1.13, figure 1.16, 1.17 A, B.

Compared with M group (15.11±0.44), the expression in PA group (9.36±0.35) and NA group (9.42±0.30) decreased significantly (P=0). See Table 1.13, figure 1.16, 1.17 B, C, E

There was no significant change in PI group and NI group (P>0.05). See Table 1.13, figure 1.16, 1.17 B, D, F.

Table 1.13: Expression of CD163 in pulmonary macrophages of mice (IOD，n=6，$\bar{x}$±s)

	CD163	P
CT	9.04±0.39	
M	15.11±0.44[##]	0
PA	9.36±0.35[**]	0
PI	14.84±0.67[##]	0.998
NA	9.42±0.30[**]	0
NI	14.86±1.18[##]	1

Comparing with the control group, ##: P<0.01. Comparing with the model group, **: P<0.01.
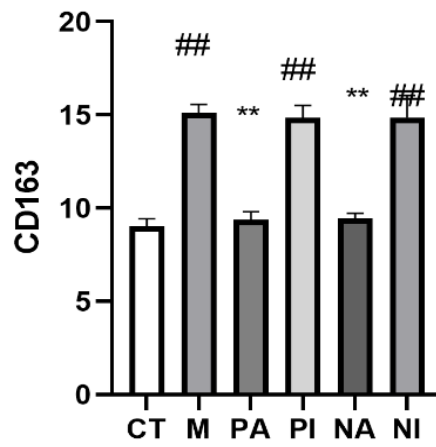
Figure 1.16: Expression of CD163 in mice alveolar macrophages

Comparing with the control group, ##: P<0.01. Comparing with the model group,

**: P<0.01.
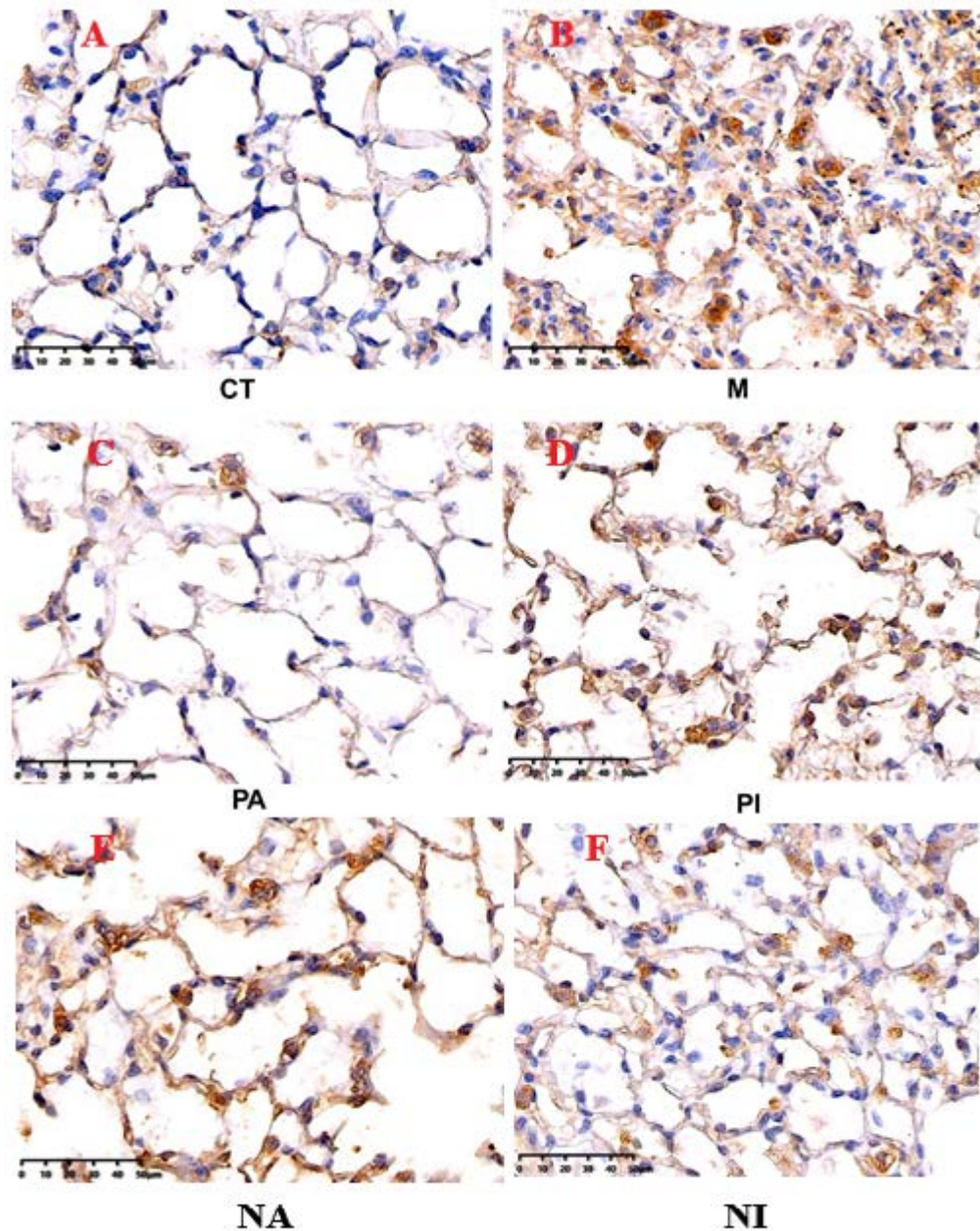
Figure 1.17: Expression of CD163 in lung tissue of mice. The brown color indicates immunohistochemical positivity.

Expression of PPAR γ in alveolar macrophages of mice

There was a statistically significant difference between groups as determined by one-way ANOVA Following modeling.

Compared with CT group (18.85±0.39), the expression of PPAR γ in alveolar macrophages of M group (12.69±0.85) decreased significantly (P=0). See Table 1.14, figure 1.18, 1.19.

Compared with M group (12.69±0.85), the expression was significantly increased in PA group (19.14±0.36, P=0) and decreased in PI group (10.39±0.40, P=0).

There was no significant change in NA group (12.87±0.45, P=0.543) and NI group (12.42±0.50, P=0.385). See Table 1.14, figure 1.18, 1.19.

Table 1.14: Expression of PPAR γ in pulmonary macrophages of mice (IOD，n=6，$\bar{x}$±s)

|	PPAR γ	P
CT	18.85±0.39	
M	12.69±0.85[##]	0
PA	19.14±0.36[**]	0
PI	10.39±0.40[##**]	0
NA	12.87±0.45[##]	0.543
NI	12.42±0.50[##]	0.385

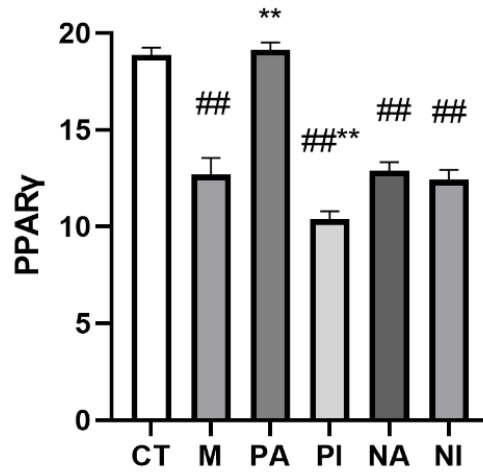Comparing with the control group, ##: P<0.01. Comparing with the model group, **: P<0.01.

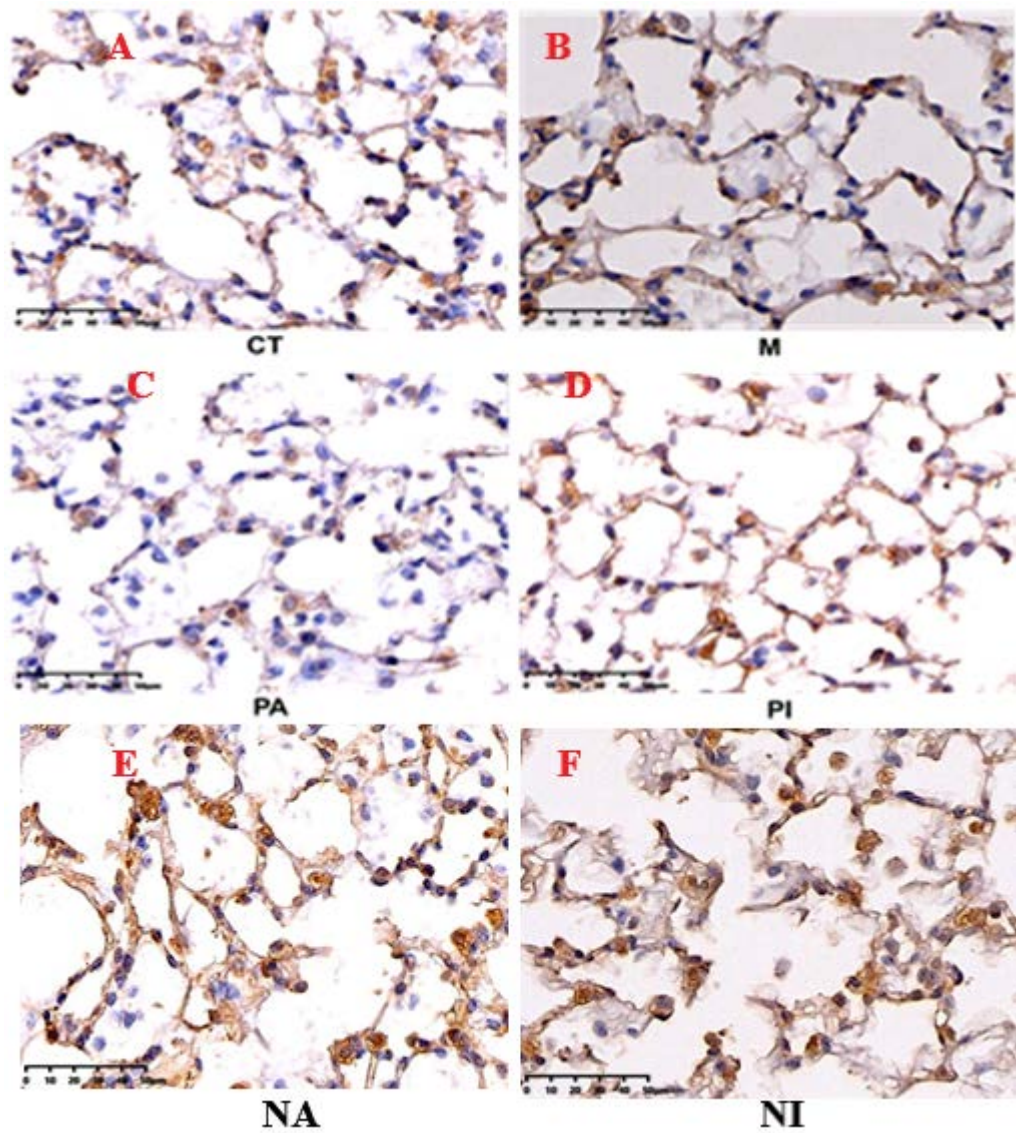**Figure 1.18: Expression of PPAR γ in mice alveolar macrophages**

Figure 1.19: Expression of PPAR γ in lung tissue of mice. The brown color

indicates immunohistochemical positivity.

Expression of Nrf2 in alveolar macrophages of mice

There was a statistically significant difference between groups as determined by one-way ANOVA Following modeling. Compared with CT group (6.04±0.62), the expression of Nrf2 in alveolar macrophages of M group (14.91±0.51) increased significantly (P=0). See table 1.15, figure 1.20, 1.21 A, B.

Compared with M group (14.91±0.51), the expression in NA group (20.33±0.82) increased significantly (P=0). See table 1.15, figure 1.20, 1.21 B, E.

There was no significant change in PA (15.36±1.87), PI (14.98±1.21), NI (14.64±0.62) groups (P=1, P=1, P=0.998). See table 1.15, figure 1.20, 1.21 B, C, D, F.

Table 1.15: Expression of Nrf2 in pulmonary macrophages of mice (IOD，n=6，$\bar{x}$±s)

	Nrf2	P
CT	6.04±0.62	
M	14.91±0.51[##]	0
PA	15.36±1.87[##]	1
PI	14.98±1.21[##]	1
NA	20.33±0.82[##**]	0
NI	14.64±0.62[##]	0.998

Comparing with the control group, ##: P<0.01. Comparing with the model group,
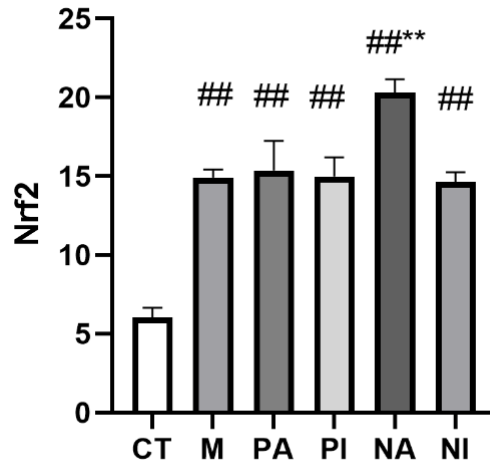
**: P<0.01.

Figure 1.20: Expression of Nrf2 in mice alveolar macrophages

Comparing with the control group, ##: P<0.01. Comparing with the model group,

**: P<0.01.
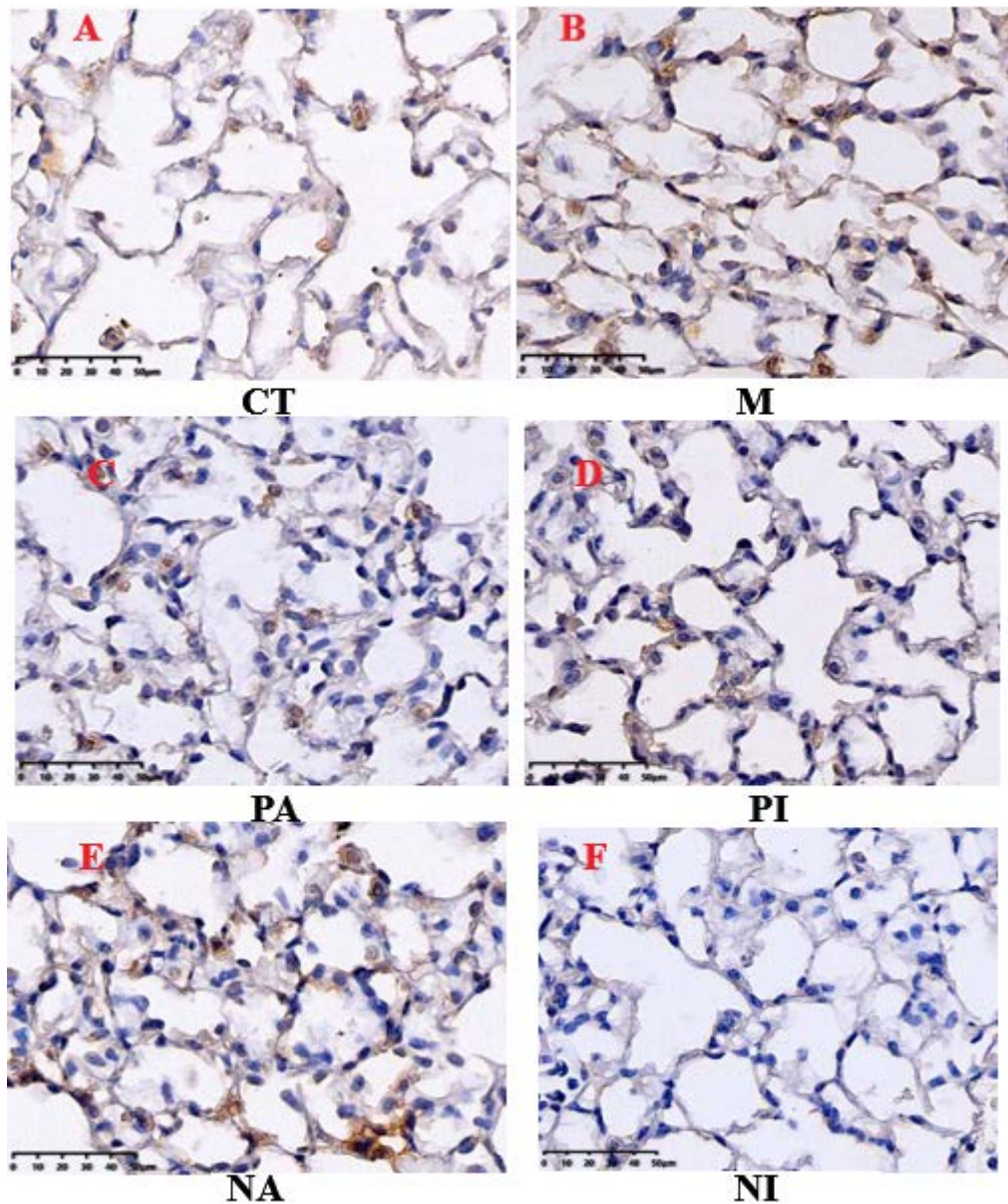
Figure 1.21: Expression of Nrf2 in alveolar macrophages of mice in each group. The brown color indicates immunohistochemical positivity.

4.2 Comparison results among CT, M, PA, NA, and BYF groups

4.2.1 Physical Overview

In the BPI group, 1 mouse died in the 11th week due to improper gavage operation, and another mouse died from fatal injuries caused by biting. In the

BNI group, two mice died in the 6th week, and post-mortem examination revealed purulent spots in the lungs, suggesting death from pulmonary abscess. In the BPNI group, 1 mouse died in the 7th week from injuries caused by biting, and another mouse died in the 12th week due to improper gavage operation.

4.2.2 Weight change

The body weight of mice in each group increased over time. There was a statistically significant difference between groups as determined by one-way ANOVA Following modeling. The M group (24.10±2.32 g) exhibited a significant decrease in body weight compared to the CT group (26.85±1.53 g) (P=0.023).

Following drug intervention, there were no significant changes in body weight in the NA (24.28±1.88 g, P=0.873), PA (25.00±1.20 g, P=0.437), and BYF groups (24.41±2.61 g, P=0.783) compared to the M group (24.10±2.32 g).

Table 2.1: Changes of body weight in mice (g, $\bar{x}\pm s$)

	N	0	P	4 weeks	P	8 weeks	P	12 weeks	P
CT	12	21.12±0.93		23.92±1.64		25.67±1.53		26.85±1.53	
M	10	20.32±1.35	0.126	20.25±1.90[#]	0.043	21.40±2.22[##]	0	24.10±2.32[#]	0.023
PA	12	20.90±0.70	0.260	20.88±0.61[#]	0.990	22.87±1.42[#]	0.180	25.00±1.20	0.437
NA	12	21.03±0.56	0.169	21.93±1.21	0.550	23.58±2.08	0.050	24.28±1.88[#]	0.873
BYF	10	21.22±0.59	0.087	21.78±1.10	0.622	23.00±1.81[##]	0.145	24.41±2.61[#]	0.783

Comparing with the control group, #: $P<0.05$, ##: $P<0.01$.
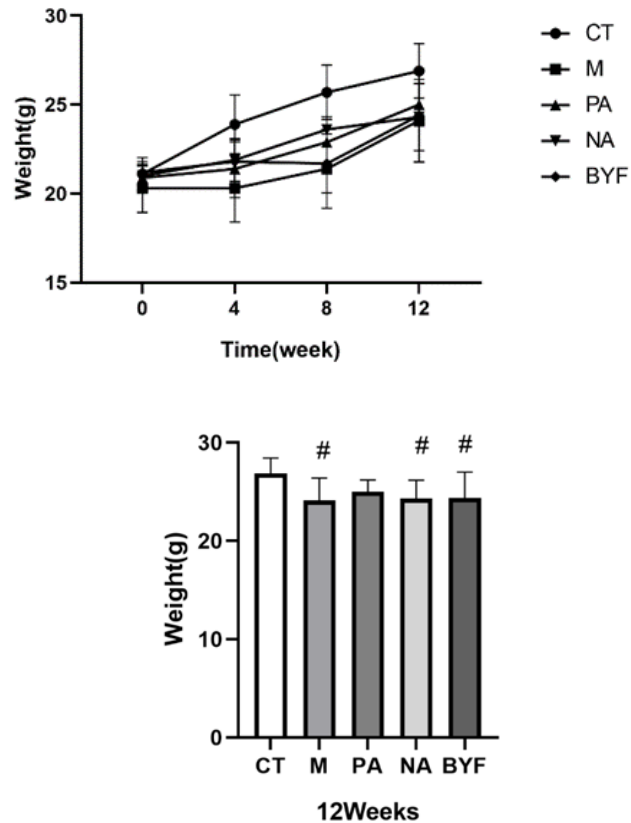
Figure 2.1: The change of body weight of mice and the weight of mice at the 12th week

Comparing with the control group, #: P<0.05, ##: P<0.01. Comparing with the model group, **: P<0.01.

4.2.3 Pulmonary function(TV、MV、PEF、EF50)

There was a statistically significant difference between groups as determined by one-way ANOVA Following modeling. Compared to the CT group (0.39±0.02 mL, 179.32±17.70 mL/min, 9.99±0.67 mL/s, 0.49±0.04 mL/s), the M group showed a significant decrease in TV (0.28±0.03 mL, P=0), MV (120.35±13.01 mL/min, P=0), PEF (5.72±0.38 mL/s, P=0), and EF50 (0.27±0.05

mL/s, P=0). Please refer to Tables 2.2, 2.3, 2.4, and 2.5, as well as Figures 2.2, 2.3, 2.4, and 2.5.

Compared to the M group (0.28±0.03 mL, 120.35±13.01 mL/min, 5.72±0.38 mL/s, 0.27±0.05 mL/s), the PA (0.33±0.01 mL, P=0.003. 151.24±9.37 mL/min, P=0.001. 6.84±0.59 mL/s, P=0.016. 0.36±0.05 mL/s, P=0.009) and NA groups (0.36±0.03 mL, P=0. 162.15±14.4 mL/min, P=0. 7.83±0.96 mL/s, P=0. 0.39±0.06 mL/s, P=0.001) exhibited an increased TV, MV, PEF, and EF50. Please refer to Tables 2.2, 2.3, 2.4, and 2.5, as well as Figures 2.2, 2.3, 2.4, and 2.5.

The BYF group showed an upregulation of TV (0.33±0.04 mL, P=0.010), MV (150.93±17.70 mL/min, P=0.001), PEF (7.07±0.96 mL/s, P=0.004) and EF50 (0.38±0.06 mL/s, P=0.002) (P<0.05). Please refer to Tables 2.2, 2.3, 2.4, and 2.5, as well as Figures 2.2, 2.3, 2.4, and 2.5.

Table 2.2: Changes of TV in mice (mL, $\bar{x}\pm s$)

	N	0	P	4 weeks	P	8 weeks	P	12 weeks	P
CT	12	0.27±0.01		0.36±0.03		0.34±0.03		0.39±0.02	
M	10	0.26±0.02	1	0.29±0.01[##]	0	0.27±0.01[##]	0	0.28±0.03[##]	0
PA	12	0.26±0.02	1	0.31±0.03[##]	0.105	0.29±0.02[##*]	0.048	0.33±0.01[##**]	0.003
NA	12	0.25±0.01	0.889	0.30±0.02[##]	0.211	0.30±0.01[#**]	0.005	0.36±0.03[#**]	0
BYF	10	0.26±0.01	0.999	0.31±0.03[##]	0.063	0.29±0.03[##]	0.137	0.33±0.04[##*]	0.010

Comparing with the control group, #: $P<0.05$, ##: $P<0.01$. Comparing with the model group, *: $P<0.05$, **: $P<0.01$.

Table 2.3: Changes of MV in mice (mL/min, $\bar{x}\pm s$)

	N	0	P	4 weeks	P	8 weeks	P	12 weeks	P
CT	12	133.23±13.09		169.03±31.61		148.64±21.04		179.32±17.70	
M	10	128.49±14.59	0.999	133.82±17.83[##]	0.006	114.04±12.67[##]	0	120.35±13.01[##]	0
PA	12	130.26±12.65	1	137.31±21.91[#]	0.770	122.62±11.30[##]	0.274	151.24±9.37[##**]	0.001
NA	12	132.09±9.47	1	146.56±11.06	0.290	121.73±4.23[##]	0.325	162.15±14.4[**]	0
BYF	10	132.09±4.46	0.999	158.76±12.60[*]	0.044	115.31±11.43[##]	0.870	150.93±17.70[##**]	0.001

Comparing with the control group, #: $P<0.05$, ##: $P<0.01$. Comparing with the model group, *: $P<0.05$, **: $P<0.01$.

Table 2.4: Changes of PEV in mice (mL/s，$\bar{x}\pm s$)

	N	0	P	4 weeks	P	8 weeks	P	12 weeks	P
CT	12	6.63±0.38		8.86±0.81		7.58±0.92		9.99±0.67	
M	10	7.33±0.88	0.580	6.98±0.33##	0	6.19±0.71##**	0.001	5.72±0.38##	0
PA	12	7.04±0.24	0.987	7.82±0.66#	0.052	6.40±0.32##	0.562	6.84±0.59##*	0.016
NA	12	6.55±0.29	0.433	8.40±0.64**	0.002	6.17±0.28##	0.963	7.83±0.96##**	0
BYF	10	6.75±0.42	0.766	8.39±0.94**	0.002	6.74±0.62#	0.141	7.07±0.96##**	0.004

Comparing with the control group, #: P<0.05, ##: P<0.01. Comparing with the model group, *: P<0.05, **: P<0.01.

**Table 2.5 Changes of EF50 in mice (mL/s，$\bar{x}\pm s$)**

	N	0	P	4 weeks	P	8 weeks	P	12 weeks	P
CT	12	0.25±0.01		0.27±0.03		0.29±0.05		0.49±0.04	
M	10	0.27±0.04	0.240	0.23±0.03##	0.003	0.21±0.02##	0	0.27±0.05##	0
PA	12	0.26±0.02	0.894	0.23±0.02##	0.623	0.23±0.02##	0.197	0.36±0.05##**	0.009
NA	12	0.26±0.01	0.674	0.25±0.02*	0.042	0.22±0.02##	0.424	0.39±0.06##**	0.001
BYF	10	0.25±0.02	0.365	0.23±0.02##	0.672	0.24±0.01##	0.058	0.38±0.06##**	0.002

Comparing with the control group, #: P<0.05, ##: P<0.01. Comparing with the model group, *: P<0.05, **: P<0.01.
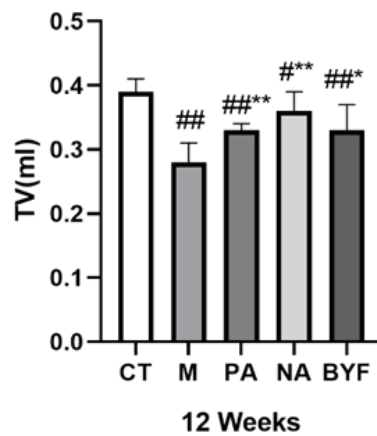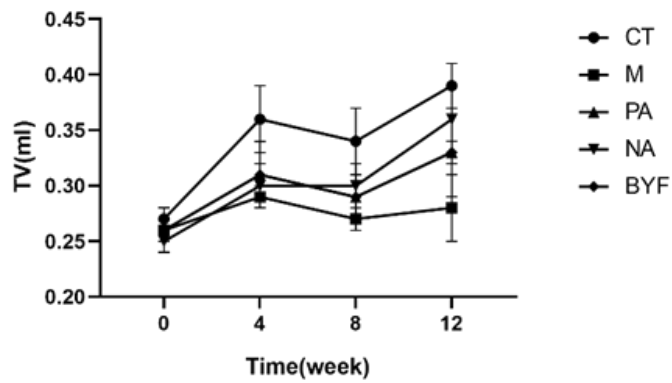
Figure 2.2: Changes of TV in mice and TV value of each group at the 12th week.

Comparing with the control group, #: P<0.05, ##: P<0.01. Comparing with the model group, *: P<0.05, **: P<0.01.
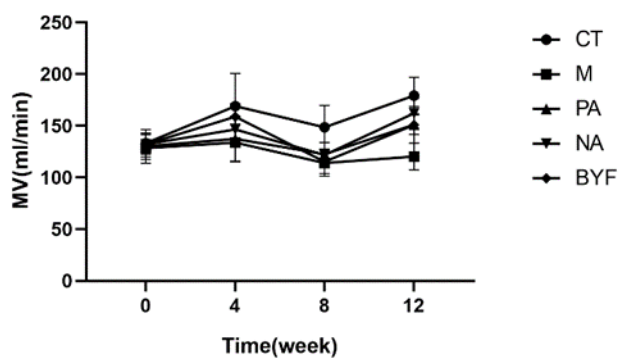
Figure 2.3: Changes of MV and MV value of each group at the 12th week

Comparing with the control group, ##: P<0.01. Comparing with the model group,
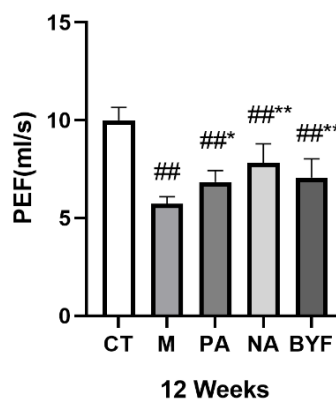
**: P<0.01.

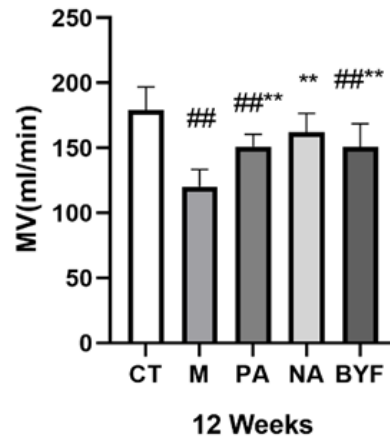**Figure 2.4: Changes of PEF in mice and PEF value of each group at the**

12th week

Comparing with the control group, ##: P<0.01. Comparing with the model group,

*: P<0.05, **: P<0.01.
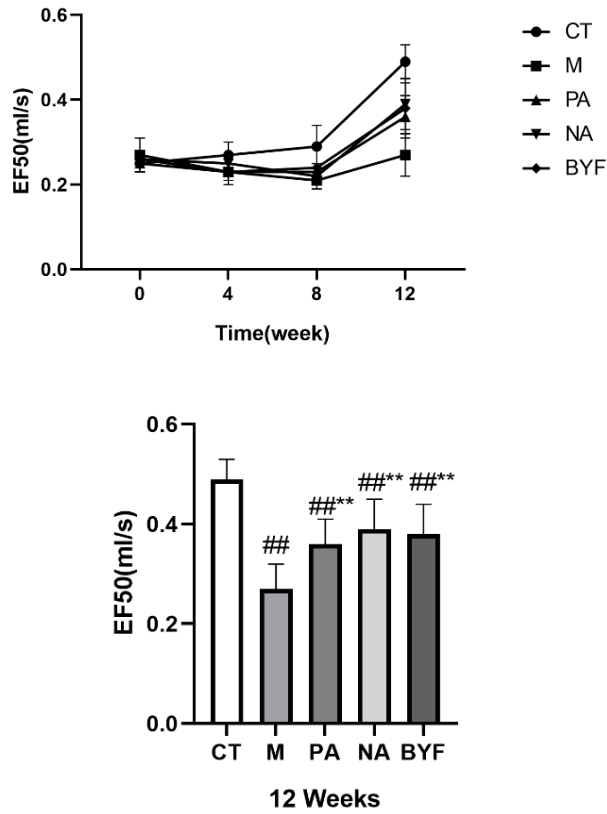
Figure 2.5: Changes of EF50 in mice and EF50 value of each group at the

12th week

Comparing with the control group, ##: P<0.01. Comparing with the model group,

**: P<0.01.

4.2.4 Pathological changes of lung tissues
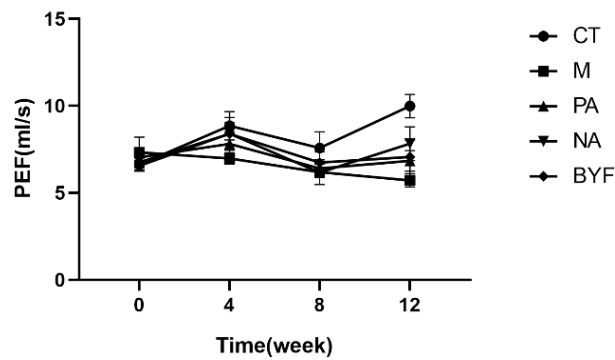
The CT, M, PA, NA group has been discussed in 4.1.1. In the BYF group, the

alveolar size was relatively uniform, and the alveolar wall structure appeared

intact. Please refer to Figure 2.6 B, E.
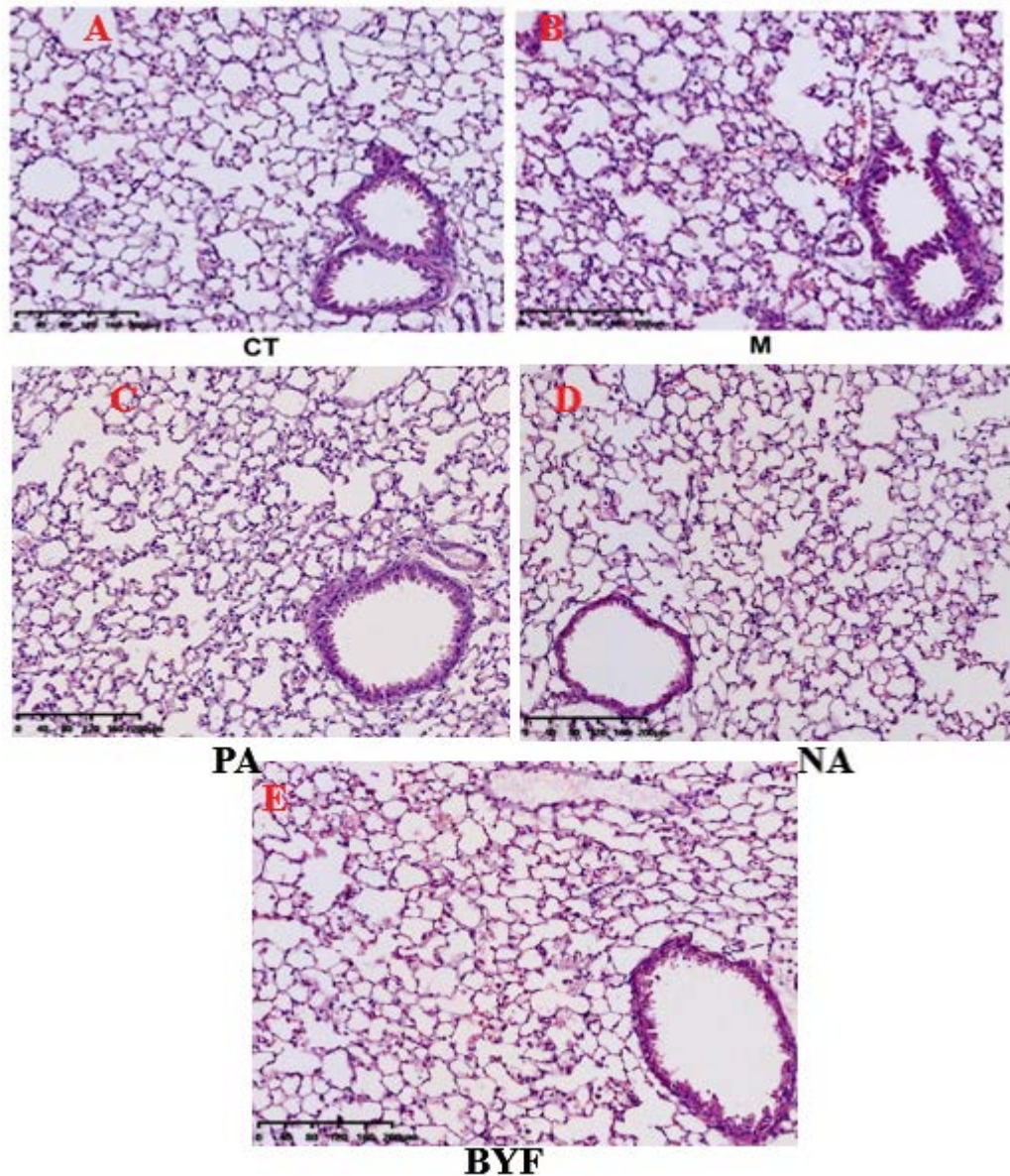
Figure 2.6: Lung histopathology of mice in each group

4.2.5 Determination of TNF α and IL-4 in lung tissue homogenate

There was a statistically significant difference between groups as determined by one-way ANOVA Following modeling. Compared to the M group (642.16±146.03 pg/mL, 431.39±50.17 pg/mL), the expression of TNFα and IL-4 in the BYF group (345.41±70.47 pg/mL, 267.07±111.37 pg/mL, P=0)

exhibited a significant decrease. Please refer to Tables 2.6, Figures 2.7.

Table 2.6: Expression of TNF α and IL-4 in lung homogenate of mice (pg/mL, n=6, $\bar{x}$±s)

	TNFα	P	IL-4	P
CT	325.99±84.63		343.24±48.87	
M	642.16±146.03##	0	431.39±50.17#	0.032
PA	286.57±44.66**	0	237.05±32.05#**	0
NA	322.22±52.66**	0	270.59±65.95**	0
BYF	345.41±70.47**	0	267.07±111.37**	0

Comparing with the control group, #: P<0.05, ##: P<0.01. Comparing with the model group, **: P<0.01.
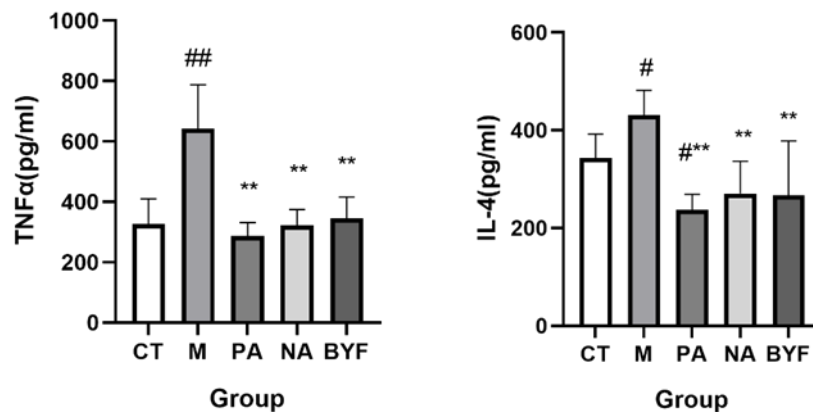
Figure. 2.7: Expression of TNF α and IL-4 in lung homogenate of mice

Comparing with the control group, #: P<0.05, ##: P<0.01. Comparing with the model group, **: P<0.01.

4.2.6 Detection of cellular efferocytosis function of alveolar macrophages in

COPD mice

There was a statistically significant difference between groups as determined by one-way ANOVA Following modeling. Compared to the M group (81.0±12.70), the efferocytosis ability in the BYF group (102.86±8.18) showed a significant increase (P=0.003). See Table 2.7, Figure 2.8.

Table 2.7: Cell efferocytosis of mice alveolar macrophages (n=6, RFU, $\bar{x}$±s)

	Geo Mean	P
CT	122.29±6.29	
M	81.0±12.70[##]	0
PA	111.65±13.90[**]	0
NA	116.75±13.97[**]	0
BYF	102.86±8.18[##**]	0.003

Comparing with the control group, ##: P<0.01. Comparing with the model group, **: P<0.01.
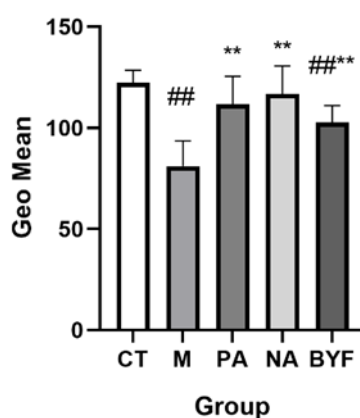
Figure 2.8: Detection of cell efferocytosis ability of alveolar macrophages in mice

Comparing with the control group, ##: P<0.01. Comparing with the model group,

**: P<0.01.

4.2.7 Detection of apoptosis in lung tissue of mice

Compared to the M group (61.68±4.37%), there was a significant decrease in

the BYF group (41.30±1.25%, P=0). See Table 2.8, Figure 2.9, 2.10 B, E.

Table 2.8: Apoptosis index of lung tissue in mice (n=6, %, $\bar{x}$±s)

	AI400	P
CT	41.34±1.69	
M	61.68±4.37[##]	0
PA	38.78±3.65[**]	0
NA	43.40±1.25[**]	0.001
BYF	41.30±1.25[**]	0

Comparing with the control group, ##: P<0.01. Comparing with the model group,
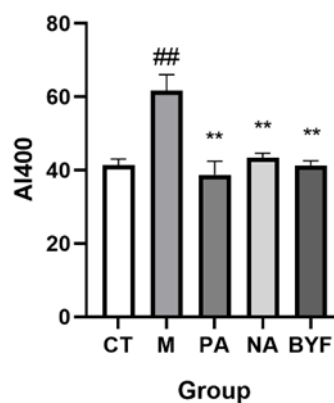
**: P<0.01.

Figure. 2.9: Detection of apoptosis in lung tissue of mice

Comparing with the control group, ##: P<0.01. Comparing with the model group,

**: P<0.01.
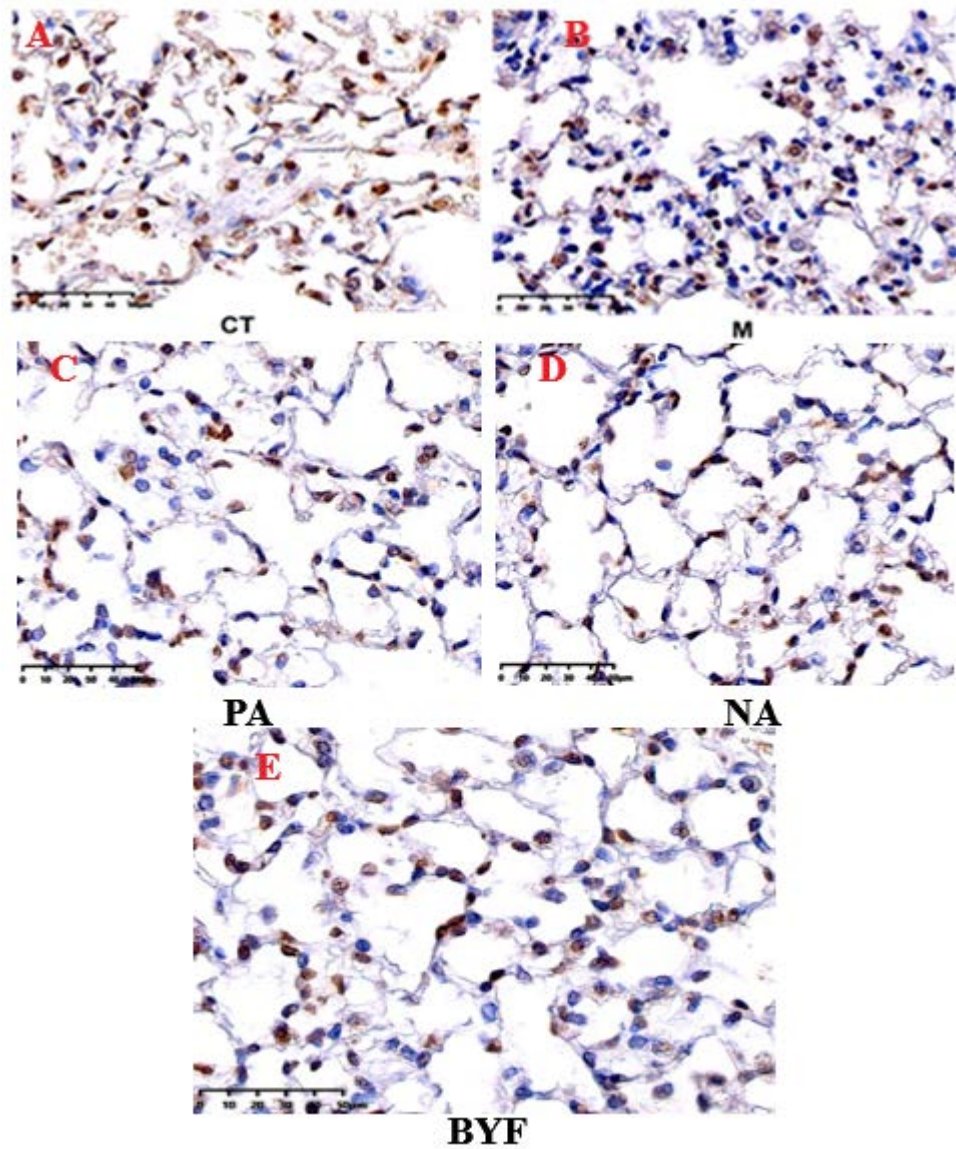
Figure. 2.10: Apoptosis detected by TUNEL method. The brown portion represents apoptotic cells, while the blue corresponds to normal cells.

4.2.8 The expression of CD68, INOS, CD163, PPAR γ, and Nrf2 in alveolar macrophages of mice

**Expression of CD68 in alveolar macrophages of mice**

CD68 mark alveolar macrophages. There was a statistically significant difference between groups as determined by one-way ANOVA Following

modeling. Compared to the M group (13.76±0.44), there was a significant

decrease in the BYF group (8.34±0.45, P=0.003). See Table 2.9, Figure 2.11,

2.12 B, E.

Table 2.9: Expression of CD68 in pulmonary macrophages of mice (n=6,

IOD, $\bar{x}$±s)

	CD68	P
CT	9.62±1.29	
M	13.76±0.44##	0
PA	7.65±0.23**	0
NA	7.74±0.49**	0
BYF	8.34±0.45**	0.003

Comparing with the control group, ##: P<0.01. Comparing with the model group,

**: P<0.01.

Figure 2.11: Expression of CD68 in mice alveolar macrophages

Comparing with the control group, ##: P<0.01. Comparing with the model group,

**: P<0.01.
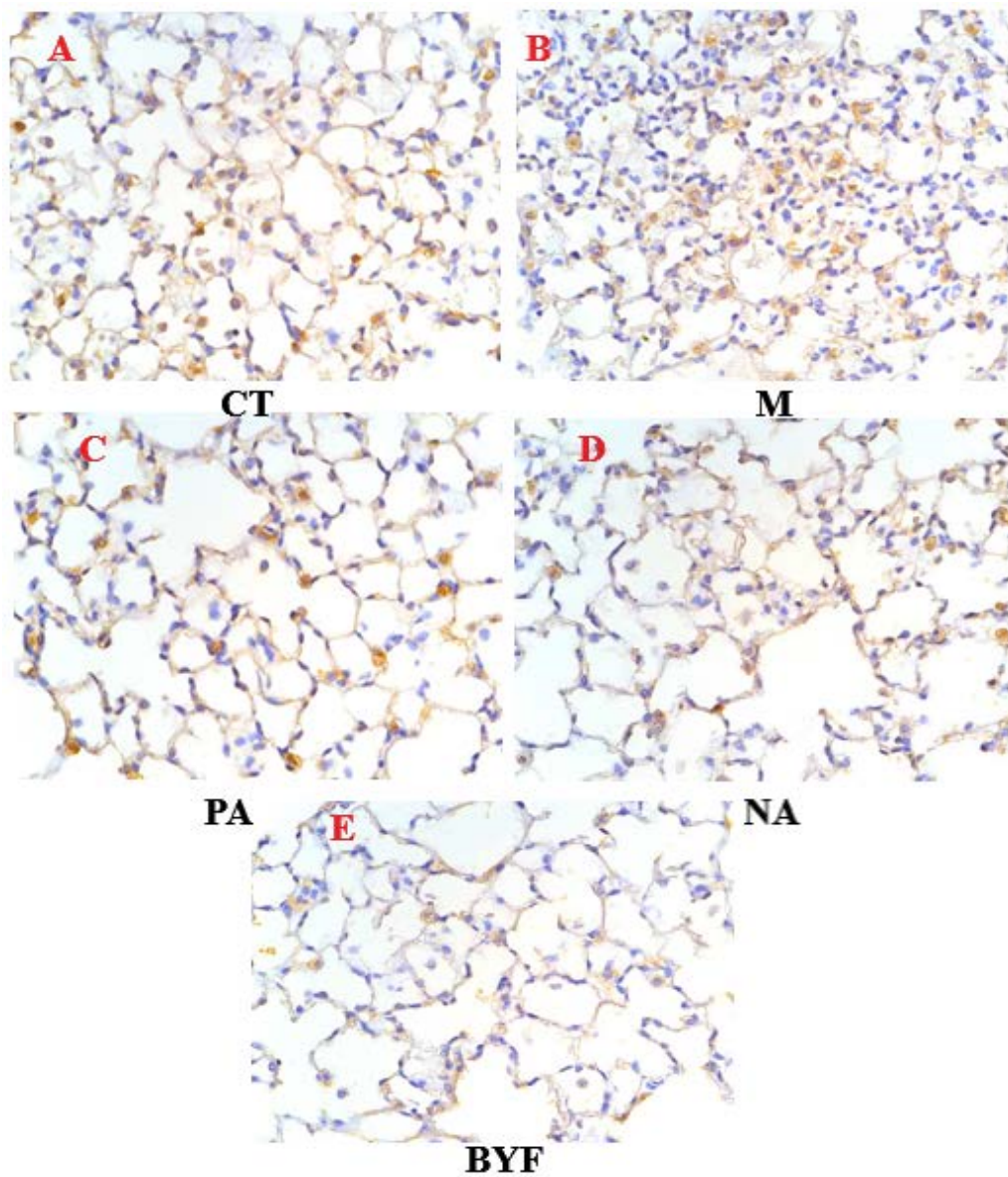
**Figure 2.12: Expression of CD68 in lung tissue of mice. The brown color indicates immunohistochemical positivity.**

Expression of INOS in alveolar macrophages of mice

INOS mark M1 alveolar macrophages. There was a statistically significant difference between groups as determined by one-way ANOVA Following

modeling. Compared to the M group (19.77±2.19), the expression in the BYF group (9.77±0.63) showed a significant decrease (P=0). See Table 2.10, and Figure 2.13, 2.14 B, E.

Table 2.10: Expression of INOS in pulmonary macrophages of mice (n=6, IOD, $\bar{x}$±s)

	INOS	P
CT	8.58±0.84	
M	19.77±2.19[##]	0
PA	9.07±0.78[**]	0
NA	9.29±0.68[**]	0
BYF	9.77±0.63[**]	0

Comparing with the control group, ##: P<0.01. Comparing with the model group, **: P<0.01.

Figure 2.13 Expression of INOS in mice alveolar macrophages

Comparing with the control group, ##: P<0.01. Comparing with the model group, **: P<0.01.
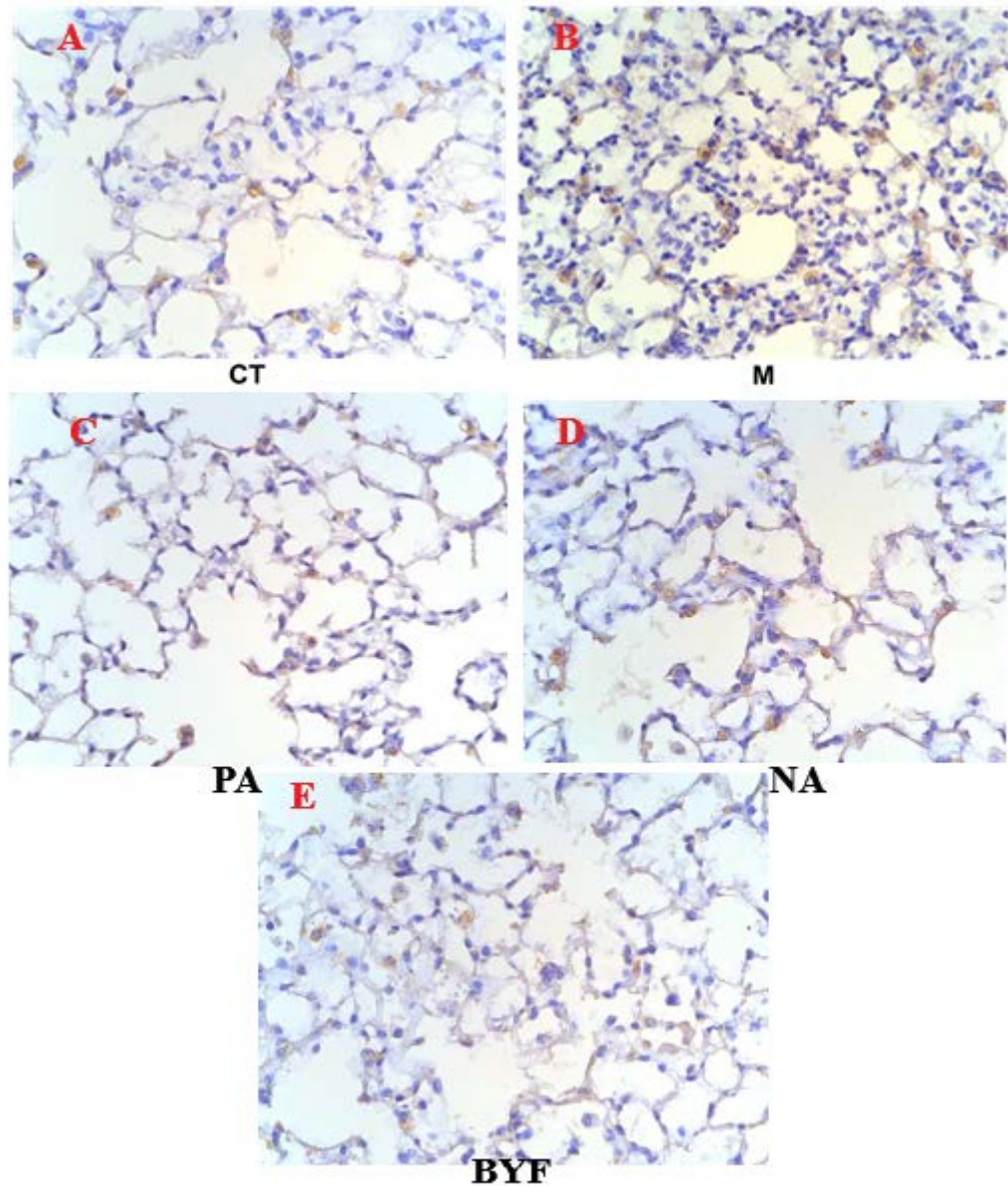
Figure 2.14: Expression of INOS in lung tissue of mice. The brown color indicates immunohistochemical positivity.

Expression of CD163 in alveolar macrophages of mice

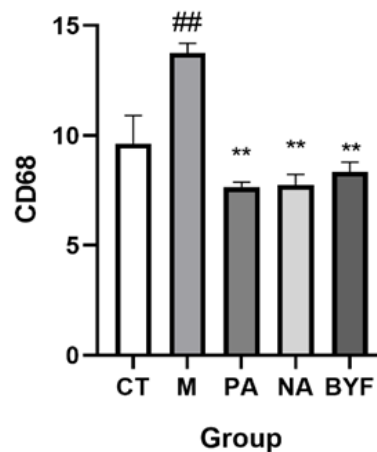CD163 mark M2 alveolar macrophages. There was a statistically significant difference between groups as determined by 3one-way ANOVA Following modeling. Compared to the M group (15.11±0.44), the expression in the BYF group (9.63±0.37) showed a significant decrease (P=0). See Table 2.11, and

Figure 2.15, 2.16 B, E.

Table 2.11: Expression of CD163 in pulmonary macrophages of mice (IOD，n=6，$\bar{x}\pm s$)

	CD163	P
CT	9.04±0.39	
M	15.11±0.44[##]	0
PA	9.36±0.45[**]	0
NA	9.42±0.30[**]	0
BYF	9.63±0.37[#**]	0

Comparing with the control group, #: P<0.05, ##: P<0.01. Comparing with the model group, **: P<0.01.
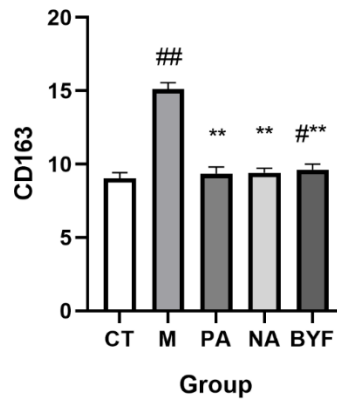
Figure 2.15: Expression of CD163 in mice alveolar macrophages

Comparing with the control group, #: P<0.05, ##: P<0.01. Comparing with the model group, **: P<0.01.
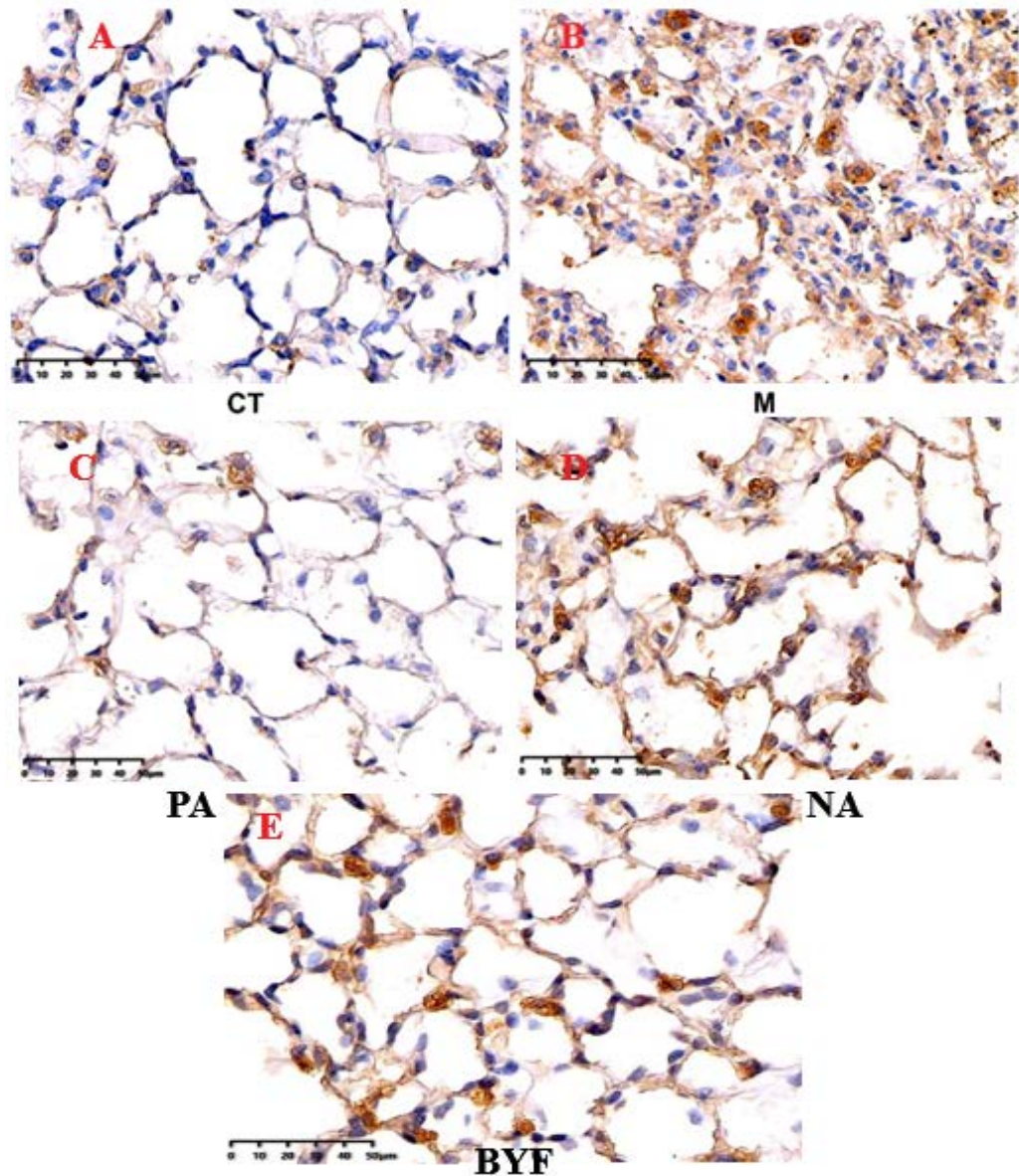
Figure 2.16: Expression of CD163 in lung tissue of mice. The brown color indicates immunohistochemical positivity.
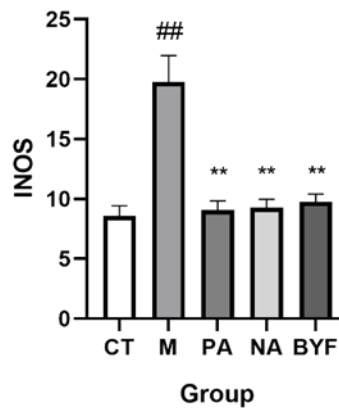
Expression of PPAR γ in alveolar macrophages of mice

There was a statistically significant difference between groups as determined by 3one-way ANOVA Following modeling. Compared to the M group (12.69±0.85), the expression in the BYF group (17.04±0.41) showed a significant increase (P=0). See Table 2.12, and Figure 2.17, 2.18 B, E.

Table 2.12: Expression of PPAR γ in pulmonary macrophages of mice

(IOD，n=6，$\bar{x}\pm s$)

	PPAR γ	P
CT	18.85±0.39	
M	12.69±0.85[##]	0
PA	19.14±0.36[**]	0
NA	12.87±0.45[##]	0.549
BYF	17.04±0.41[##**]	0

Comparing with the control group, ##: P<0.01. Comparing with the model group,
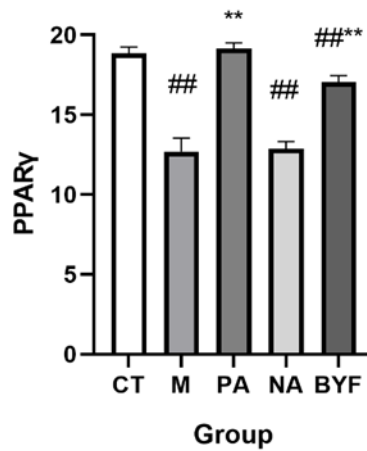
**: P<0.01.

Figure 2.17: Expression of PPAR γ in mice alveolar macrophages

Comparing with the control group, ##: P<0.01. Comparing with the model group,

**: P<0.01.
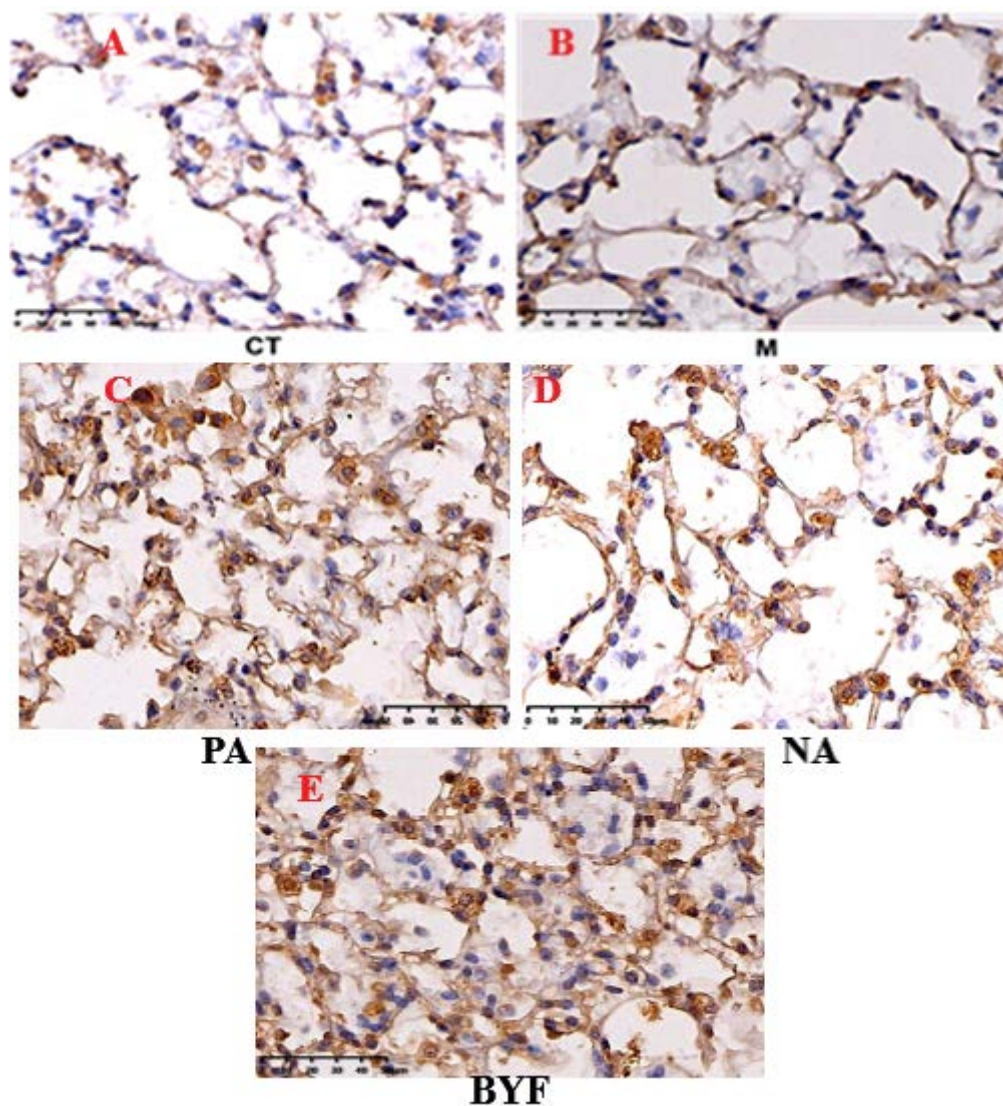
Figure 2.18: Expression of PPAR γ in lung tissue of mice. The brown color indicates immunohistochemical positivity.

Expression of Nrf2 in alveolar macrophages of mice

There was a statistically significant difference between groups as determined by 3one-way ANOVA Following modeling. Compared to the M group (14.91±0.51), the expression in the BYF group (20.82±0.49) showed a significant increase (P=0). See Table 2.13, and Figure 2.19, 2.20 B, E.

Table 2.13: Expression of Nrf2 in pulmonary macrophages of mice (IOD，

n=6，$\bar{x}\pm s$)

	Nrf2	P
CT	6.04±0.62	
M	14.91±0.51##	0
PA	15.36±1.87##	0.999
NA	20.33±0.82##**	0
BYF	20.82±0.49##**	0

Comparing with the control group, ##: P<0.01. Comparing with the model group,
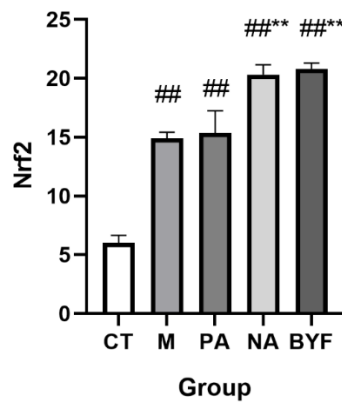
**: P<0.01.

Figure 2.19: Expression of Nrf2 in mice alveolar macrophages

Comparing with the control group, ##: P<0.01. Comparing with the model group,

**: P<0.01.
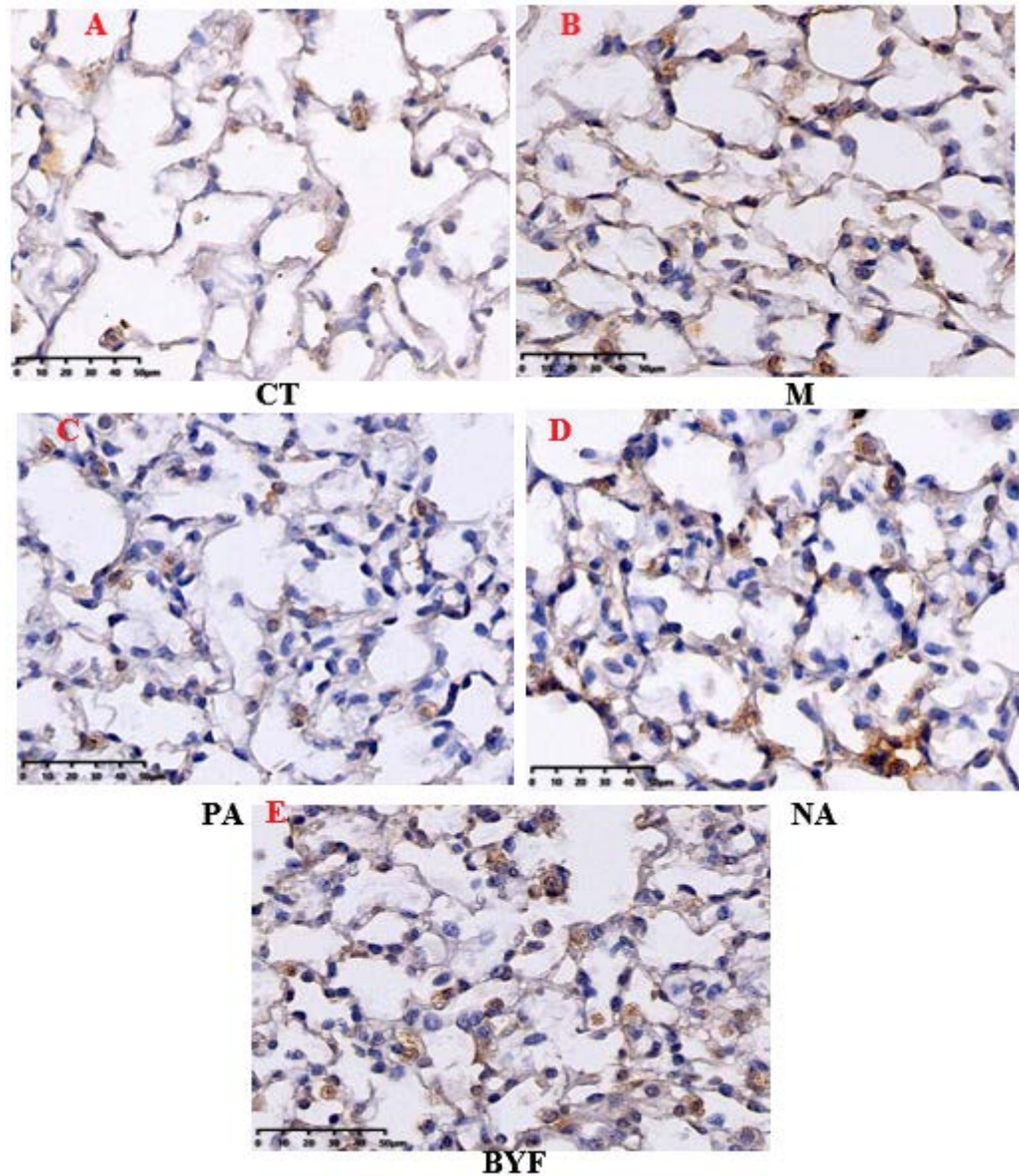
Figure 2.20: Expression of Nrf2 in alveolar macrophages of mice in each group. The brown color indicates immunohistochemical positivity.

4.3 Comparison results among CT, M, BPI, BNI, BYF and BPNI groups

4.3.1 Physical Overview

During the modeling period of 1-8 weeks COPD mice, the mice in CT group had good mental state, agile activity, smooth hair, normal diet, normal

defecation, and normal weight gain. Since the second week, the mice in group M showed restlessness, frequent bites and fights, and bites on the head, neck, abdomen, and tail of most mice. At the 6th week, the mice showed decreased irritability, dry hair, dispirited spirit, slow movement, reduced intake of food and water, and slow weight growth. The above symptoms of mice in BPI group, BNI group and BPNI group were relieved, but not as good as those in BYF group. In the BPI group, 1 mouse died of improper intragastric administration, and 1 mouse died of bite in the 11th week. In the BNI group, 2 mice died at the 6th week, and lung abscess was found after dissection, which was the death of lung abscess. In the BYF group, 2 mice died at the 12th and 13th week, respectively. After dissection, it was found that there was residual drug fluid in the bronchus. In the BPNI group, 1 mouse died of bite at the 7th week and 1 mouse died of improper intragastric administration at the 12th week.

4.3.2 Weight change

There was a statistically significant difference between groups as determined by one-way ANOVA Following modeling. Compared to the M group (24.10±2.32 g), the BPNI group (0.016 g) exhibited a decrease in body weight (P=0.016), while other groups showed no significant changes. See Table 3.1 and figure 3.1.

Table 3.1: Changes of body weight in mice (g, $\overline{x}\pm s$)

	N	0	P	4 Weeks	P	8 Weeks	P	12 Weeks	P
CT	12	21.12±0.93		23.92±1.64		25.67±1.53		26.85±1.53	
M	10	20.32±1.35	0.089	20.25±1.90	0.073	21.40±2.22##	0	24.10±2.32##	0.001
BPI	10	20.82±0.40	0.280	21.17±0.82	0.972	20.98±1.07##	0.623	21.42±0.90##	0.288
BNI	10	20.75±0.48	0.348	20.70±0.66#	0.978	20.65±0.86##	0.378	20.47±0.84##	0.619
BYF	10	21.22±0.59	0.057	21.78±1.10	0.974	23.00±1.81	0.066	24.42±2.61	0.286
BPNI	10	20.65±0.54	0.469	20.10±1.43#	0.794	22.87±0.45	0.090	23.92±1.05#*	0.016

Comparing with the control group, #: P<0.05, ##: P<0.01. Comparing with the model group, *: P<0.05
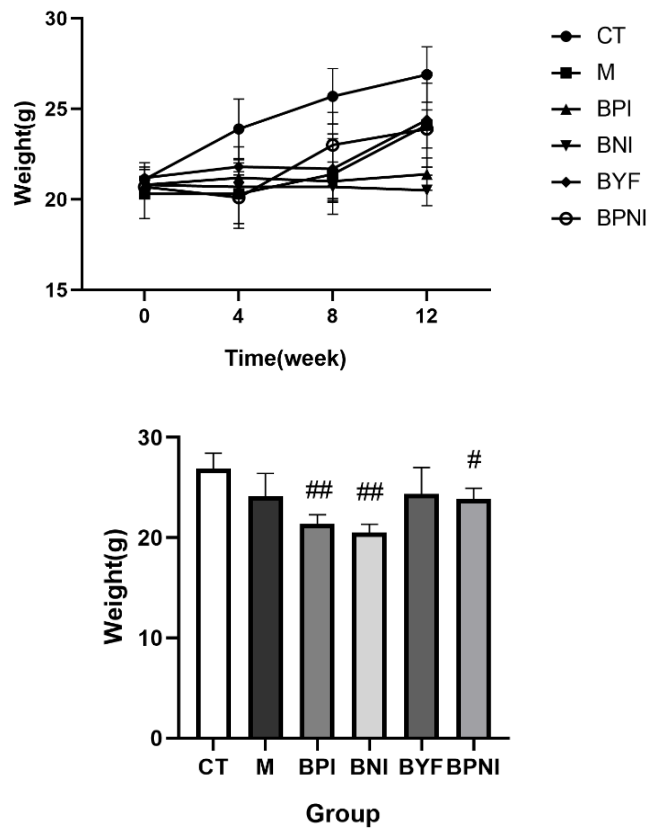
Figure 3.1: The change of body weight of mice and the weight of mice at the 12th week

Comparing with the control group, #: P<0.05, ##: P<0.01.

4.3.3 Pulmonary function(TV、MV、PEF、EF50)

Compared to the M group, there were no statistically significant differences in TV, MV, PEF, and EF50 in the BPI (P=0.994, P=0.516, P=0.991, P=0.916), BNI (P=1, P=0.341, P=0.351, P=0.334), and BPNI groups (P=0.877, P=0.392, P=0.999, P=0.797). Please refer to Tables 3.2, 3.3, 3.4, and 3.5, as well as Figures 3.2, 3.3, 3.4, and 3.5.

Table 3.2: Changes of TV in mice (mL, $\bar{x}\pm s$)

	N	0	P	4 Weeks	P	8 Weeks	P	12 Weeks	P
CT	12	0.27±0.01		0.36±0.03		0.34±0.03		0.39±0.02	
M	10	0.26±0.02	1	0.29±0.01[##]	0.003	0.27±0.01[##]	0.005	0.28±0.03[##]	0
BPI	10	0.27±0.03	0.999	0.30±0.01[##]	0.657	0.29±0.03	0.796	0.27±0.01[##]	0.994
BNI	10	0.27±0.01	1	0.30±0.01[#]	0.328	0.28±0.01[#]	0.242	0.29±0.01[##]	1
BYF	10	0.26±0.01	1	0.31±0.03	0.600	0.29±0.03	0.820	0.33±0.04	0.328
BPNI	10	0.26±0.01	1	0.29±0.02[##]	1	0.28±0.01[#]	0.532	0.30±0.01[##]	0.877

Comparing with the control group, #: P<0.05, ##: P<0.01

Table 3.3: Changes of MV in mice (mL/min, $\bar{x}\pm s$)

	N	0	P	4 Weeks	P	8 Weeks	P	12 Weeks	P
CT	12	133.23±13.09		169.03±31.61		148.64±21.04		179.32±17.70	
M	10	128.49±14.59	1	133.82±17.83	0.368	114.04±12.67##	0	120.35±13.01##	0
BPI	10	133.75±14.40	1	134.88±5.07	1	120.14±6.44##	0.382	125.51±13.81##	0.516
BNI	10	125.95±6.66	1	130.44±12.04	1	121.89±4.91##	0.262	127.96±3.55##	0.341
BYF	10	132.09±4.46	1	158.76±12.60	0.203	115.31±11.43##	0.855	150.93±17.70##**	0.001
BPNI	10	130.07±8.75	1	123.97±8.71	0.945	117.42±7.08##	0.627	127.17±10.52##	0.392

Comparing with the control group, ##: $P<0.01$. Comparing with the model group, **: $P<0.01$.

Table 3.4: Changes of PEV in mice (mL/s，$\bar{x}\pm s$)

	N	0	P	4 Weeks	P	8 Weeks	P	12 Weeks	P
CT	12	6.63±0.38		8.86±0.81		7.58±0.92		9.99±0.67	
M	10	7.33±0.88	0.680	6.98±0.33[##]	0	6.19±0.71	0.167	5.72±0.38[##]	0
BPI	10	6.93±0.32	0.972	7.18±0.46[#]	0.585	5.50±0.32[#]	0.479	5.50±0.40[##]	0.991
BNI	10	6.43±0.31	0.384	7.53±0.36	0.130	6.37±0.26	1	6.20±0.31[##]	0.351
BYF	10	6.75±0.42	0.852	8.39±0.94[**]	0	6.74±0.62	0.886	7.07±0.96[##]	0.151
BPNI	10	7.21±0.89	1	7.08±0.47[#]	0.784	5.60±0.28[#]	0.634	5.91±0.45[##]	0.999

Comparing with the control group, #: P<0.05, ##: P<0.01. Comparing with the model group, **: P<0.01.

Table 3.5 Changes of EF50 in mice (mL/s，$\bar{x}\pm s$)

	N	0	P	4 Weeks	P	8 Weeks	P	12 Weeks	P
CT	12	0.25±0.01		0.27±0.03		0.29±0.05		0.49±0.04	
M	10	0.27±0.04	0.981	0.23±0.03$^{\#\#}$	0.004	0.21±0.02	0.057	0.27±0.05$^{\#\#}$	0
BPI	10	0.26±0.01	1	0.25±0.02	0.110	0.23±0.01	0.633	0.28±0.06$^{\#\#}$	0.916
BNI	10	0.25±0.03	1	0.25±0.02*	0.031	0.23±0.02	0.887	0.30±0.01$^{\#\#}$	0.334
BYF	10	0.25±0.02	1	0.23±0.02$^{\#}$	0.686	0.24±0.01	0.211	0.38±0.06$^{\#\#**}$	0
BPNI	10	0.25±0.05	0.999	0.22±0.02$^{\#\#}$	0.895	0.25±0.02	0.188	0.27±0.03$^{\#\#}$	0.797

Comparing with the control group, #: P<0.05, ##: P<0.01. Comparing with the model group, *: P<0.05, **: P<0.01.

Figure 3.2: Changes of TV in mice and TV value of each group at the 12th week.

Comparing with the control group, ##: P<0.01
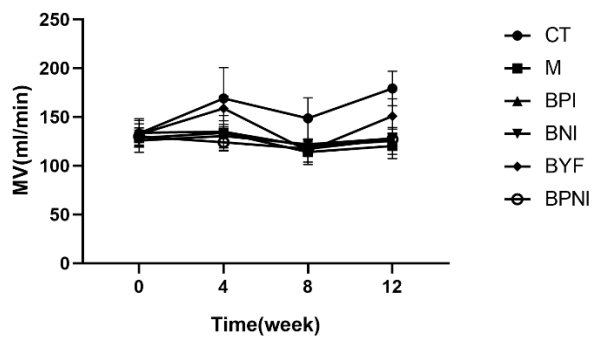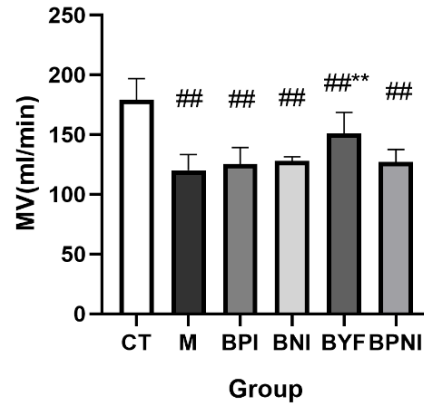
Figure 3.3: Changes of MV and MV value of each group at the 12th week

Comparing with the control group, ##: P<0.01. Comparing with the model group,
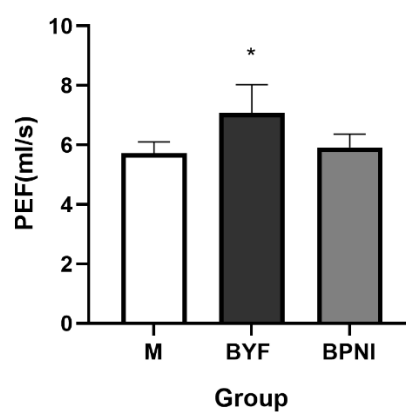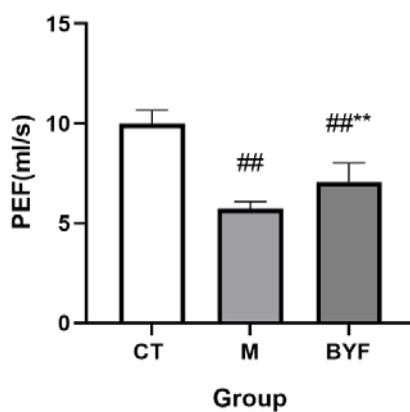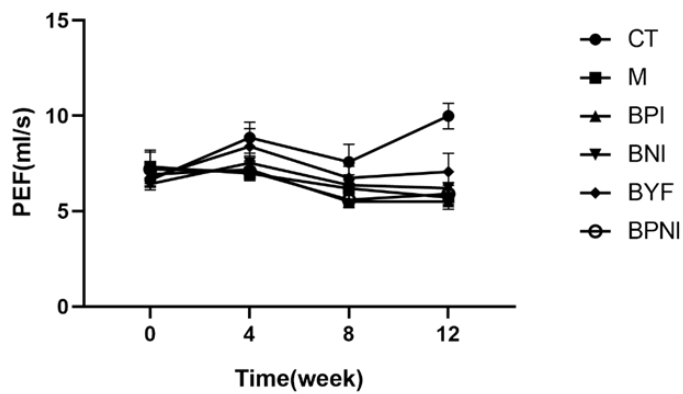
**: P<0.01.

Figure 3.4: Changes of PEF in mice and PEF value of each group at the
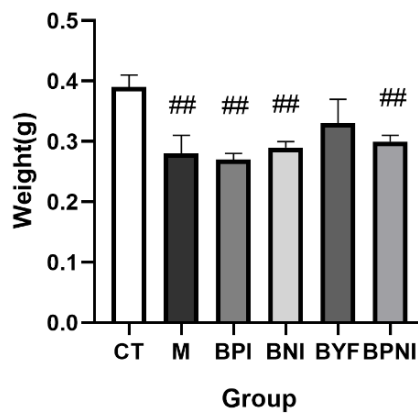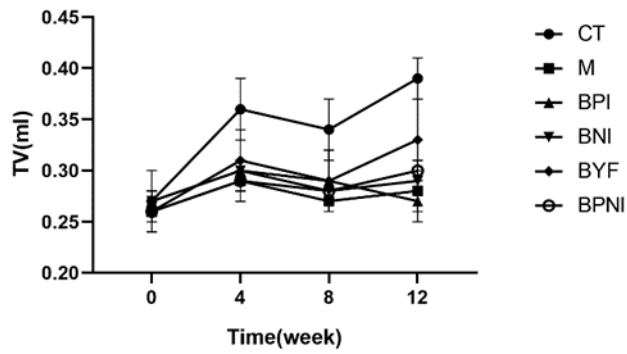
12th week

Comparing with the control group, ##: P<0.01. Comparing with the model group,

*: P<0.05, **: P<0.01.
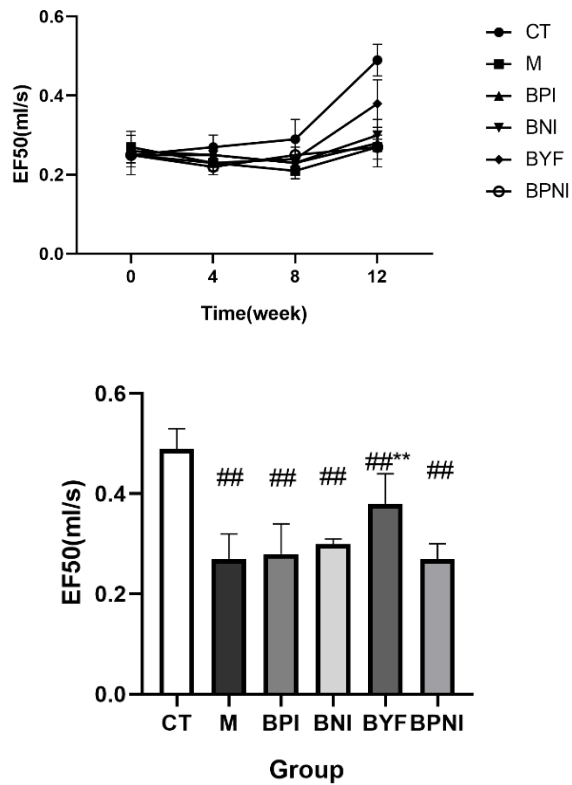
Figure 3.5: Changes of EF50 in mice and EF50 value of each group at the

12th week

Comparing with the control group, ##: P<0.01. Comparing with the model group,

**: P<0.01.

4.3.4 Pathological changes of lung tissues

Compared to the M group, the BPI group showed bronchial lumen narrowing,

see figure 3.6 B, C. The BNI group exhibited aggravated bronchial lumen

narrowing with increased inflammatory cell infiltration, see figure 3.6 B, D. In

the BPNI group, mice displayed exacerbated bronchial wall fibrosis, increased

narrowing of the bronchial lumen, enhanced inflammatory cell infiltration, and

hyperplasia of goblet cells, see figure 3.6 B, F.
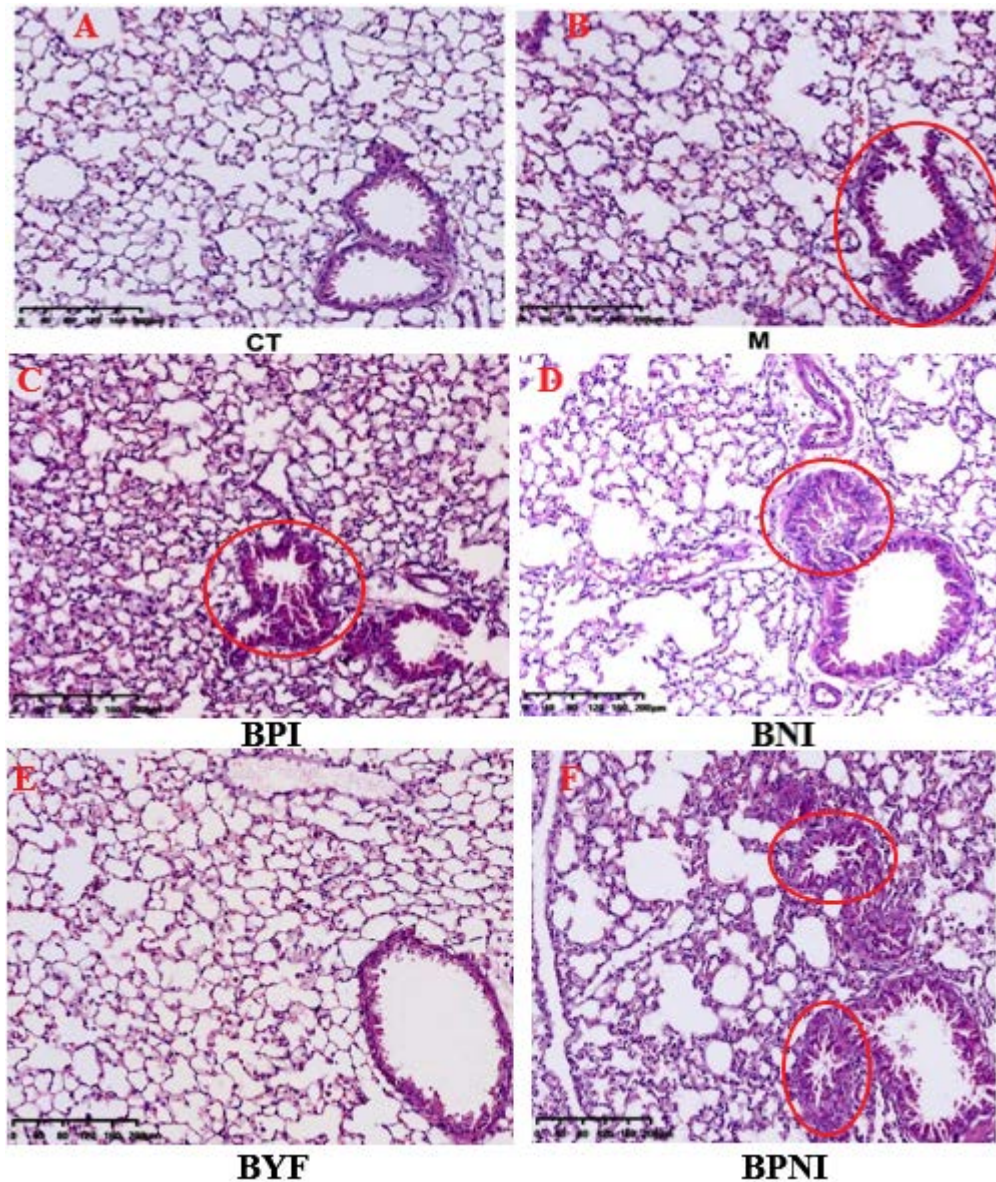
Figure 3.6: Lung histopathology of mice in each group

4.3.5 Determination of TNF α and IL-4 in lung tissue homogenate

There was a statistically significant difference between groups as determined by one-way ANOVA Following modeling. Compared to the M group, the BPI ($P=0$, $P=0.040$), BNI ($P=0$, $P=0.001$), and BPNI groups ($P=0$, $P=0.001$) exhibited a decrease in the expression of TNFα and IL-4. See table 3.6, and

figure 3.7.

Table 3.6: Expression of TNF α and IL-4 in lung homogenate of mice

(pg/ml，n=6，$\bar{x}\pm s$)

|	TNFα	P	IL-4	P
CT	325.99±84.63		343.24±48.87	
M	642.16±146.03[##]	0	431.39±50.17[#]	0.040
BPI	380.42±113.89[**]	0	281.25±51.41[**]	0.001
BNI	392.69±141.94[**]	0	273.96±90.07[**]	0.001
BYF	345.41±70.47[**]	0	267.07±111.37[**]	0
BPNI	334.49±78.02[**]	0	283.15±46.00[**]	0.001

Comparing with the control group, #: P<0.05, ##: P<0.01. Comparing with the
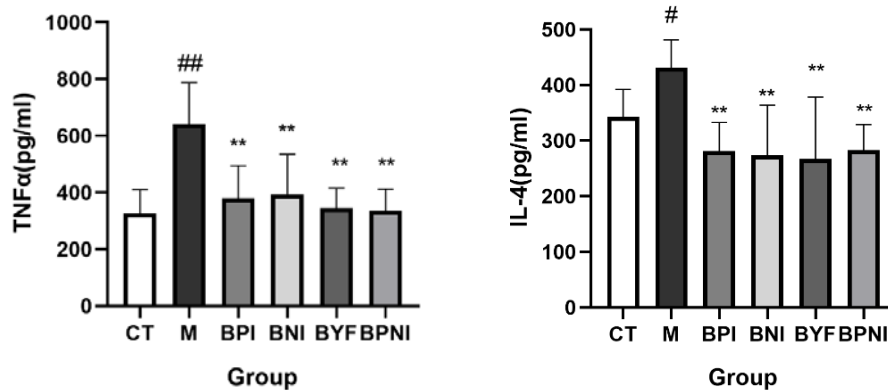
model group, **: P<0.01.

Figure 3.7: Expression of TNF α and IL-4 in lung homogenate of mice

Comparing with the control group, #: P<0.05, ##: P<0.01. Comparing with the

model group, **: P<0.01.

4.3.6 Detection of cellular efferocytosis function of alveolar macrophages in COPD mice

Compared to the M group, the BPI (P=0), BNI (P=0), and BPNI groups (P=1)

showed no statistically significant differences. See Table 3.7, and figure 3.8.

Table 3.7: Cell efferocytosis of mice alveolar macrophages (RFU, n=6, $\bar{x}\pm s$)

	Geo Mean	P
CT	122.29±6.29	
M	81.00±12.70##	0
BPI	74.67±8.32##	0
BNI	92.34±15.36##	0
BYF	102.86±8.18##**	0.004
BPNI	81.00±14.24##	1

Comparing with the control group, ##: P<0.01. Comparing with the model group,
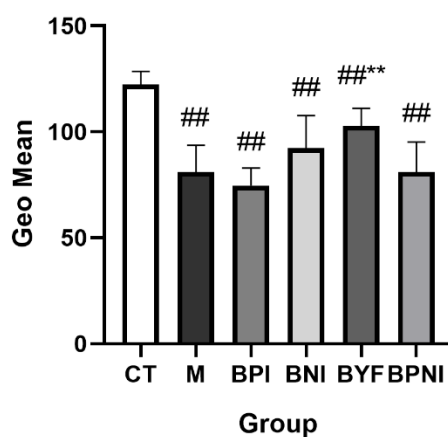
**: P<0.01.

Figure 3.8: Detection of cell efferocytosis ability of alveolar macrophages

in mice

Comparing with the control group, ##: P<0.01. Comparing with the model group,

**: P<0.01.

4.3.7 Detection of apoptosis in lung tissue of mice

There was a statistically significant difference between groups as determined by one-way ANOVA Following modeling. Compared to the M group, both the BPI (P=0.006) and BNI groups (P=0.038) exhibited a decrease, see Table 3.8, and figure 3.9, 3.10 B, C, D The BPNI group (P=0.283) showed no statistically significant difference. See Table 3.8, and figure 3.9, 3.10 B, F.

Table 3.8: Apoptosis index of lung tissue in mice (n=6, %, $\bar{x}\pm s$)

	AI400	P
CT	41.34±1.69	
M	61.68±4.37[##]	0
BPI	49.77±3.56[#**]	0.006
BNI	53.00±3.14[##*]	0.038
BYF	41.30±1.25[**]	0
BPNI	56.72±0.90[##]	0.283

Comparing with the control group, ##: P<0.01. Comparing with the model group, *: P<0.05, **: P<0.01.

Figure 3.9: Detection of apoptosis in lung tissue of mice

Comparing with the control group, ##: P<0.01. Comparing with the model group,

*: P<0.05, **: P<0.01.
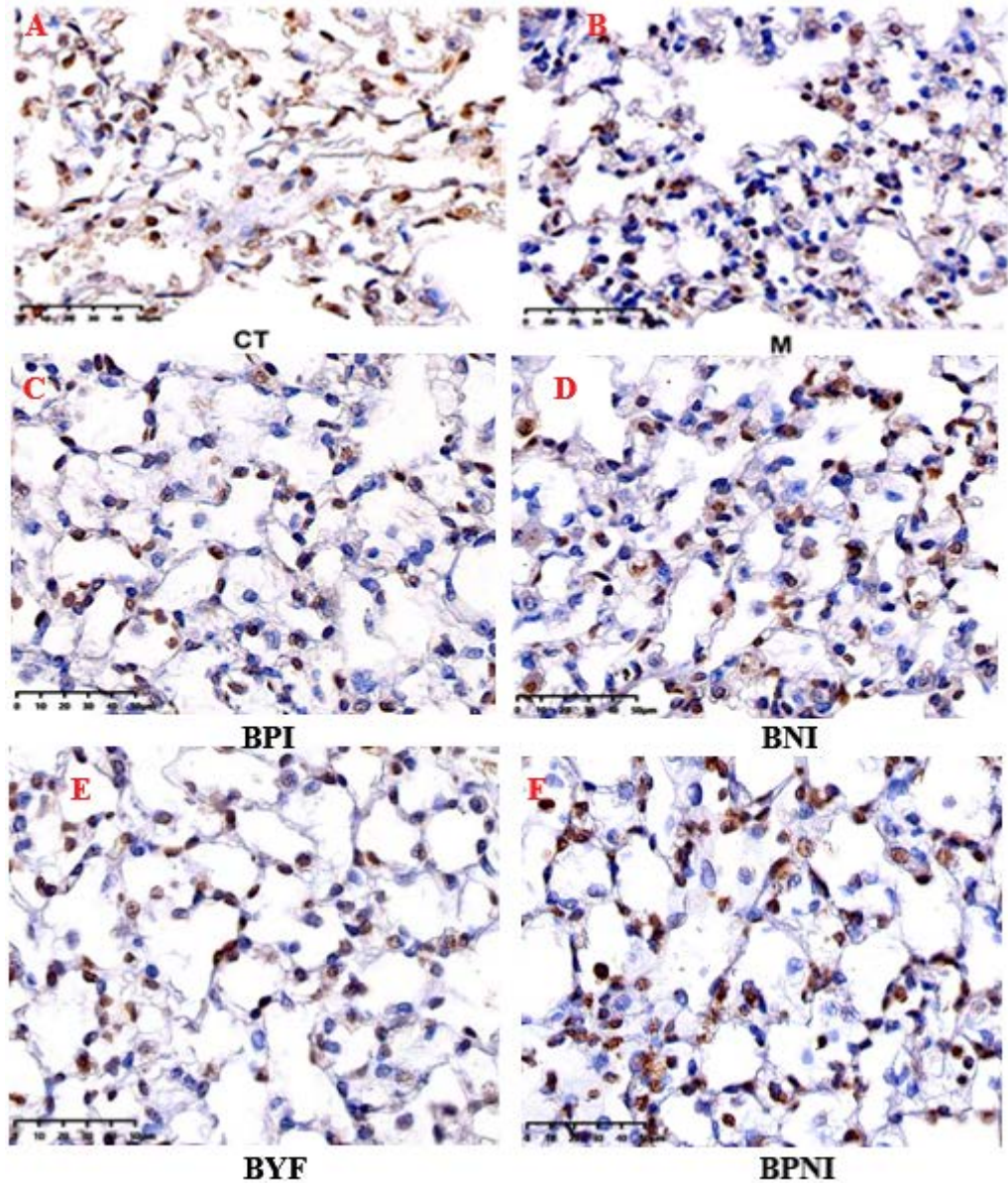
Figure 3.10: Apoptosis detected by TUNEL method The brown portion

represents apoptotic cells, while the blue corresponds to normal cells.

4.3.8 The expression of CD68, INOS, CD163, PPAR γ, and Nrf2 in alveolar macrophages of mice

Expression of CD68 in alveolar macrophages of mice

There was a statistically significant difference between groups as determined by one-way ANOVA Following modeling. Compared to the M group, the BPI group (P=0.222) showed no statistically significant difference, see table 3.9, figure 3.11 and 3.12 B, C.

The BNI group (P=0.049) exhibited a decrease, see table 3.9, figure 3.11 and 3.12 B, D.

The BPNI group (P=0.952) showed no statistically significant difference. See table 3.9, figure 3.11 and 3.12 B, F.

Table 3.9: Expression of CD68 in pulmonary macrophages of mice (IOD，n=6，$\bar{x}\pm$s)

	CD68	P
CT	9.62±1.29	
M	13.76±0.44##	0
BPI	14.48±1.02##	0.222
BNI	12.59±1.02##*	0.049
BYF	8.34±0.45#**	0
BPNI	13.80±1.32##	0.952

Comparing with the control group, #: P<0.05, ##: P<0.01. Comparing with the model group, *: P<0.05, **: P<0.01.
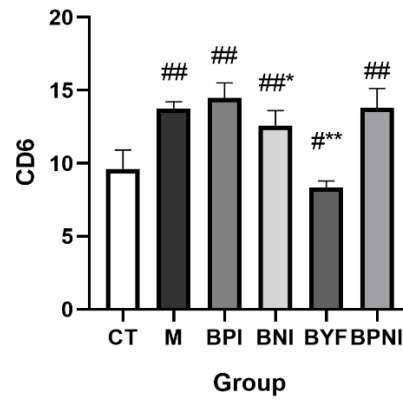
Figure 3.11: Expression of CD68 in mice alveolar macrophages

Comparing with the control group, #: $P<0.05$, ##: $P<0.01$. Comparing with the

model group, *: $P<0.05$, **: $P<0.01$.
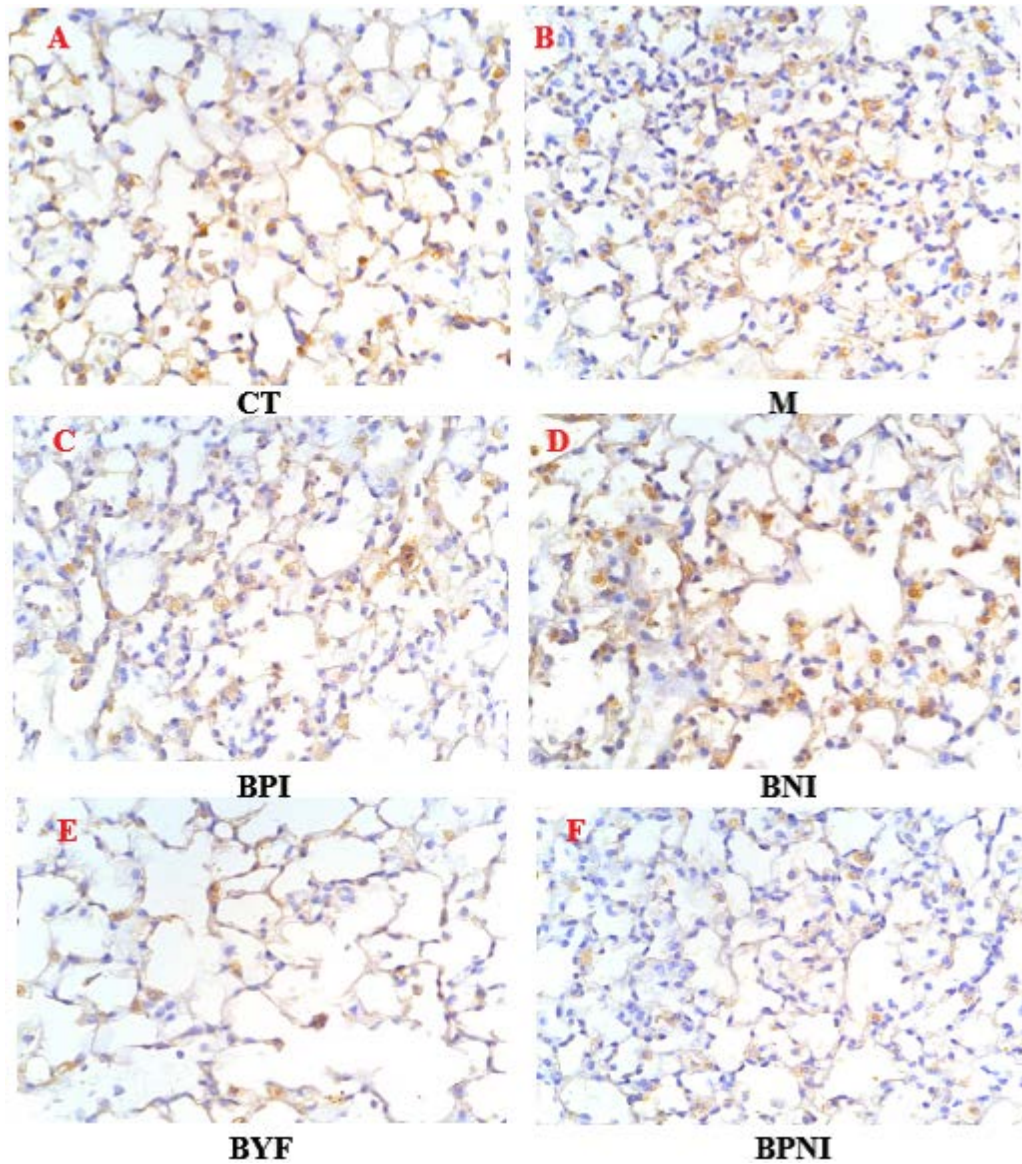
Figure 3.12: Expression of CD68 in lung tissue of mice. The brown color indicates immunohistochemical positivity.

Expression of INOS in alveolar macrophages of mice

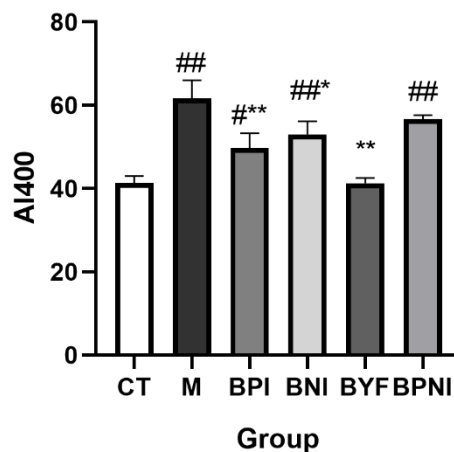There was a statistically significant difference between groups as determined by one-way ANOVA Following modeling. Compared to the M group, the BPI (P=0.001) and BNI groups (P=0.003) exhibited a significant decrease in expression, see table 3.10, figure 3.13 and 3.14 B, C, D. The BPNI group

(P=0.999) showed no statistically significant difference. See table 3.10, figure

3.13 and 3.14 B, F.

Table 3.10: Expression of INOS in pulmonary macrophages of mice

(IOD，n=6，$\bar{x}\pm$s)

	INOS	P
CT	8.58±0.84	
M	19.77±2.19[##]	0
BPI	11.50±0.84[##**]	0.001
BNI	12.63±0.75[##**]	0.003
BYF	9.77±0.63[**]	0
BPNI	18.86±2.00[##]	0.999

Comparing with the control group, ##: P<0.01. Comparing with the model group,
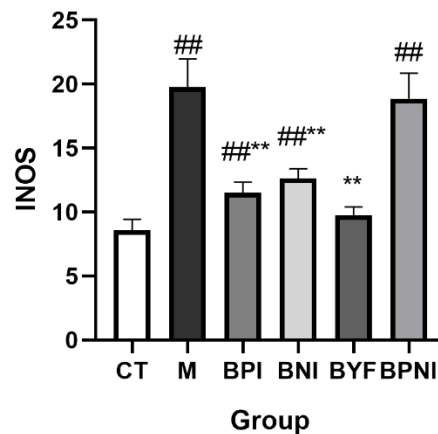
**: P<0.01.

Figure 3.13 Expression of INOS in mice alveolar macrophages

Comparing with the control group, ##: P<0.01. Comparing with the model group,

**: P<0.01.
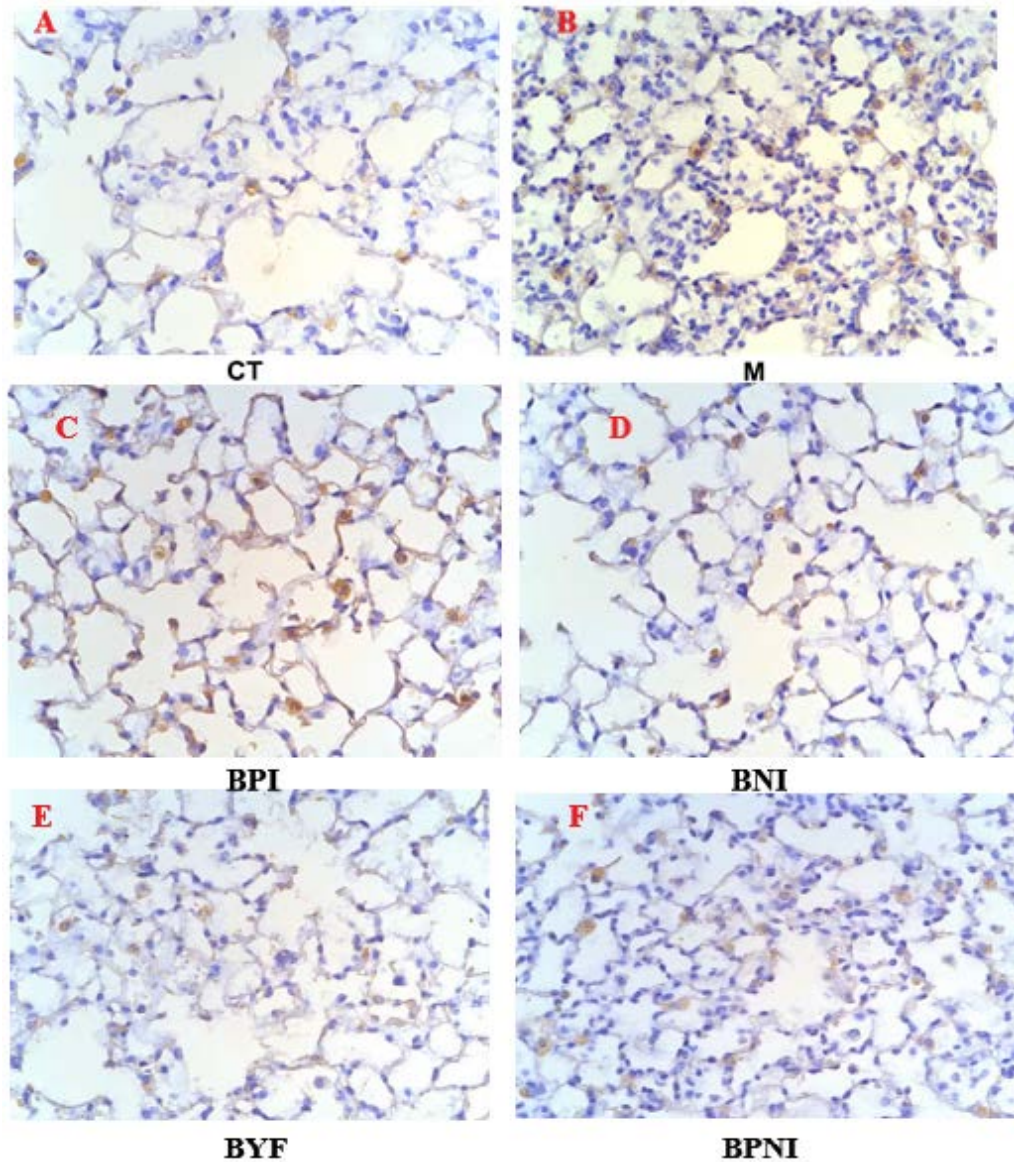
Figure 3.14: Expression of INOS in lung tissue of mice. The brown color indicates immunohistochemical positivity.

Expression of CD163 in alveolar macrophages of mice

Compared to the M group, the BPI (P=0.477), BNI (P=0.160), and BPNI groups (P=1) showed no statistically significant difference. Please refer to Table 3.11 and Figure 3.15, 3.16 B, C, D, F.

Table 3.11: Expression of CD163 in pulmonary macrophages of mice

(IOD，n=6，$\bar{x}\pm s$)

	CD163	P
CT	9.04±0.39	
M	15.11±0.44##	0
BPI	13.98±1.19##	0.477
BNI	13.82±0.92##	0.160
BYF	9.63±0.37**	0
BPNI	14.99±0.57##	1

Comparing with the control group, ##: P<0.01. Comparing with the model group,
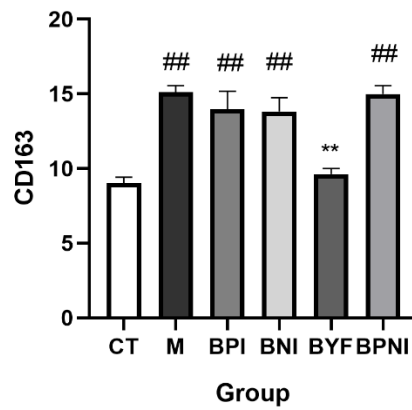
**: P<0.01.

Figure 3.15: Expression of CD163 in mice alveolar macrophages

Comparing with the control group, ##: P<0.01. Comparing with the model group,

**: P<0.01.
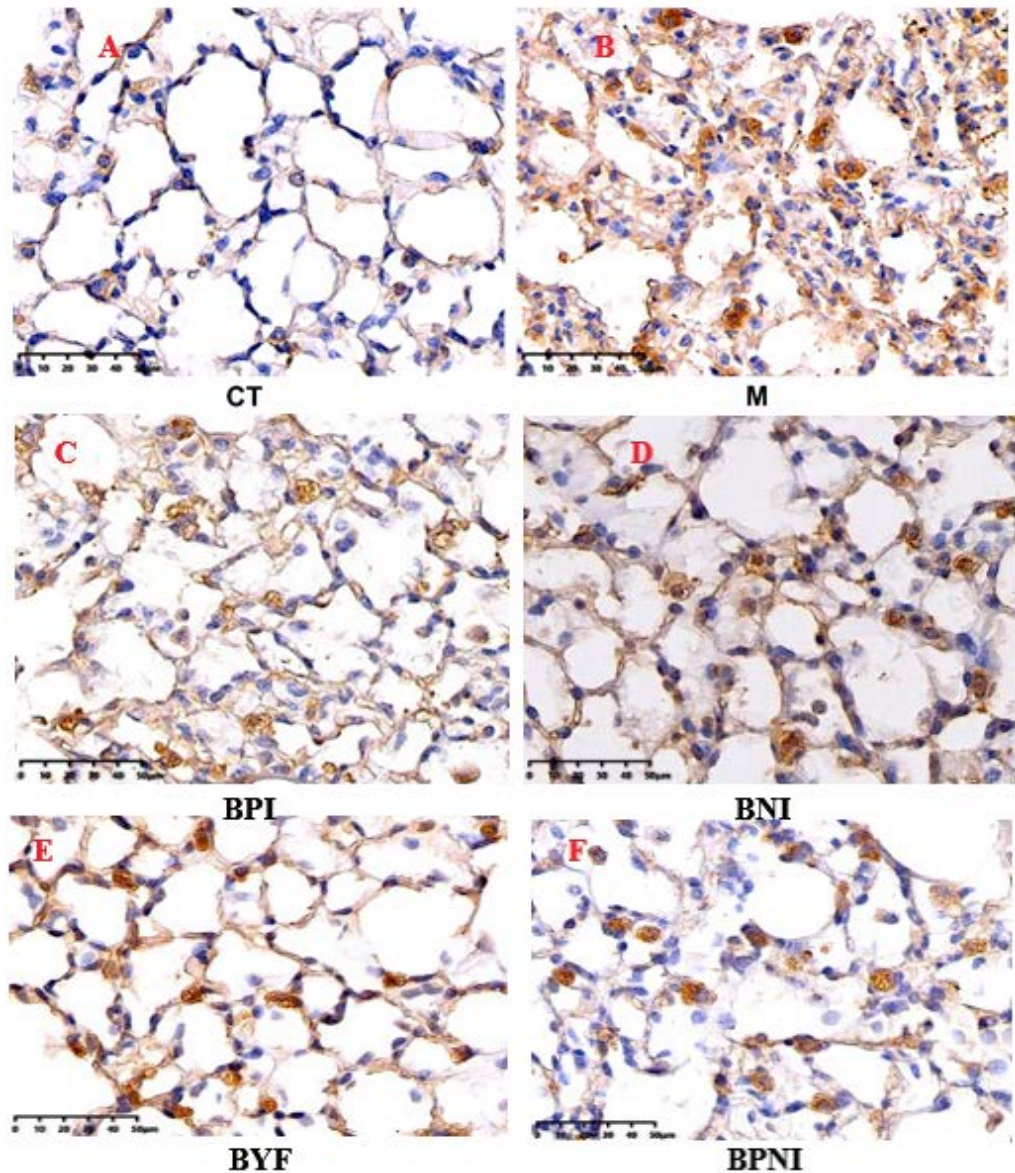
Figure 3.16: Expression of CD163 in lung tissue of mice. The brown color indicates immunohistochemical positivity.

Expression of PPAR γ in alveolar macrophages of mice

There was a statistically significant difference between groups as determined by one-way ANOVA Following modeling. Compared to the M group, the BNI (P=0) and BPI groups (P=0,069) showed no significant changes, while the BPNI group (0.001) exhibited a significant decrease in expression. Please refer to

Table 3.12 and Figure 3.17, 3.18 B, F.

Table 3.12: Expression of PPAR γ in pulmonary macrophages of mice

(IOD，n=6，$\bar{x}\pm$s)

	PPAR γ	P
CT	18.85±0.39	
M	12.69±0.85[##]	0
BPI	11.97±0.46[##]	0.069
BNI	14.79±0.60[##**]	0
BYF	17.04±0.41[##**]	0
BPNI	11.27±1.00[##**]	0.001

Comparing with the control group, ##: P<0.01. Comparing with the model group,
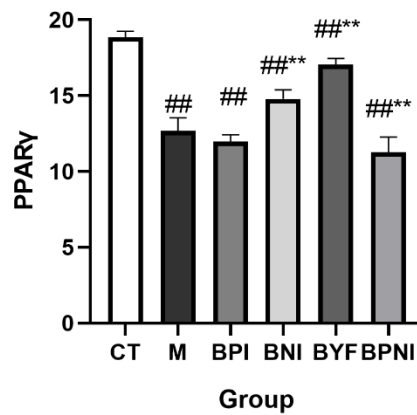
**: P<0.01.

Figure 3.17: Expression of PPAR γ in mice alveolar macrophages

Comparing with the control group, ##: P<0.01. Comparing with the model group,

**: P<0.01.
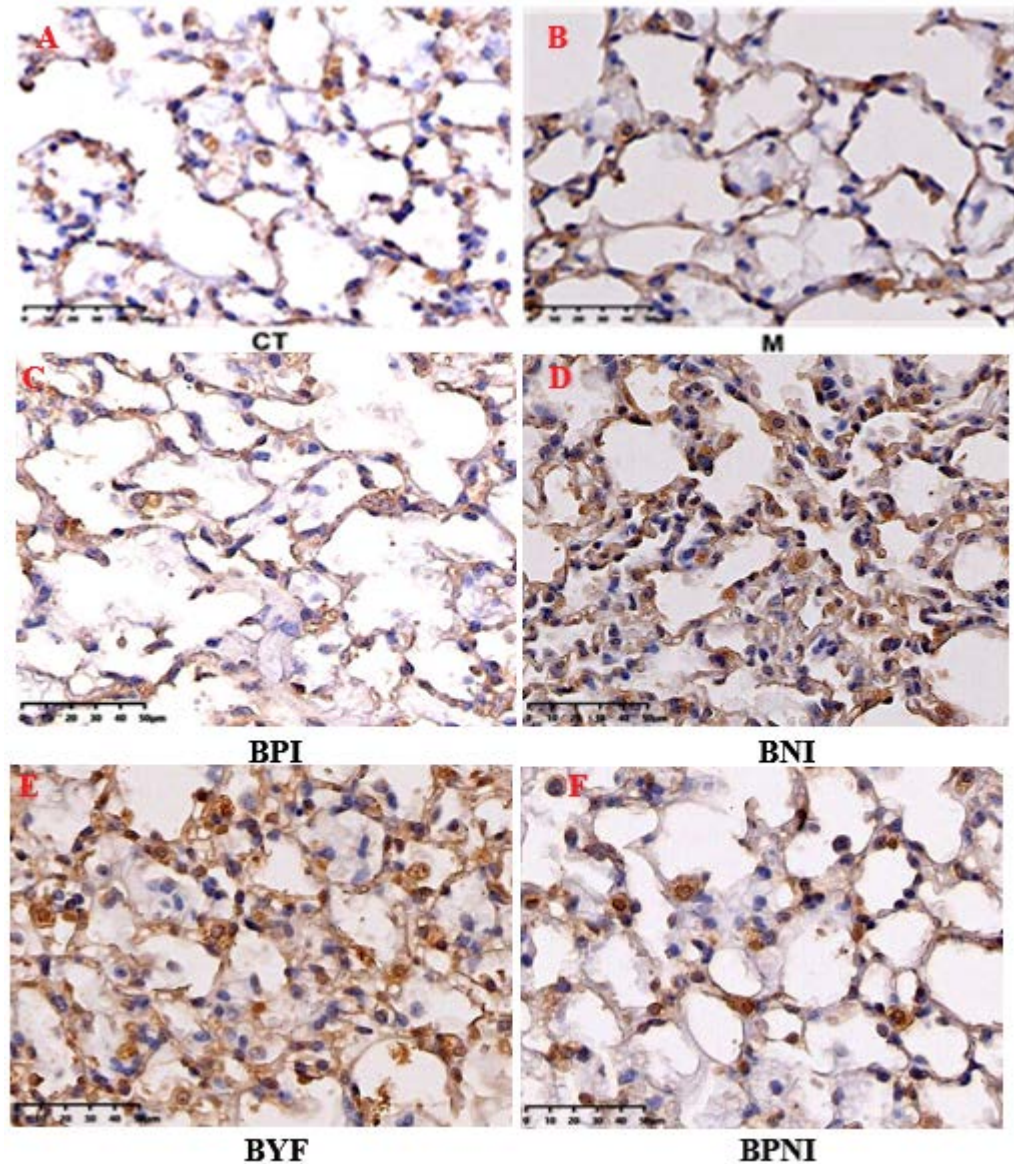
Figure 3.18: Expression of PPAR γ in lung tissue of mice. The brown color indicates immunohistochemical positivity.

Expression of Nrf2 in alveolar macrophages of mice

There was a statistically significant difference between groups as determined by one-way ANOVA Following modeling. Compared to the M group, the BPI (P=0), BNI (P=0), and BPNI groups (P=0) exhibited a significant decrease in expression. Please refer to Table 3.13 and Figure 3.19, 3.20 B, C, D, F.

Table 3.13: Expression of Nrf2 in pulmonary macrophages of mice (IOD，n=6，$\bar{x}\pm$s)

	Nrf2	P
CT	6.04±0.62	
M	14.91±0.51[##]	0
BPI	16.90±0.86[##**]	0
BNI	11.06±0.89[##**]	0
BYF	20.82±0.49[##**]	0
BPNI	9.02±1.15[##**]	0

Comparing with the control group, ##: P<0.01. Comparing with the model group,
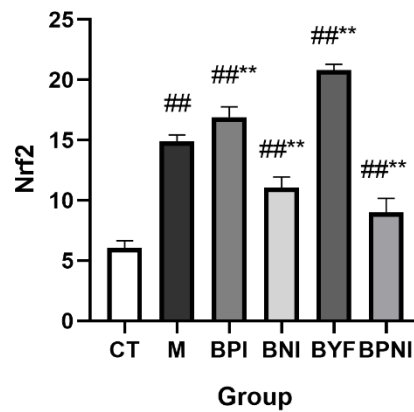
**: P<0.01.

Figure 3.19: Expression of Nrf2 in mice alveolar macrophages

Comparing with the control group, ##: P<0.01. Comparing with the model group,

**: P<0.01.
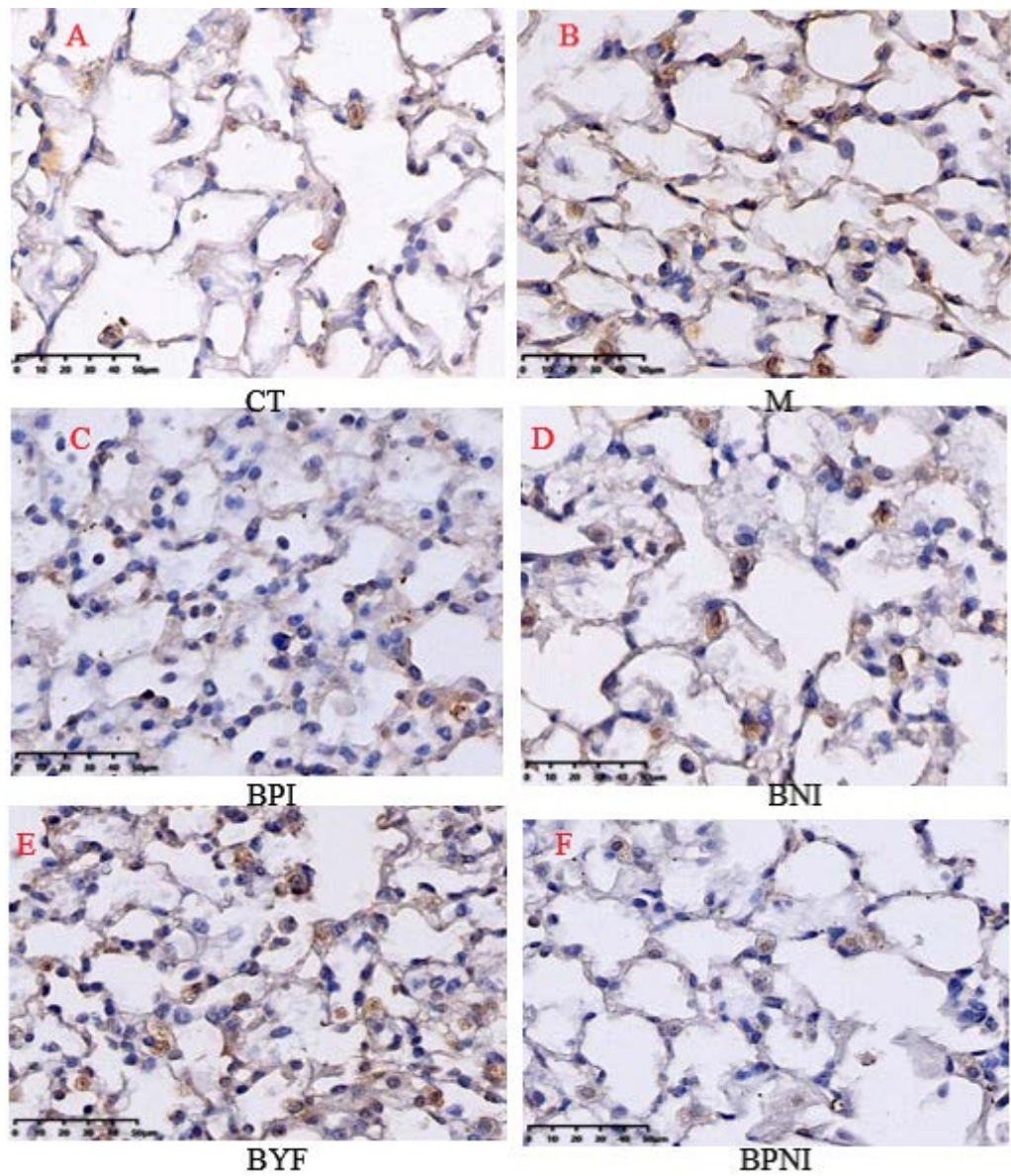
Figure 3.20: Expression of Nrf2 in alveolar macrophages of mice in each group. The brown color indicates immunohistochemical positivity.

Chapter 5.0: Discussion

It is well recognized that correlation does not imply causation. In this experiment, the comparative results among the CT, M, PA, NA, PI, and NI groups were utilized to validate the therapeutic potential of the PPAR γ and Nrf2 signaling pathways in treating COPD by modulating macrophage efferocytosis. The comparative results among the CT, M, PA, NA, and BYF groups were utilized to validate the therapeutic efficacy of Bufei Yishen prescription in COPD. The positive validation of Bufei Yishen prescription through the PPAR γ, Nrf2 signaling pathways in treating COPD was confirmed by comparing the results among the CT, M, PA, NA, and BYF groups. Lastly, the negative validation of Bufei Yishen prescription in treating COPD through the activation of the PPAR γ, Nrf2 signaling pathways and modulation of macrophage efferocytosis function was confirmed by comparing the results among the CT, M, BPI, BNI, BYF, and BPNI groups.

5.1 Physical Overview and body weight change of COPD mice model

Cigarette smoke (CS) is the primary risk factor for COPD. Prolonged exposure to the inflammatory environment induced by CS can lead to various pathological and physiological changes in the body, including anorexia, malnutrition, weight loss, hormonal alterations, systemic inflammatory responses, osteoporosis, and skeletal muscle atrophy. These pathological

changes are closely associated with the severity and major symptoms of COPD patients. Cigarette smoke can stimulate the expression of hypothalamic neuropeptide Y in mice, reduce the secretion of gastric growth hormone, decrease food intake, and lead to weight loss due to insufficient energy (Kamiide et al., 2015).

The study found that when the BMI of patients is below 18.5, FEV1, FEV1/FVC, and skeletal muscle mass are significantly reduced. With the increasing severity of the condition, the loss of muscle mass becomes more prominent, the muscle tension index weakens, and the patient's demand for a respirator also increases (Mete et al., 2018).

Meanwhile, it was also discovered that the loss of muscle mass is an important factor in the mortality rate of COPD patients, unrelated to lung function, smoking status, and BMI. The intake of certain nutrients such as vitamin E, vitamin C, and total carotenoids is positively correlated with FEV1 (Mete et al., 2018).

But currently, research results are inconsistent. Cazzola, et al. (2013) found that the probability of developing COPD increases with an increase in body mass, regardless of smoking status.

In the results of this study, the M group exhibited clinical symptoms of weight loss consistent with COPD patients. The lack of significant changes in the PA, PI, NA, BYF, BPI, and BNI groups may be attributed to the duration of drug treatment and the sample size.

5.2 Changes of pulmonary function in COPD mice model

Pulmonary function was used as the standard gold method in diagnosis and evaluation of COPD (Mirza et al., 2018). Zhang et al. (2019) used conventional lung function tests combined with impulse oscillometry to discover that, after treatment, patients exhibited a significant decrease in total airway resistance, central airway resistance, and peripheral airway resistance. Ventilation function improved, and the greater the baseline lung function impairment, the more pronounced the improvement in peripheral airway resistance. This indicates that lung function is a crucial basis for assessing COPD.

Tantucci and Modina (2012) pointed out that the decline in forced expiratory volume in one second (FEV1) is more rapid in the initial stages of COPD. The FEV1 of COPD patients continues to decrease with age, especially after middle age.

A study by Luan et al. (2021) indicated that patients aged 40 and above have more severe conditions, with lower forced vital capacity (FVC), forced

expiratory volume in one second (FEV1), percentage of carbon monoxide diffusion volume in its predicted value (DLCO), and a higher ratio of residual volume to total lung volume (RV/TLC).

In this study, the lung function parameters in mice were challenging to detect. Therefore, we employed a non-invasive whole-body plethysmograph for unrestrained small animals to assess lung function. The main parameters being measured included tidal volume (TV), minute ventilation (MV), peak expiratory flow (PEF), and 50% tidal volume expiratory flow (EF50) to evaluate mice lung function.

Whether during the modeling period from weeks 1-8 or at the final collection in week 12, mice in the M group exhibited a significant decrease in TV, MV, PEF, and EF50. This aligns with the clinical characteristics of COPD patients. This suggests the successful establishment of the COPD model

The TV, MV, PEF, and EF50 increased in the PA and NA groups, while in the PI and NI groups, these parameters either showed no statistical significance or decreased. This suggests that the activation of the PPAR γ and Nrf2 signaling pathways can improve lung function in the COPD mice model.

The TV, MV, PEF, and EF50 of mice in the BYF group all increased, indicating

that Bufei Yishen prescription could improve lung function in the COPD mice model. In contrast, the TV, MV, PEF, and EF50 of mice in the BPNI group showed no statistical significance, suggesting that the addition of PPAR γ and Nrf2 signaling pathway inhibitors resulted in the loss of Bufei Yishen prescription's ability to improve lung function in the COPD mice model.

5.3 Pathological changes of lung tissue in COPD mice model

Based on all the pathological features of COPD, it can be summarized into two main components: emphysema and small airway disease. Small airway remodeling is the most crucial aspect of small airway disease, characterized primarily by fibrosis, thickening of the small airway walls, narrowing of the lumen, and progressive obstruction.

The pathological changes in emphysema are mainly characterized by lung overinflation, reduced elasticity, a gray-white or pale appearance, enlarged alveolar spaces, thinning of alveolar septa, and destruction of alveolar walls.

The study has shown that in GOLD stage IV patients, the cross-sectional area of terminal bronchioles in lung tissue decreases by 81.0% to 99.7%, and the number of terminal bronchioles decreases by 72% to 89%. Moreover, the narrowing and disappearance of terminal bronchioles precede the development of emphysema. The lumens of terminal bronchioles become narrowed, the walls become thinner,

and they are more susceptible to the influence of various inflammatory substances (McDonough et al., 2011). The specific mechanism has been discussed in section 2.3.

Pathological images of mice lung tissues in the M group show uneven alveolar size, disrupted alveolar wall structure, and many alveolar wall fractures. The bronchial wall is significantly thickened, with pronounced fibrosis in the surrounding tissue. The bronchial lumen is narrow, goblet cell hyperplasia is observed, and there is a substantial infiltration of inflammatory cells. These features exhibit typical pathological characteristics of emphysema, including alveolar wall destruction, fusion of alveolar walls, and enlargement of alveolar spaces, which are consistent with the general pathological symptoms of COPD patients. This indicates that the pathological changes in lung tissue of mice in the model group align with the characteristics of COPD parenchymal damage.

In the PA and NA groups, there was an improvement in bronchial wall thinning and lumen narrowing, while in the PI and NI groups, bronchial lumen narrowing worsened. This indicates that the activation of the PPAR γ and Nrf2 signaling pathways can improve the pathological conditions in the COPD mice model.

In the BYF group, there is a certain improvement observed, including thinning of the bronchial wall and a decrease in bronchial lumen narrowing. This suggests

that Bufei Yishen prescription may inhibit the inflammatory response in the COPD mice model and improve the pathological condition of COPD mice.

In the BPNI group, there is no significant improvement observed, indicating that after the addition of PPAR γ and Nrf2 pathway inhibitors, Bufei Yishen prescription loses its ability to improve the pathological condition of the COPD mice model.

5.4 Changes of inflammatory cytokines expression in COPD mice model

Inflammation is a biological response of cells and blood vessels triggered by external or internal stimuli, such as trauma, chemical substances, pathogens, toxins, and physical factors. It can initiate the self-healing functions of tissues and is one of the primary defense systems in the body (Kolac et al., 2017).

However, sustained inflammatory responses can lead to a series of pathological changes in the body. Chronic airway inflammation is a crucial characteristic of COPD. Airway inflammation is a key factor that exacerbates and drives the progression of COPD. The conditions of airway and systemic inflammatory responses are closely associated with the onset and survival rates of patients (Vogelmeier et al., 2017, Wang et al., 2018).

Lung parenchymal damage, emphysema, small airway inflammation, and

chronic bronchitis with central airway inflammation are the main pathological features of COPD. Airway inflammation leads to a rapid increase in the number of inflammatory cells such as macrophages, T lymphocytes, and neutrophils within the lungs. It also stimulates the secretion of inflammatory factors such as TNFα, IL-4, IL-10, and IL-8, resulting in a persistent inflammatory state that damages alveolar structure and leads to a decline in lung function (Bohr et al., 2017, Brightling and Greening, 2019).

High in neutrophils count is the key marker of inflammation. However, the detection results of neutrophil expression were not satisfactory. TNFα, as a neutrophil chemotactic protein, is highly expressed in the lungs, indicating an increased number of neutrophils and heightened airway reactivity (Caramori et al., 2014).

TNF-α is a pleiotropic cytokine that can participate in stimulating inflammation and is present in most inflammatory sites (McPhillips et al., 2007). TNF-α can induce oxidative stress, airway hyperresponsiveness, and airway remodeling (Malaviya et al., 2017). The study has shown that significant levels of TNF-α can be detected in smokers and COPD patients. During acute exacerbations of COPD, the levels of TNF-α continue to rise (Strzelak et al., 2018). TNF-α, as a pro-inflammatory cytokine, may play a central role in the pathogenesis of COPD by promoting and sustaining the expression and release of various pro-

inflammatory mediators (Tanni et al., 2010).

IL-4 belongs to type 2 immune response driving factors, mainly released by helper T cells (TH-2). The close association between inflammation, airway remodeling in COPD lung tissue, and high expression of IL-4 is evident. Factors such as bacteria, allergies, and cigarette smoke exposure put the lungs in a state of heightened airway reactivity, promoting the activation and proliferation of TH2 cells. This, in turn, disrupts the body's defense mechanisms by activating the Stat6 signaling pathway, enhancing tracheal inflammatory responses. (Ho and Miaw, 2016).

IL-4 can stimulate B cells to secrete immunoglobulin E (IgE), promoting inflammation and stimulating increased airway mucus secretion, airway fibrosis, and airway remodeling. (Barnes, 2018). When IL-4R is activated, the related signal transduction can result in excessive mucus secretion, pulmonary inflammation, and elevated serum IgE levels (Wei et al., 2014).

A study by Mitra and team (2018) has found that smokers with COPD have significantly increased concentrations of GM-CSF, IFN-γ, and IL-4 in serum compared to non-smoking COPD patients. Smoking also leads to higher IgE levels in COPD patients, confirming that IL-4 may exacerbate COPD by increasing IgE production.

In this study, compared to the CT group, the levels of TNFα and IL-4 in the lung homogenate of mice in the M group were significantly elevated, consistent with the increased inflammatory factors observed in COPD patients. This suggests the successful establishment of the COPD model.

In the PA and NA groups, there was a decrease in TNFα and IL-4, indicating that the activation of the PPAR γ and Nrf2 signaling pathways can reduce the levels of inflammatory factors in the COPD mice model. In the PI and NI groups, the decrease in TNFα and IL-4 may be attributed to issues related to sample size or duration of drug treatment.

In the BYF group, the levels of TNFα and IL-4 were significantly decreased, indicating that Bufei Yishen prescription could reduce TNFα and IL-4 in the COPD mice model. In the BPNI group, there was a significant decrease in TNFα and IL-4, which may be related to sample size and duration of medication, considering the correlation.

5.5 Detection of efferocytosis of alveolar macrophages in COPD mice model

Apoptosis is a form of cell death characterized by nuclear and cytoplasmic condensation, DNA fragmentation, and the formation of apoptotic bodies, which encapsulate cellular contents and are eventually engulfed and cleared by

macrophages. (Qi Hui-Li and Yao Li-Fen, 2016).

Liu Xue Ning and team (2019) pointed out that COPD patients exhibit impaired macrophage efferocytosis, which can induce or exacerbate pulmonary inflammation. Studies have shown that there is a significant presence of apoptotic cells in the lung tissue of COPD patients, and the deteriorating severity of COPD is associated with impaired phagocytic function of alveolar macrophages (Eltboli et al., 2014).

Efferocytosis is a physiological process of mutual adaptation and coordination between apoptotic cells and phagocytic cells. Impaired efferocytosis results in the inability to clear many apoptotic cells. Apoptotic cells release various hydrolytic enzymes and pro-inflammatory factors, leading to the degradation of alveolar protein structures and the disruption of various cellular functions.

McCubbrey and Curtis (2013) validated the impaired efferocytosis in COPD patients through *in vivo* and *in vitro* methods. The degree of impairment was found to be associated with the severity and frequency of COPD exacerbations.

Hodge and team (2006) demonstrated that the increased number of apoptotic cells detected in the lungs of COPD patients is attributed to significantly impaired phagocytic function of alveolar macrophages. In comparison to never-smoking healthy individuals, both COPD smokers and healthy smokers exhibit

a notable reduction in the ability of alveolar macrophages to engulf apoptotic bronchial epithelial cells. Additionally, alveolar macrophages in these groups show decreased.

In this study, the apoptotic index in the M group mice significantly increased, accompanied by a notable decrease in the efferocytosis capacity of alveolar macrophages. This indicates the presence of impaired efferocytosis ability in the alveolar macrophages of the COPD mice model. The findings align with the characteristic impaired efferocytosis observed in COPD patients, confirming the successful establishment of the COPD model

In the PA and NA groups, there was a decrease in the apoptosis index, and the efferocytosis ability of alveolar macrophages increased. Meanwhile, in the PI and NI groups, there were no statistically significant changes, suggesting that the activation of the PPAR γ and Nrf2 signaling pathways can improve the efferocytosis ability of alveolar macrophages in the COPD mice model. The observed increase in efferocytosis ability in the PI group may be influenced by issues related to sample size.

The apoptotic index decreased in the BYF group and the efferocytosis capacity of alveolar macrophages increased. This suggests that Bufei Yishen prescription can reduce the apoptotic index in the COPD mice model and enhance the

efferocytosis ability of alveolar macrophages.

In contrast, the BPNI group exhibited a significant increase in the apoptotic index, accompanied by a notable decrease in the efferocytosis capacity of alveolar macrophages. This indicates that, after the addition of PPAR γ and Nrf2 signaling pathway inhibitors, Bufei Yishen prescription lost its ability to enhance efferocytosis in alveolar macrophages in the COPD mice model.

5.6 The expression of CD68, INOS, CD163 in alveolar macrophages of mice model

Macrophages are generally presence in non-polarized form in body. Under sustained inflammatory stimuli, macrophages can polarize into M1 and M2 phenotypes (Barnes, 2016). In animal models of COPD, the expression of M1 and M2 macrophages is significantly increased compared to normal animals (Arora et al., 2018; Bazzan et al., 2017).

M1 macrophages are activated by factors such as LPS and IFN-γ, leading to the release of pro-inflammatory cytokines such as TNFα, IL-1β, and IL-12. This activation stimulates the pulmonary immune response system but simultaneously inhibits the proliferation of surrounding cells, resulting in tissue damage. On the other hand, M2 macrophages are activated by stimuli like apoptotic cells, IL-4, and IL-13. They release anti-inflammatory factors such as

IL-10 and TNFβ, contribute to the phagocytosis of apoptotic cells, promote wound healing, and participate in the repair of necrotic tissue. However, M2 activation is also associated with pulmonary fibrosis and other parenchymal injuries (Arora et al., 2018).

Any imbalance in macrophage polarization during the process can potentially affect the body's state, leading to various diseases or inflammatory conditions. In COPD, this is often manifested by an expansion of M1 macrophage-mediated pro-inflammatory responses and deficiencies in M2-mediated phagocytosis and tissue repair functions. (Yamasaki and Eeden, 2018).

The study observed that with the progression of smoking and COPD, the proportion of M1 macrophages increased with the severity of the disease. Additionally, smoking was identified as a significant factor in M1 macrophage polarization. After smoking cessation, the percentage of M1 macrophages significantly decreased. However, the reduction in M1 polarization was only observed in non-COPD smokers and smokers with mild COPD, with no significant difference noted in smokers with severe COPD (Bazzan et al., 2017b).

Therefore, the improvement in macrophage polarization in the COPD mice model is not simply characterized by a decrease in M1 macrophages and an increase in M2 macrophages. Instead, both M1 and M2 macrophages are reduced,

indicating an overall decrease in macrophage population.

CD68 is a glycosylated type I transmembrane protein that belongs to the lysosome/endosome-associated membrane glycoprotein family. In terms of expression, CD68 is exclusively expressed in the monocyte/macrophage cell lineage. In the lung tissue of COPD patients, there is high expression of CD68, and its expression can be reduced after treatment (Bourbeau et al., 2007). Therefore, it is often used as a marker for macrophages.

INOS, utilizing L-arginine as a substrate to generate NO, participates in the bactericidal action of macrophages against ingested microorganisms and is commonly used as a marker for M1 macrophages (Eapen et al., 2017)

CD163 is a type I transmembrane protein that mediates the engulfment of haptoglobin-hemoglobin complexes by cells and is only expressed in cells of the monocyte lineage. Binding of CD163 to its ligands regulates CD163 expression and the secretion of anti-inflammatory cytokines, making it a common marker for M2 macrophages (He et al., 2017c).

In this study, the expression of CD68, iNOS, and CD163 in alveolar macrophages of the M group mice significantly increased. This indicates an increased quantity and polarization of alveolar macrophages in the COPD mice

model, consistent with the characteristic macrophage polarization observed in COPD patients. It suggests that the COPD mice model is successful.

The expression of CD68, iNOS, and CD163 in the PA and NA groups decreased, while there was no significant change in the expression of CD68, iNOS, and CD163 in the PI and NI groups. This suggests that the activation of the PPAR γ and Nrf2 signaling pathways can improve macrophage polarization in the COPD mice model.

The decrease in the expression of CD68, iNOS, and CD163 in the BYF group indicates that Bufei Yishen prescription can improve alveolar macrophage polarization. The lack of significant changes in the expression of CD68, iNOS, and CD163 in the BPNI group suggests that the addition of PPAR γ and Nrf2 signaling pathway inhibitors diminishes the ability of Bufei Yishen prescription to improve macrophage polarization.

5.7 The expression of PPAR γ and Nrf2 in alveolar macrophages of mice model

In this study, the expression of PPAR γ and Nrf2 increased in the BYF group mice, while there were no significant changes or a decrease in PPAR γ and Nrf2 expression in the BPNI group. This suggests that Bufei Yishen prescription can activate the PPAR γ and Nrf2 signaling pathways.

6.0: Conclusion

After cigarette smoke induction, the changes of physical overview, lung function, pathophysiology of lung tissue and the expression level of inflammatory factors in mice accorded with the characteristics of COPD, and the efferocytosis function of alveolar macrophages was abnormal. The above results proved that the experimental model was established successfully, and the efferocytosis dysfunction of alveolar macrophages may be the potential mechanism of the continuous progression of inflammatory reaction in COPD.

Activation of PPAR γ and Nrf2 signal pathway could improve the physical overview, lung function, inhibit the expression of inflammatory factors and promote the efferocytosis ability of alveolar macrophages in COPD mice, while inhibiting the expression of PPAR γ and Nrf2 signal pathway could not significantly improve the main pathological features and macrophage efferocytosis function of COPD mice. It is suggested that PPAR γ and Nrf2 signal pathway are involved in regulating the efferocytosis ability of alveolar macrophages and inhibiting inflammation in COPD mice.

Bufei Yishen prescription can effectively improve the physical overview, lung function and lung tissue injury of COPD mice model, reduce the expression level of pulmonary inflammatory factors, improve the efferocytosis function of alveolar macrophages in COPD mice model, reduce the apoptosis rate of lung

tissue, and inhibit the number and polarization of macrophages.

Bufei Yishen Prescription exerts its therapeutic effects on COPD through the regulation of PPAR γ and Nrf2, which in turn modulate macrophage efferocytosis function and suppress inflammatory responses.

Limitations and novelty

    The related signaling pathways of COPD are still worthy of further study, and the specific mechanism is still unclear. From the perspective of macrophage cell efferocytosis, there is few related literatures to study the molecular mechanism of traditional Chinese medicine in the prevention and treatment of COPD. The clinical effect of Bufei Yishen prescription on COPD has been confirmed, but the exact mechanism is still unclear. This study provides some possible answers to these three questions. But more decisive evidence of molecular biology and clinical research is still needed.

PUBLICATIONS

许聪,Te Kian Keong,李晨旭,孟丹华,武颖烁,周哲旭,吴耀松,陈玉龙.PPAR γ 信号通路对香烟烟雾所致COPD模型小鼠肺泡巨噬细胞的影响[J].中国中合急救杂志,2022,29(6):663-669.DOI:10.3969/j.issn.1008-9691.2022.06.005.

9 References

Adeloye, D., Chua, S., Lee, C., Basquill, C., Papana, A., Theodoratou, E., Nair, H., Gasevic, D., Sridhar, D., Campbell, H., Chan, K. Y., Sheikh, A. & Rudan, I. (2015), "Global And Regional Estimates Of Copd Prevalence: Systematic Review And Meta-Analysis", *J Glob Health,* Vol. 5 No. 2, Pp. 020415.

Arora, S., Ahmad, S., Irshad, R., Goyal, Y., Rafat, S., Siddiqui, N., Dev, K., Husain, M., Ali, S., Mohan, A. & Syed, M. A. (2019), "Tlrs In Pulmonary Diseases", *Life Sci,* Vol. 233116671.

Baird, L. & Dinkova-Kostova, A. T. (2011), "The Cytoprotective Role Of The Keap1-Nrf2 Pathway", *Arch Toxicol,* Vol. 85 No. 4, Pp. 241-72.

Barnes, P. J. (2016), "Inflammatory Mechanisms In Patients With Chronic Obstructive Pulmonary Disease", *J Allergy Clin Immunol,* Vol. 138 No. 1, Pp. 16-27.

Barnes, P. J. (2018), "Targeting Cytokines To Treat Asthma And Chronic Obstructive Pulmonary Disease", *Nat Rev Immunol,* Vol. 18 No. 7, Pp. 454-466.

Barnes, P. J. (2019), "Inflammatory Endotypes In Copd", *Allergy,* Vol. 74 No. 7, Pp. 1249-1256.

Belchamber, K. & Donnelly, L. E. (2017), "Macrophage Dysfunction In Respiratory Disease", *Results Probl Cell Differ,* Vol. 62299-313.

Blanco, I., Diego, I., Bueno, P., Fernandez, E., Casas-Maldonado, F., Esquinas, C., Soriano, J. B. & Miravitlles, M. (2018), "Geographical Distribution Of Copd Prevalence In Europe, Estimated By An Inverse Distance Weighting Interpolation Technique", *Int J Chron Obstruct Pulmon Dis,* Vol. 1357-67.

Boada-Romero, E., Martinez, J., Heckmann, B. L. & Green, D. R. (2020), "The Clearance Of Dead Cells By Efferocytosis", *Nat Rev Mol Cell Biol,* Vol. 21 No. 7, Pp. 398-414.
Ccdc (2022), 中国死因监测数据集-2021, 中国科学技术出版社.

Chamitava, L., Cazzoletti, L., Ferrari, M., Garcia-Larsen, V., Jalil, A., Degan, P., Fois, A. G., Zinellu, E., Fois, S. S., Fratta, P. A., Nicolis, M., Olivieri, M., Corsico, A., Bono, R., Pirina, P. & Zanolin, M. E. (2020), "Biomarkers Of Oxidative Stress And Inflammation In Chronic Airway Diseases", *Int J Mol Sci,* Vol. 21 No. 12, Pp.

Cho, H. Y. & Kleeberger, S. R. (2014), "Noblesse Oblige: Nrf2 Functions In The Airways", *Am J Respir Cell Mol Biol,* Vol. 50 No. 5, Pp. 844-7.

Cho, H. Y., Gladwell, W., Wang, X., Chorley, B., Bell, D., Reddy, S. P. & Kleeberger, S. R. (2010), "Nrf2-Regulated Ppar{Gamma} Expression Is Critical To Protection Against Acute Lung Injury In Mice", *Am J Respir Crit Care Med,* Vol. 182 No. 2, Pp. 170-82.

Collaborators, G. D. A. I. (2020), "Global Burden Of 369 Diseases And Injuries In 204 Countries And Territories, 1990-2019: A Systematic Analysis For The Global Burden Of Disease Study 2019", *Lancet,* Vol. 396 No. 10258, Pp. 1204-1222.

Delmas, M. C., Benezet, L., Ribet, C., Iwatsubo, Y., Zins, M., Nadif, R., Roche, N. & Leynaert, B. (2021), "Underdiagnosis Of Obstructive Lung Disease: Findings From The French Constances Cohort", *Bmc Pulm Med,* Vol. 21 No. 1, Pp. 319.

Diver, W. R., Jacobs, E. J. & Gapstur, S. M. (2018), "Secondhand Smoke Exposure In Childhood And Adulthood In Relation To Adult Mortality Among Never Smokers", *Am J Prev Med,* Vol. 55 No. 3, Pp. 345-352.

Doran, A. C., Yurdagul, A. J. & Tabas, I. (2020), "Efferocytosis In Health And Disease", *Nat Rev Immunol,* Vol. 20 No. 4, Pp. 254-267.

Elliott, M. R., Koster, K. M. & Murphy, P. S. (2017), "Efferocytosis Signaling In The Regulation Of Macrophage Inflammatory Responses", *J Immunol,* Vol. 198 No. 4, Pp. 1387-1394.

Fang, L., Gao, P., Bao, H., Tang, X., Wang, B., Feng, Y., Cong, S., Juan, J., Fan, J., Lu, K., Wang, N., Hu, Y. & Wang, L. (2018), "Chronic Obstructive Pulmonary Disease In China: A Nationwide Prevalence Study", *Lancet Respir Med,* Vol. 6 No. 6, Pp. 421-430.

Forey, B. A., Thornton, A. J. & Lee, P. N. (2011), "Systematic Review With Meta-Analysis Of The Epidemiological Evidence Relating Smoking To Copd, Chronic Bronchitis And Emphysema", *Bmc Pulm Med,* Vol. 1136.

Gao Y, Chu S, Zhang Z, Chen N, Et Al. Hepatoprotective Effects Of Ginsenoside Rg1 - A Review. J Ethnopharmacol, 2017, 206:178-183

Gbd, G. D. A. I. (2018), "Global, Regional, And National Incidence, Prevalence, And Years Lived With Disability For 354 Diseases And Injuries For 195 Countries And Territories, 1990-2017: A Systematic Analysis For The Global Burden Of Disease Study 2017", *Lancet,* Vol. 392 No. 10159, Pp. 1789-1858.

Gold, T. G. I. F. (2023) Global Strategy For Prevention, Diagnosis And

Management Of Copd: 2023 Report..

He, Y., Jiang, B., Li, L. S., Li, L. S., Ko, L., Wu, L., Sun, D. L., He, S. F., Liang, B. Q., Hu, F. B. & Lam, T. H. (2012), "Secondhand Smoke Exposure Predicted Copd And Other Tobacco-Related Mortality In A 17-Year Cohort Study In China", *Chest,* Vol. 142 No. 4, Pp. 909-918.

Henson, P. M. & Bratton, D. L. (2013), "Antiinflammatory Effects Of Apoptotic Cells", *J Clin Invest,* Vol. 123 No. 7, Pp. 2773-4.

Imboden, M., Wielscher, M., Rezwan, F. I., Amaral, A., Schaffner, E., Jeong, A., Beckmeyer-Borowko, A., Harris, S. E., Starr, J. M., Deary, I. J., Flexeder, C., Waldenberger, M., Peters, A., Schulz, H., Chen, S., Sunny, S. K., Karmaus, W., Jiang, Y., Erhart, G., Kronenberg, F., Arathimos, R., Sharp, G. C., Henderson, A. J., Fu, Y., Piirila, P., Pietilainen, K. H., Ollikainen, M., Johansson, A., Gyllensten, U., De Vries, M., Van Der Plaat, D. A., De Jong, K., Boezen, H. M., Hall, I. P., Tobin, M. D., Jarvelin, M. R., Holloway, J. W., Jarvis, D. & Probst-Hensch, N. M. (2019), "Epigenome-Wide Association Study Of Lung Function Level And Its Change", *Eur Respir J,* Vol. 54 No. 1, Pp.

Issemann, I. & Green, S. (1990), "Activation Of A Member Of The Steroid Hormone Receptor Superfamily By Peroxisome Proliferators", *Nature,* Vol. 347 No. 6294, Pp. 645-50.

Jubrail, J., Kurian, N. & Niedergang, F. (2017), "Macrophage Phagocytosis Cracking The Defect Code In Copd", *Biomed J,* Vol. 40 No. 6, Pp. 305-312.

Kliewer, S. A., Forman, B. M., Blumberg, B., Ong, E. S., Borgmeyer, U., Mangelsdorf, D. J., Umesono, K. & Evans, R. M. (1994), "Differential Expression And Activation Of A Family Of Murine Peroxisome Proliferator-Activated Receptors", *Proc Natl Acad Sci U S A,* Vol. 91 No. 15, Pp. 7355-9.

Kojima, K., Asai, K., Kubo, H., Sugitani, A., Kyomoto, Y., Okamoto, A., Yamada, K., Ijiri, N., Watanabe, T., Hirata, K. & Kawaguchi, T. (2019), "Isoflavone Aglycones Attenuate Cigarette Smoke-Induced Emphysema Via Suppression Of Neutrophilic Inflammation In A Copd Murine Model", *Nutrients,* Vol. 11 No. 9, Pp.

Kong L, Liu J, Wang J, Luo Q, Zhang H, Liu B, Xu F, Pang Q, Liu Y, Dong J. Icariin Inhibits Tnf-A/Ifn-Γ Induced Inflammatory Response Via Inhibition Of The Substance P And P38-Mapk Signaling Pathway In Human Keratinocytes. Int Immunopharmacol.2015 Dec;29(2):401-407. Doi: 10.1016/J.Intimp.2015.10.023. Epub 2015 Oct 24. Pmid: 26507164.

Kurihara, N., Fujimoto, S., Kohno, M., Ohta, K., Hirata, K. & Takeda, T. (1989), "[Exercise Induced Hypoxemia And Exercise Tolerance In Patients With Copd And The   Benefits Of Oxygen Supplementation]", *Nihon Kyobu Shikkan Gakkai Zasshi,* Vol. 27 No. 2, Pp. 155-62.

Lee, C. (2017), "Collaborative Power Of Nrf2 And Ppargamma Activators Against Metabolic And   Drug-Induced Oxidative Injury", *Oxid Med Cell Longev,* Vol. 20171378175.

Leung, J. M. & Sin, D. D. (2017), "Asthma-Copd Overlap Syndrome: Pathogenesis, Clinical Features, And Therapeutic   Targets", *Bmj,* Vol. 358j3772.

Li, J. S., Li, S. Y., Xie, Y., Yu, X. Q., Wang, M. H., Sun, Z. K., Ma, L. J., Jia, X. H., Zhang, H. L., Xu, J. P. & Hou, C. X. (2013), "The Effective Evaluation On Symptoms And Quality Of Life Of Chronic Obstructive Pulmonary Disease Patients Treated By Comprehensive Therapy Based On Traditional Chinese Medicine Patterns", *Complement Ther Med,* Vol. 21 No. 6, Pp. 595-602.

Li, J. S., Li, S. Y., Yu, X. Q., Xie, Y., Wang, M. H., Li, Z. G., Zhang, N. Z.,Shao, S. J., Zhang, Y. J., Zhu, L., Guo, L. X., Bai, Y. P. & Wang, Y. F.(2012), "Bu-Fei Yi-Shen Granule Combined With Acupoint Sticking Therapy In Patients With Stable Chronic Obstructive Pulmonary Disease: A Randomized, Double-Blind, Double-Dummy, Active-Controlled, 4-Center Study", *J Ethnopharmacol,* Vol. 141 No. 2, Pp. 584-91.

Li, J. S., Xie, Y., Li, S. Y. & Yu, X. Q. (2014), "Comparison Of Conventional Medicine, Tcm Treatment, And Combination Of Both Conventional Medicine And Tcm Treatment For Patients With Chronic Obstructive Pulmonary Disease: Study Protocol Of A Randomized Comparative Effectiveness Research Trial", *Trials,* Vol. 15153.

Li J, Zhao P, Li Y, Tian Y, Wang Y. Systems Pharmacology-Based Dissection Of Mechanisms Of Chinese Medicinal Formula Bufei Yishen As An Effective Treatment For Chronic Obstructive Pulmonary Disease. Sci Rep. 2015 Oct 15;5:15290. Doi: 10.1038/Srep15290. Pmid: 26469778; Pmcid: Pmc4606809.

Li J, Zhao P, Yang L, Li Y, Tian Y, Li S. System Biology Analysis Of Long-Term Effect And Mechanism Of Bufei Yishen On Copd Revealed By System Pharmacology And 3-Omics Profiling. Sci Rep. 2016 May 5;6:25492. Doi:

10.1038/Srep25492. Pmid: 27146975; Pmcid: Pmc4857103.

Li Jiansheng, 2018, Zhengzhou, 201811115372.3

Li, S. T., Dai, Q., Zhang, S. X., Liu, Y. J., Yu, Q. Q., Tan, F., Lu, S. H., Wang, Q., Chen, J. W., Huang, H. Q., Liu, P. Q. & Li, M. (2018), "Ulinastatin Attenuates Lps-Induced Inflammation In Mouse Macrophage Raw264.7 Cells By Inhibiting The Jnk/Nf-Kappab Signaling Pathway And Activating The Pi3k/Akt/Nrf2 Pathway", *Acta Pharmacol Sin,* Vol. 39 No. 8, Pp. 1294-1304.

Li Y, Li Sy, Li Js, Deng L, Tian Yg, Jiang Sl, Wang Y, Wang Yy. A Rat Model For Stable Chronic Obstructive Pulmonary Disease Induced By Cigarette Smoke Inhalation And Repetitive Bacterial Infection. Biol Pharm Bull. 2012;35(10):1752-60. Doi: 10.1248/Bpb.B12-00407. Epub 2012 Aug 3. Pmid: 22863994.

Liu, D., Geng, Z., Zhu, W., Wang, H., Chen, Y. & Liang, J. (2014), "15-Deoxy-Delta(1)(2),(1)(4)-Prostaglandin J(2) Ameliorates Endotoxin-Induced Acute Lung Injury In Rats", *Chin Med J (Engl),* Vol. 127 No. 5, Pp. 815-20.

Liu, S., Zhou, Y., Wang, X., Wang, D., Lu, J., Zheng, J., Zhong, N. & Ran, P. (2007), "Biomass Fuels Are The Probable Risk Factor For Chronic Obstructive Pulmonary Disease In Rural South China", *Thorax,* Vol. 62 No. 10, Pp. 889-97.

Liu Y, Li C, Wu H, Xie X, Sun Y, Dai M. Paeonol Attenuated Inflammatory Response Of Endothelial Cells Via Stimulating Monocytes-Derived Exosomal Microrna-223. Front Pharmacol. 2018 Nov 20;9:1105. Doi: 10.3389/Fphar.2018.01105. Pmid: 30515094; Pmcid: Pmc6256086.

Liu, Z. J., Liu, W., Liu, L., Xiao, C., Wang, Y. & Jiao, J. S. (2013), "Curcumin Protects Neuron Against Cerebral Ischemia-Induced Inflammation Through Improving Ppar-Gamma Function", *Evid Based Complement Alternat Med,* Vol. 2013470975.

Liu Z, Han Y, Zhao F, Zhao Z, Tian J, Jia K. Nobiletin Suppresses High-Glucose-Induced Inflammation And Ecm Accumulation In Human Mesangial Cells Through Stat3/Nf-Kb Pathway. J Cell Biochem. 2019 Mar;120(3):3467-3473. Doi: 10.1002/Jcb.27621. Epub 2018 Nov 30. Pmid: 30499124.

Li W, Zhao R, Wang X, Liu F, Zhao J, Yao Q, Zhi W, He Z, Niu X. Nobiletin-Ameliorated Lipopolysaccharide-Induced Inflammation In Acute Lung Injury By Suppression Of Nf-Kb Pathway In Vivo And Vitro. Inflammation. 2018 Jun;41(3):996-1007. Doi: 10.1007/S10753-018-0753-3. Pmid: 29541888.

Lu, J., Liu, L., Zhu, Y., Zhang, Y., Wu, Y., Wang, G., Zhang, D., Xu, J., Xie, X., Ke, R., Han, D., Li, S., Feng, W., Xie, M., Liu, Y., Fang, P., Shi, H., He, P., Liu, Y., Sun, X. & Li, M. (2014), "Ppar-Gamma Inhibits Il-13-Induced Collagen Production In Mouse Airway Fibroblasts", *Eur J Pharmacol,* Vol. 737133-9.

Lytras, T., Kogevinas, M., Kromhout, H., Carsin, A. E., Anto, J. M., Bentouhami, H., Weyler, J., Heinrich, J., Nowak, D., Urrutia, I., Martinez-Moratalla, J., Gullon, J. A., Pereira-Vega, A., Raherison-Semjen, C., Pin, I., Demoly, P., Leynaert, B., Villani, S., Gislason, T., Svanes, C., Holm, M., Forsberg, B., Norback, D., Mehta, A. J., Probst-Hensch, N., Benke, G., Jogi, R., Toren, K., Sigsgaard, T., Schlunssen, V., Olivieri, M., Blanc, P. D., Vermeulen, R., Garcia-Aymerich, J., Jarvis, D. & Zock, J. P. (2018), "Occupational Exposures And 20-Year Incidence Of Copd: The European Community Respiratory Health Survey", *Thorax,* Vol. 73 No. 11, Pp. 1008-1015.

Mansure, J. J., Nassim, R. & Kassouf, W. (2009), "Peroxisome Proliferator-Activated Receptor Gamma In Bladder Cancer: A Promising Therapeutic Target", *Cancer Biol Ther,* Vol. 8 No. 7, Pp. 6-15.

Marshall, D. C., Al, O. O., Goodall, R., Shalhoub, J., Adcock, I. M., Chung, K. F. & Salciccioli, J. D. (2022), "Trends In Prevalence, Mortality, And Disability-Adjusted Life-Years Relating To Chronic Obstructive Pulmonary Disease In Europe: An Observational Study Of The Global Burden Of Disease Database, 2001-2019", *Bmc Pulm Med,* Vol. 22 No. 1, Pp. 289.

Mehrotra, P. & Ravichandran, K. S. (2022), "Drugging The Efferocytosis Process: Concepts And Opportunities", *Nat Rev Drug Discov,* Vol. 21 No. 8, Pp. 601-620.

Meng, Y., Feng, R., Yang, Z., Liu, T., Huo, T. & Jiang, H. (2022), "Oxidative Stress Induced By Realgar In Neurons: P38 Mapk And Erk1/2 Perturb Autophagy And Induce The P62-Keap1-Nrf2 Feedback Loop To Activate The Nrf2 Signalling Pathway", *J Ethnopharmacol,* Vol. 282114582.

Mirza, S., Clay, R. D., Koslow, M. A. & Scanlon, P. D. (2018), "Copd Guidelines: A Review Of The 2018 Gold Report", *Mayo Clin Proc,* Vol. 93 No. 10, Pp. 1488-1502.

Nioi, P., Nguyen, T., Sherratt, P. J. & Pickett, C. B. (2005), "The Carboxy-Terminal Neh3 Domain Of Nrf2 Is Required For Transcriptional Activation", *Mol Cell Biol,* Vol. 25 No. 24, Pp. 10895-906.

Ntritsos, G., Franek, J., Belbasis, L., Christou, M. A., Markozannes, G., Altman,

P., Fogel, R., Sayre, T., Ntzani, E. E. & Evangelou, E. (2018), "Gender-Specific Estimates Of Copd Prevalence: A Systematic Review And   Meta-Analysis", *Int J Chron Obstruct Pulmon Dis,* Vol. 131507-1514.

Persson, L. J., Aanerud, M., Hardie, J. A., Miodini, N. R., Bakke, P. S., Eagan, T. M. & Hiemstra, P. S. (2017), "Antimicrobial Peptide Levels Are Linked To Airway Inflammation, Bacterial   Colonisation And Exacerbations In Chronic Obstructive Pulmonary Disease", *Eur Respir J,* Vol. 49 No. 3, Pp.

Pilling, D., Vakil, V., Cox, N. & Gomer, R. H. (2015), "Tnf-Alpha-Stimulated Fibroblasts Secrete Lumican To Promote Fibrocyte   Differentiation", *Proc Natl Acad Sci U S A,* Vol. 112 No. 38, Pp. 11929-34.

Puttur, F., Gregory, L. G. & Lloyd, C. M. (2019), "Airway Macrophages As The Guardians Of Tissue Repair In The Lung", *Immunol Cell Biol,* Vol. 97 No. 3, Pp. 246-257.

Rabe, K. F. & Watz, H. (2017), "Chronic Obstructive Pulmonary Disease", *Lancet,* Vol. 389 No. 10082, Pp. 1931-1940.

Rangasamy, T., Cho, C. Y., Thimmulappa, R. K., Zhen, L., Srisuma, S. S., Kensler, T. W., Yamamoto, M., Petrache, I., Tuder, R. M. & Biswal, S. (2004), "Genetic Ablation Of Nrf2 Enhances Susceptibility To Cigarette Smoke-Induced   Emphysema In Mice", *J Clin Invest,* Vol. 114 No. 9, Pp. 1248-59.

Safiri, S., Carson-Chahhoud, K., Noori, M., Nejadghaderi, S. A., Sullman, M., Ahmadian, H. J., Ansarin, K., Mansournia, M. A., Collins, G. S., Kolahi, A. A. & Kaufman, J. S. (2022), "Burden Of Chronic Obstructive Pulmonary Disease And Its Attributable Risk Factors   In 204 Countries And Territories, 1990-2019: Results From The Global Burden Of   Disease Study 2019", *Bmj,* Vol. 378e069679.

Salvi, S. S., Brashier, B. B., Londhe, J., Pyasi, K., Vincent, V., Kajale, S. S., Tambe, S., Mandani, K., Nair, A., Mak, S. M., Madas, S., Juvekar, S., Donnelly, L. E. & Barnes, P. J. (2020), "Phenotypic Comparison Between Smoking And Non-Smoking Chronic Obstructive   Pulmonary Disease", *Respir Res,* Vol. 21 No. 1, Pp. 50.

Shen, J., Cheng, J., Zhu, S., Zhao, J., Ye, Q., Xu, Y., Dong, H. & Zheng, X. (2019), "Regulating Effect Of Baicalin On Ikk/Ikb/Nf-Kb Signaling Pathway And   Apoptosis-Related Proteins In Rats With Ulcerative Colitis", *Int Immunopharmacol,* Vol. 73193-200.

Sidhaye, V. K., Holbrook, J. T., Burke, A., Sudini, K. R., Sethi, S., Criner, G. J.,

Fahey, J. W., Berenson, C. S., Jacobs, M. R., Thimmulappa, R., Wise, R. A. & Biswal, S. (2019), "Compartmentalization Of Anti-Oxidant And Anti-Inflammatory Gene Expression In Current And Former Smokers With Copd", *Respir Res,* Vol. 20 No. 1, Pp. 190.

Soriano, J. B., Polverino, F. & Cosio, B. G. (2018), "What Is Early Copd And Why Is It Important?", *Eur Respir J,* Vol. 52 No. 6, Pp.

Stampfli, M. R. & Anderson, G. P. (2009), "How Cigarette Smoke Skews Immune Responses To Promote Infection, Lung Disease And Cancer", *Nat Rev Immunol,* Vol. 9 No. 5, Pp. 377-84.

Strange, C. (2020), "Alpha-1 Antitrypsin Deficiency Associated Copd", *Clin Chest Med,* Vol. 41 No. 3, Pp. 339-345.

Straus, D. S., Pascual, G., Li, M., Welch, J. S., Ricote, M., Hsiang, C. H., Sengchanthalangsy, L. L., Ghosh, G. & Glass, C. K. (2000), "15-Deoxy-Delta 12,14-Prostaglandin J2 Inhibits Multiple Steps In The Nf-Kappa B Signaling Pathway", *Proc Natl Acad Sci U S A,* Vol. 97 No. 9, Pp. 4844-9.

Subramani, P. A., Reddy, M. C. & Narala, V. R. (2013), "The Need For Physiologically Relevant Peroxisome Proliferator-Activated Receptor-Gamma (Ppar-Gamma) Ligands", *Endocr Metab Immune Disord Drug Targets,* Vol. 13 No. 2, Pp. 175-83.

Sun, Y., He, L., Wang, T., Hua, W., Qin, H., Wang, J., Wang, L., Gu, W., Li, T., Li, N., Liu, X., Chen, F. & Tang, L. (2020), "Activation Of P62-Keap1-Nrf2 Pathway Protects 6-Hydroxydopamine-Induced Ferroptosis In Dopaminergic Cells", *Mol Neurobiol,* Vol. 57 No. 11, Pp. 4628-4641.

Suzuki, T. & Yamamoto, M. (2015), "Molecular Basis Of The Keap1-Nrf2 System", *Free Radic Biol Med,* Vol. 88 No. Pt B, Pp. 93-100.

Taniguchi, A., Tsuge, M., Miyahara, N. & Tsukahara, H. (2021), "Reactive Oxygen Species And Antioxidative Defense In Chronic Obstructive Pulmonary Disease", *Antioxidants (Basel),* Vol. 10 No. 10, Pp.

Tang Y, Huang W, Song Q, Zheng X, He R, Liu J. Paeonol Ameliorates Ovalbumin-Induced Asthma Through The Inhibition Of Tlr4/Nf-*K*b And Mapk Signaling. Evid Based Complement Alternat Med. 2018 Aug 15;2018:3063145. Doi: 10.1155/2018/3063145. Pmid: 30186353; Pmcid: Pmc6114069.

Venkatesan, P. (2022), "Gold Report: 2022 Update", *Lancet Respir Med,* Vol. 10 No. 2, Pp. E20.

Verma, A., Gudi, N., Yadav, U. N., Roy, M. P., Mahmood, A., Nagaraja, R. & Nayak, P. (2021), "Prevalence Of Copd Among Population Above 30 Years In India: A Systematic Review And Meta-Analysis", *J Glob Health,* Vol. 1104038.

Vidya, M. K., Kumar, V. G., Sejian, V., Bagath, M., Krishnan, G. & Bhatta, R. (2018), "Toll-Like Receptors: Significance, Ligands, Signaling Pathways, And Functions In Mammals", *Int Rev Immunol,* Vol. 37 No. 1, Pp. 20-36.

Wang, C., Xu, J., Yang, L., Xu, Y., Zhang, X., Bai, C., Kang, J., Ran, P., Shen, H., Wen, F., Huang, K., Yao, W., Sun, T., Shan, G., Yang, T., Lin, Y., Wu, S., Zhu, J., Wang, R., Shi, Z., Zhao, J., Ye, X., Song, Y., Wang, Q., Zhou, Y., Ding, L., Yang, T., Chen, Y., Guo, Y., Xiao, F., Lu, Y., Peng, X., Zhang, B., Xiao, D., Chen, C. S., Wang, Z., Zhang, H., Bu, X., Zhang, X., An, L., Zhang, S., Cao, Z., Zhan, Q., Yang, Y., Cao, B., Dai, H., Liang, L. & He, J. (2018a), "Prevalence And Risk Factors Of Chronic Obstructive Pulmonary Disease In China (The China Pulmonary Health [Cph] Study): A National Cross-Sectional Study", *Lancet,* Vol. 391 No. 10131, Pp. 1706-1717.

Wang, M., Luo, X., Xu, S., Liu, W., Ding, F., Zhang, X., Wang, L., Liu, J., Hu, J. & Wang, W. (2019), "Trends In Smoking Prevalence And Implication For Chronic Diseases In China: Serial National Cross-Sectional Surveys From 2003 To 2013", *Lancet Respir Med,* Vol. 7 No. 1, Pp. 35-45.

Wang, N., Cong, S., Fan, J., Bao, H., Wang, B., Yang, T., Feng, Y., Liu, Y., Wang, L., Wang, C., Hu, W. & Fang, L. (2020), "Geographical Disparity And Associated Factors Of Copd Prevalence In China: A Spatial Analysis Of National Cross-Sectional Study", *Int J Chron Obstruct Pulmon Dis,* Vol. 15367-377.

Wheaton, A. G., Liu, Y., Croft, J. B., Vanfrank, B., Croxton, T. L., Punturieri, A., Postow, L. & Greenlund, K. J. (2019), "Chronic Obstructive Pulmonary Disease And Smoking Status - United States, 2017", *Mmwr Morb Mortal Wkly Rep,* Vol. 68 No. 24, Pp. 533-538.

Who, 2022, International Standard Terminologies On Traditional Chinese Medicine [Online], Who. Available Through: Aru Library Website <Https://Www.Who.Int/Publications/I/Item/9789240042322> [Accessed 3 March 2022]

Wortham, B. W., Eppert, B. L., Flury, J. L., Morgado, G. S. & Borchers, M. T. (2013), "Tlr And Nkg2d Signaling Pathways Mediate Cs-Induced Pulmonary Pathologies", *Plos One,* Vol. 8 No. 10, Pp. E78735.

Xian, X., Ding, Y., Dieckmann, M., Zhou, L., Plattner, F., Liu, M., Parks, J. S., Hammer, R. E., Boucher, P., Tsai, S. & Herz, J. (2017), "Lrp1 Integrates Murine Macrophage Cholesterol Homeostasis And Inflammatory Responses In Atherosclerosis", *Elife,* Vol. 6.

Xie, W., Dumas, O., Varraso, R., Boggs, K. M., Camargo, C. J. & Stokes, A. C. (2021), "Association Of Occupational Exposure To Inhaled Agents In Operating Rooms With Incidence Of Chronic Obstructive Pulmonary Disease Among Us Female Nurses", *Jama Netw Open,* Vol. 4 No. 9, Pp. E2125749.

Xu Cq, Liu Bj, Wu Jf, Xu Yc, Duan Xh, Cao Yx, Dong Jc. Icariin Attenuates Lps-Induced Acute Inflammatory Responses: Involvement Of Pi3k/Akt And Nf-Kappab Signaling Pathway. Eur J Pharmacol. 2010 Sep 10;642(1-3):146-53. Doi: 10.1016/J.Ejphar.2010.05.012. Epub 2010 May 25. Pmid: 20519138.

Yan, J., Li, J., Zhang, L., Sun, Y., Jiang, J., Huang, Y., Xu, H., Jiang, H. & Hu, R. (2018), "Nrf2 Protects Against Acute Lung Injury And Inflammation By Modulating Tlr4 And Akt Signaling", *Free Radic Biol Med,* Vol. 12178-85.

Yang, W., Li, F., Li, C., Meng, J. & Wang, Y. (2021), "Focus On Early Copd: Definition And Early Lung Development", *Int J Chron Obstruct Pulmon Dis,* Vol. 163217-3228.

Yin, P., Wu, J., Wang, L., Luo, C., Ouyang, L., Tang, X., Liu, J., Liu, Y., Qi, J., Zhou, M. & Lai, T. (2022), "The Burden Of Copd In China And Its Provinces: Findings From The Global Burden Of Disease Study 2019", *Front Public Health,* Vol. 10859499.

Zha, Z., Leng, R., Xu, W., Bao, H., Chen, Y., Fang, L., Liu, Z. & Ye, D. (2019), "Prevalence And Risk Factors Of Chronic Obstructive Pulmonary Disease In Anhui Province, China: A Population-Based Survey", *Bmc Pulm Med,* Vol. 19 No. 1, Pp. 102.

Zhang, W., Feng, C. & Jiang, H. (2021), "Novel Target For Treating Alzheimer's Diseases: Crosstalk Between The Nrf2 Pathway And Autophagy", *Ageing Res Rev,* Vol. 65101207.

Zheng, D. J., Abou, T. M. & Heit, B. (2021), "Role Of Apoptotic Cell Clearance In Pneumonia And Inflammatory Lung Disease", *Pathogens,* Vol. 10 No. 2, Pp.

Zhou, D. G., Diao, B. Z., Zhou, W. & Feng, J. L. (2016), "Oroxylin A Inhibits Allergic Airway Inflammation In Ovalbumin (Ova)-Induced Asthma Murine Model", *Inflammation,* Vol. 39 No. 2, Pp. 867-72.

Zhou, X. M., Hou, G., Gu, D. X., Wang, Q. Y. & Zhao, L. (2017), "Peroxisome Proliferator-Activated Receptor-Gamma In Induced Sputum Is Correlated With Mmp-9/Timp-1 Imbalance And Formation Of Emphysema In Copd Patients", *J Thorac Dis,* Vol. 9 No. 10, Pp. 3703-3710.

Zhu, Y., Qi, C., Korenberg, J. R., Chen, X. N., Noya, D., Rao, M. S. & Reddy, J. K. (1995), "Structural Organization Of Mouse Peroxisome Proliferator-Activated Receptor Gamma (Mppar Gamma) Gene: Alternative Promoter Use And Different Splicing Yield Two Mppar Gamma Isoforms", *Proc Natl Acad Sci U S A,* Vol. 92 No. 17, Pp. 7921-5.

包海鹏, 史琦, 阎玥, 高龙霞, 司东旭, 于明霞, 李春雷, 孔艳华 & 李友林 (2019), "分子生物学标志物在COPD发病机制中的作用研究概况", *辽宁中医杂志,* Vol. 46 No. 6, pp. 1334-1338.

陈玉龙,吴耀松,李建生等.调补肺肾三法对香烟烟雾提取物和脂多糖刺激A549细胞分泌细胞因子的影响[J].中华中医药杂志,2013,28(07):1989-1993.

蔡星璇, 王耀勇 & 贾俊青 (2021), "维生素D对COPD患者急性炎症指标的影响", *中国老年学杂志,* Vol. 41 No. 11, pp. 2458-2461.

季楠, 俞敏 & 林盈 (2022), "慢性阻塞性肺疾病合并肺栓塞的相关性研究进展", *心肺血管病杂志,* Vol. 41 No. 2, pp. 210-213+209.

金航, 章文强, 马新雅, 代海霞 & 栾荣生 (2021), "四川省城乡慢性阻塞性肺病患病率及影响因素分析", *预防医学情报杂志,* Vol. 37 No. 4, pp. 465-471,477.

李晨旭 （2020），"基于 PPARγ 通路探究补肺益肾法对 COPD 动物模型巨噬细胞胞葬障碍治疗作用"，河南中医药大学

李建生 (2011), "正虚积损为慢性阻塞性肺疾病的主要病机", *中华中医药杂志,* Vol. 26 No. 08, pp. 710-713.

李素云, 李建生, 马利军, 周庆伟 & 李成海 (2003), "补肺益肾颗粒对COPD缓解期患者细胞外基质的影响", *中国中医药信息杂志,* No. 09, pp. 13-15.

李素云, 周庆伟 & 吴纪珍 (2003), "补肺益肾颗粒对COPD缓解期患者肺通气功能和免疫功能的影响", *山东中医杂志,* No. 06, pp. 333-335.

李亚, 王洋, 毛静, 吴兆寰, 刘学芳, 卞晴晴, 李君子, 田燕歌, 冯素香, 郑万春 & 李素云 (2021), "补肺益肾方调控NF-κB信号通路对COPD大鼠炎

性反应的影响", *中华中医药杂志*, Vol. 36 No. 6, pp.

罗倩, 王晓园, 张海涛, 陈艺慧, 向赟, 马媛, 闵丽 & 黄玉蓉 (2019), "新疆乌鲁木齐市城乡40岁以上居民慢性阻塞性肺疾病的患病情况与相关危险因素分析", *临床肺科杂志*, Vol. 24 No. 9, pp. 1562-1567.

秦燕勤,吴耀松,李建生等.调补肺肾三方对香烟烟雾提取物和脂多糖刺激人中性粒细胞释放活性氧及弹性蛋白酶的影响 [J].中国全科医学,2016,19(36):4515-4519.

秦燕勤,陈玉龙,冯素香等. 人参、浙贝母、赤芍有效组分对A549/THP-1细胞共培养炎症模型炎症因子的影响[C]//中国中西医结合学会实验医学专业委员会.第十四次中国中西医结合实验医学学术研讨会论文汇编,2017:4.

饶敏 & 陆月明 (2017), "NF-κB信号途径在COPD中的研究进展", *国际呼吸杂志*, Vol. 37 No. 21, pp.

陶丽,范方田,刘玉萍等.中药及其组分配伍的整合作用研究实践与进展[J].中国药理学通报,2013,29(02):153-156.

田燕歌. 补肺益肾方联合舒肺贴抑制炎症反应治疗COPD大鼠的机制研究[D].北京中医药大学,2015.

吴耀松,陈玉龙,李建生等.补肺益肾方及其拆方含药血清对烟雾和脂多糖刺激细胞分泌细胞因子的影响 [J]. 中药材 ,2013,36(06):961-966.DOI:10.13863/j.issn1001-4454.2013.06.035.

韦衮政, 韦爱欢, 李琼锋, 万启南, 祁燕, 戚彦飞 & 徐莹 (2020), "方药对慢性阻塞性肺疾病信号通路作用的研究进展", *环球中医药*, Vol. 13 No. 4, pp. 752-760.

徐轶凡. 异鼠李素通过Nrf2/Keap1通路减轻慢性阻塞性肺疾病模型小鼠气道炎症的研究 [D]. 广州医科大学,2023.DOI:10.27043/d.cnki.ggzyc.2022.000242.

杨丽霞, 贾钦尧, 陈艳 & 宋珊 (2020), "Toll样受体2、4/MyD88/NF-κB信号通路及相关分子在COPD发病机制中的作用及临床意义", *西部医学*, Vol. 32 No. 12, pp.

殷蕾, 黄跃龙, 金东辉, 胡李平 & 席钊 (2020), "湖南省40岁及以上居民慢性阻塞性肺疾病患病情况及影响因素分析", *中国慢性病预防与控制*, Vol. 28 No. 10, pp. 731-734.
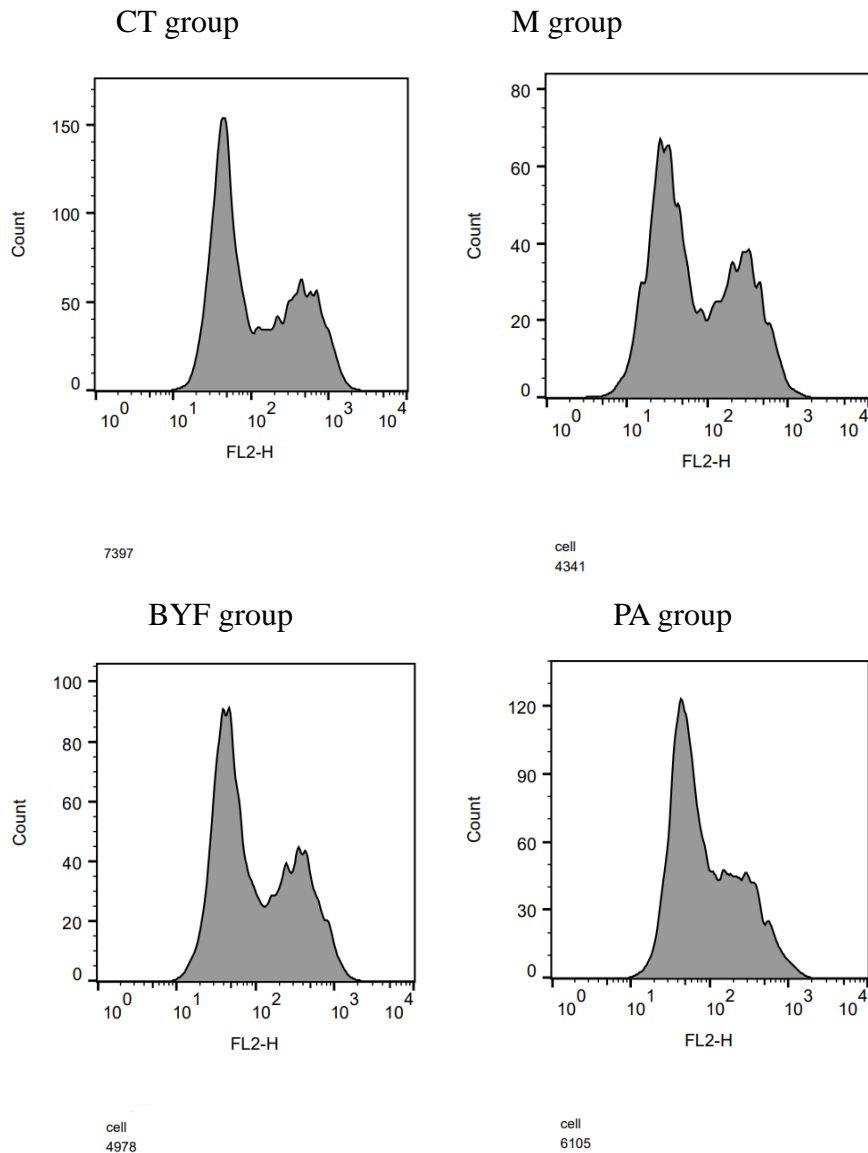
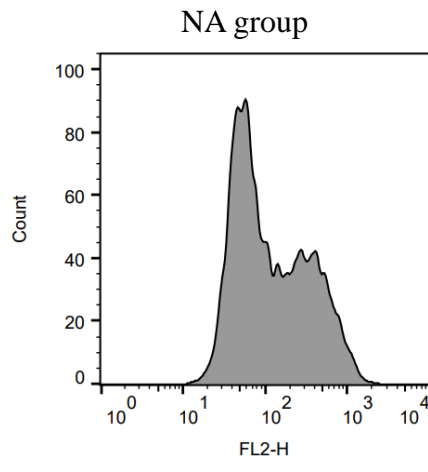张春晶,李淑艳,赵容杰等.人参皂苷Rh1对哮喘模型小鼠炎症因子表达的抑

制作用[J].中国病理生理杂志,2018,34(01):163-167.

张雍, 汤洪秀, 周琦, 彭静 & 彭焱 (2019), "重庆市渝中区成年居民慢性阻塞性肺疾病患病情况及影响因素研究", *重庆医学,* Vol. 48 No. 24, pp. 4226-4230.

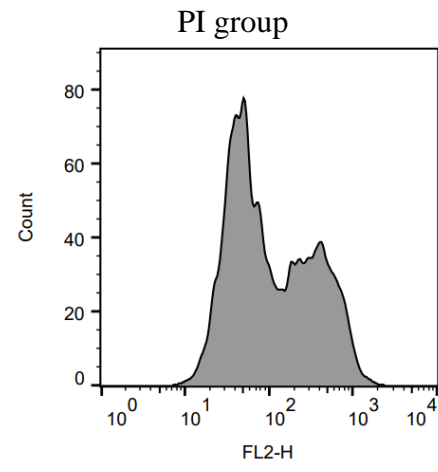张一乐,史苗颜,孙萌,高艳荣,薛艳,吴佳敏,陈麒,张炜.补肾益肺方对慢性阻塞性肺疾病稳定期患者气道黏液高分泌及肺功能影响的临床研究[J].上海中医药杂志,2021,55(12):69-73.

Appendix A

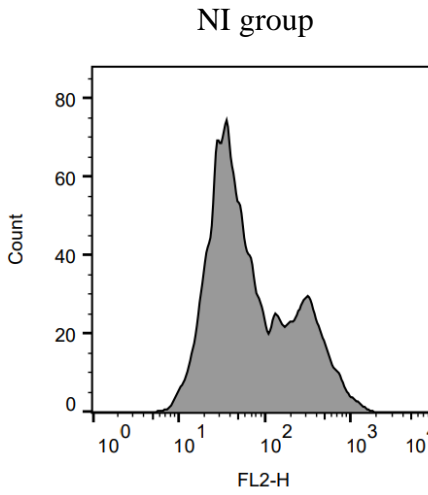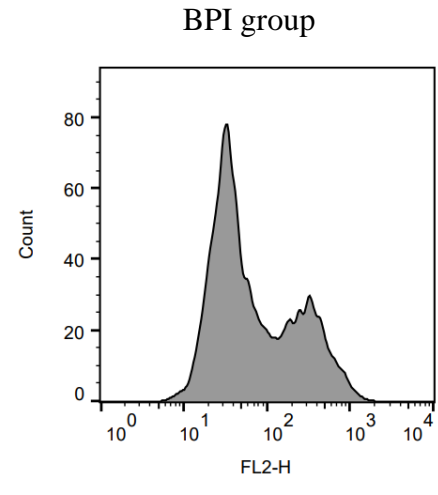Flow chart of alveolar macrophages efferocytosis in each group of mice.

CT group

M group

7397

cell
4341

BYF group

PA group

cell
4978

cell
6105

NA group

PI group

NI group

BPI group

BNI group

BPNI group